Modeling and control of an efficient asbestos removal mobile manipulator

Siddharth Bharamu Maraje

Université Clermont Auvergne

École doctorale Sciences Pour l'Ingénieur
Spécialité "Électronique et systèmes"

Ph.D. Thesis

Modeling and control of an efficient asbestos removal mobile manipulator

(Provisional Document)

Presented by
M. Siddharth Bharamu MARAJE

Defense conducted on 10th July, 2020 in front of the jury composed of:

Mathias HÜSING	Professor, RWTH Aachen University	Examiner
Med Amine LARIBI	Associate Professor HDR, Université de Poitiers	Examiner
Stéphane CARO	Director of Research, CNRS, LS2N, Nantes	Reporter
Véronique PERDEREAU	Professor, Sorbonne Université, Paris	Reporter
Belhassen-Chedli BOUZGARROU	Professor, SIGMA Clermont	Co-supervisor
Jean-Christophe FAUROUX	Associate Professor HDR, SIGMA Clermont	Supervisor
Lounis ADOUANE	Professor, Université de Technologie de Compiègne	Co-supervisor

Université Clermont Auvergne - SIGMA Clermont
Institut Pascal, UMR 6602 CNRS/UCA/SIGMA Clermont, F-63171 Aubière, France

Acknowledgement

My pleasure knows no bounds as I complete this work full of rich experience. I am overwhelmed with the assistance, guidance and blessings bestowed upon me by people directly and indirectly associated in this work. I could hardly find fitting words to express my sincerity and deep respect to them. As I am in the pensive mood and lost in the memories of the past, all the people step one by one before my memory.

Right in the beginning, I would like to express my deep sense of gratitude towards my supervisors Prof.Dr. Jean-Christophe Fauroux, Prof.Dr. Belhassen-Chedli Bouzgarrou and Prof.Dr Lounis Adouane for guiding me at all stumbling blocks and critical moments. It was because of this implicit and valuable guidance I could find a motivation and faith to complete my work. The penetrating questions they asked, made me aware of what a researcher needs to possess. I feel, I was remarkably lucky and singularly fortunate to work under them.

I am thankful to the colleagues from Bots2Rec consortium for collaboration throughout the project. I was fortunate to get feedback on my thesis development from Prof.Dr.-Ing Burkhard Corves (RWTH, Aachen) and Prof. Dr.-Ing. Mathias Hüsing (RWTH, Aachen) during consortium meetings. Dr. Dim Detert (RWTH, Aachen) as a scientific project manager did an excellent job of binding the team together. His help in terms of coordination with consortium partners was extremely useful. I had an opportunity to work with Mr. Roberto Guzman (Robotnik Automation) while performing grinding tests on Version-1 prototype. Mr. Bruno Lineatte (Directeur R&D Modes Constructifs Bâtiment) was a delight to discuss with on verity of topics related to sustainable constructions.

Alongside the academic life, my social life in France was made a great fun by my friends Corentin, Quentin, Zine, Kamal, Dana and Dong. The multicultural environment of the lab gave me an opportunity grow my personality.

I am very thankful to my father Prof.Dr. Bharmu Marje for concrete and valuable guidance and suggestions. I express deep sense of love to my mother Prof.Dr. Seema Marje and other family members who are the chief source of my inspiration.

Finally, I thank all members of jury for agreeing to review my thesis manuscript.

Yours lovely,
Siddharth MARAJE

Contents

List of figures

List of Tables

Table of notations

Abbreviations :

Bots2ReC	Robots to Re-Construction
DGM	Direct Geometric Model
IGM	Inverse Geometric Model
IKM	Inverse Kinematic Model
IGS	Interactive Geometric Software
ZMP	Zero Moment Point
CoM	Centre of Mass
CG	Centre of Gravity

Notations :

(P_G)	Plane representing the ground surface
(P_W)	Plane representing the ground surface
(P_C)	Plane representing the ground surface
h	Displacement of the vertical slider
B	Position of the arm base on the mobile platform
b	Distance of point B from (P_W)
w	Workspace of the robotic arm
(C)	Intersection of w with (P_W)
C	Center of circle (C)
T_{cp}	Tool center position.

Coordinate Frames :

$\mathcal{F}_{\mathcal{E}}$	Coordinate frame attached to the environment
$\mathcal{F}_{\mathcal{G}}$	Coordinate frame attached to the ground surface
$\mathcal{F}_{\mathcal{W}}$	Coordinate frame attached to the wall surface
$\mathcal{F}_{\mathcal{C}}$	Coordinate frame attached to the ceiling surface
$\mathcal{F}_{\mathcal{R}}$	Coordinate frame attached to the robotic unit
$\mathcal{F}_{\mathcal{S}}$	Coordinate frame attached to the support polygon of the mobile base

General Introduction

The aim of developing robotics has been to replace human labor for performing tasks with better accuracy and productivity. There are variety of tasks that involve serious risk to human life. This has motivated to bring in automation so that human lives can be avoided from getting into risks. Although the industrial automation has flourished over the years, it is not yet widespread in civil engineering. Removing asbestos contamination from real world rehabilitation sites is one such application posing a serious health hazard. As extreme safety measures significantly affect the operational efficiency, Bots2ReC project (EU funded H2020) was initiated with a goal to design, test and validate a robotic system and the associated operational process for automated asbestos decontamination. In the context of the project, SIGMA Clermont was responsible for addressing the issue of local process monitoring and stability management of the intended robotic system called 'robotic unit'. Out of the two responsibilities the later one has been addressed in this thesis.

After a careful study of asbestos removal use-case, it was found that the constraint of cleaning high ceiling requires a robotic arm with large workspace. Additionally, rehabilitation sites have narrow entry points that imposes that the robotic unit is also narrow with a compact base. From these two constraints (high and narrow robot), it can be deduced that the robotic unit will have a high aspect ratio and potential stability problems. One solution could be to use stabilizers as can be found in cranes and earth moving machines, but at the price of addition of mass, worse compactness and productivity.

There are two influential factors that tend to affect stability of the robotic unit. Firstly, dynamic machining process like grinding and scarification and secondly, the robotic arm motions during cleaning operation with acceleration that can be high. This triggers an interest of selecting a suitable arm kinematics and dimension that is capable of providing required reachability while minimizing the risk of instability. Moreover, dynamic nature of the asbestos removal process requires study of reaction forces while operating on different cleaning surfaces (wall, ground and ceiling) and arm dynamics to be integrated into the dynamic analysis.

A grinding task requires to completely cover the surface and perform optimal path planning with zigzag trajectories. To grind with a high productivity and good grinding quality, it is required to maintain the dynamic stability of the robotic unit during the process. Thus, static and dynamic stability analysis will have to be addressed during the thesis work so as to perform efficient grinding trajectories.

Organisation of the manuscript

This thesis is divided into five main chapters followed by general conclusions and future work.

Chapter 1 starts by explaining the general motivation of the **Bots2ReC** project and gives information on the use of asbestos within residential sites. Operational regulations for the process of asbestos removal are detailed to make reader aware about the stringent safety measures for human operators. Then, the conceptual framework of the robotic asbestos removal process is presented. In the end, the two prototypes of the robotic unit designed and manufactured during the timeline of the project are introduced.

Review of the literature related to stability margins and stability analysis is performed in chapter 2. A classification of stability margins is presented based on the physical parameters such as distance, angle, energy, moment and force. Approaches related to motion planning and control are revised to seek ideas regarding trajectory planning addressed later in Chapter 5.

Chapter 3 presents a geometrical approach for dimensional synthesis of the robotic arm based on the inference of design rules. Initial requirements appearing in the robotized asbestos removal process are formulated in terms of design rules. Using skeleton modeling approach, geometric modeling of the robotic arm is made in an interactive geometric software (IGS). Design features are then derived from design rules for the selected structures.

Thereafter, the dynamic model of the robotic unit for stability analysis is developed in Chapter 4. Three surfaces, ground, wall and ceiling are considered to identify reaction forces appearing during the grinding process. Then, a numerical approach for stability evaluation is proposed based on ZMP criteria. It is validated numerically in a co-simulation environment combining a numerical solver and a dynamic multibody simulation software.

In Chapter 5, static and dynamic stability analyses of prototypes Version-1 and Version-2 are presented. They are analyzed with three scenarios (ground, wall, ceiling). Version-1 prototype includes an arm supported by a vertical slider. Analysis was made for two positions of the slider so as to study the dynamic stability for different altitude of the arm base. For Version-2 prototype static stability is analyzed for the three scenarios and dynamic stability is evaluated for the wall scenario. A trajectory based on the conclusions obtained from stability analysis is demonstrated.

Chapter 1

Introduction

Contents

This chapter presents in detail the **H2020-Bot2ReC** project under which the dissertation is carried out. Initially, the issue of asbestos contamination in residential sites is presented. It is followed by a general motivation and goals of the project which motivated scientific objectives of the dissertation. Lastly, approach adapted while developing solutions is explained in brief.

1.1 Background of the Bots2ReC project

Automation and robotic solutions are getting prevalent in civil engineering domain that has applications like construction, demolition and re-rehabilitation, etc. Past few decades have shown a continuous growth in the number of robots used and applications developed for civil engineering due to enormous demand and increase in health regulations. Data released by International Federation of Robotics (IFR) stated that the number of robots and automatic systems deployed in 2015 were 568 units with expectancy to reach 2,800 units till 2019 [IFR, 2017]. On the other hand, tasks involved in the civil engineering pose multiple challenges for robotic systems like advanced perception and navigation through complex environment, obstacle avoidance, stability management, collaborative working, robust machining capacity etc. Even to operate such a system, skilled operator is required to efficiently command and supervise the system. Thus, currently, complex tasks are performed by trained labor using conventional electrical and hydraulic tools due to lack of technological advancements in automated systems.

However, cost of the automation machinery going down in recent times, research and engineering communities are motivated to implement advanced solutions replacing human labor. One such example is refurbishment of habitation sites having asbestos contamination is still performed by human operators that are subjected to them to hazardous side-effects of asbestos fibers. Additionally, productivity of human workers is limited due to muscle fatigue and tough working conditions. This led to initiation of **Robots to Re-Construction** (Bots2ReC) project under H2020 innovation action. with a goal to automate asbestos removal process in real world rehabilitation sites [Bots2ReC, 2016].

1.2 Asbestos consumption, consequences and regulations

Asbestos, a naturally found mineral, has been in demand for centuries due to its excellent sound, heat and electric insulation properties. Moreover, it possesses quite a long durability [J.E. and Mossman, 1997] making it an important ingredient for magnitude of products.

Table 1.1: Common types of asbestos products

Category	Products
Adhesives	Roofing sealant, pipe lagging, duct tape, furnace cement and glue for flooring, wall panels, ceiling tiles
Construction Mastics	Repairy or filling industrial materials such as furnaces, tile or flooring
Duct Connectors	Fabric to connect HVAC system parts
Electrical Components	Ebonized panels, electrical shielding, molded cement bases, flash guard paper, wire insulation and cable wrap
Felt	roofing, flooring and paper mills
Fireproofing	Firefighter gear, tar paper, paint and spray-on fireproofing
Gaskets	Heat-resistant seals to join machine parts, valves, hoses
Plastics	Tools, cookware, appliances and vehicles, brake pads

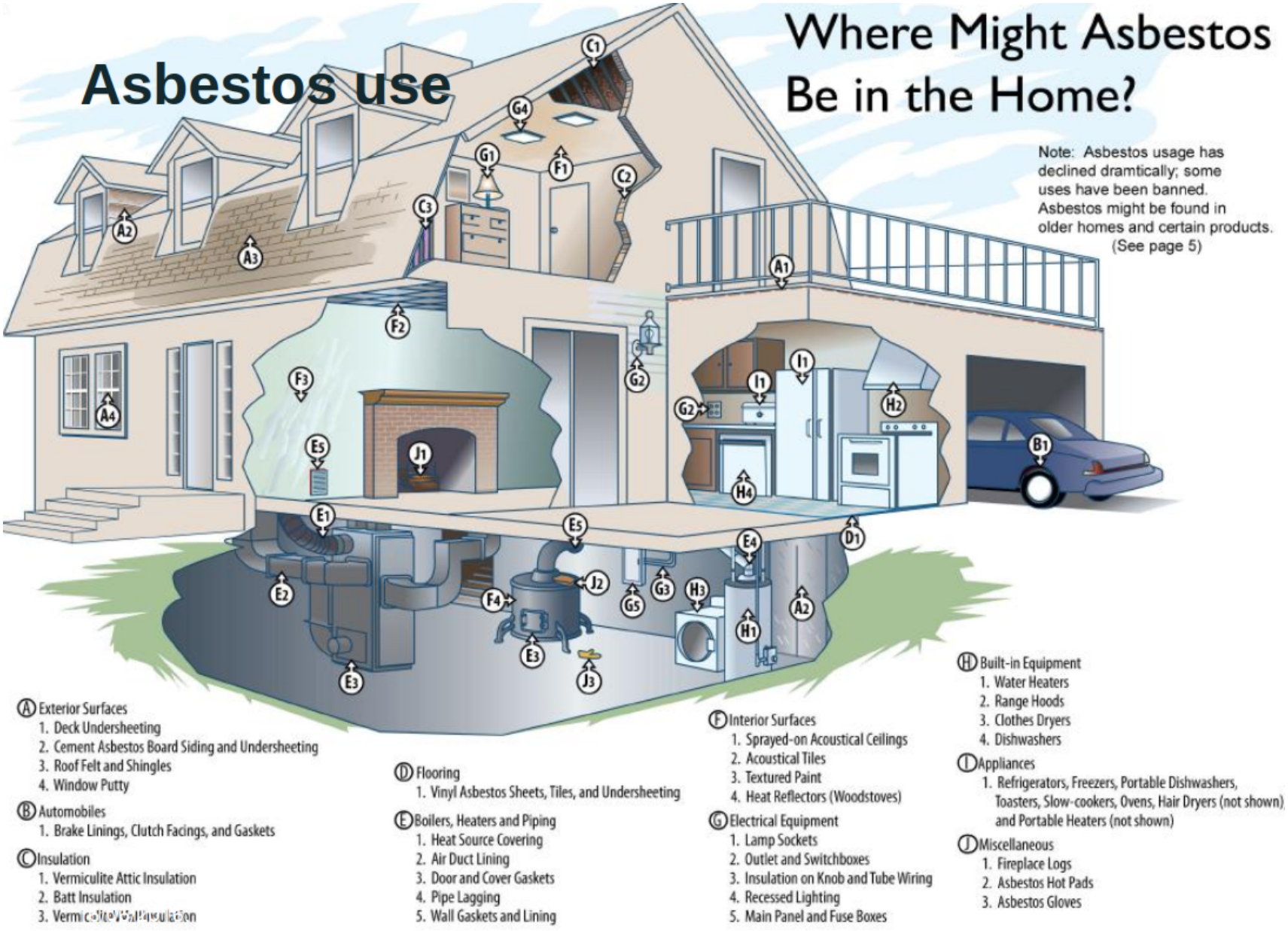

Figure 1.1: Presence of asbestos contamination inside residence-A

Figure 1.2: Presence of asbestos contamination inside residence-B

Table 1.1 presents category of products that containing asbestos [Centre-Mosothelioma, 2006]. Ill-effects of asbestos have been observed since the time of 20th century, where Romans observed sickness induced in slaves who worked with asbestos. Thus there was a ban introduced on buying asbestos quarry slaves due to their early age deaths [UNRV]. In recent times, more research on the asbestos-hazards resulted in identifying generation of fibers being released into air while working with products containing the

asbestos. Workers were then most likely to inhale microscopic fibers leading them to serious health problems like mesothelioma and lung cancer [Straif et al., 2009]. It was observed that after inhaling, asbestos fibers make their way into lining of lungs, abdomen and heart. Figures 1.3 and 1.4 indicate sharp increase in the use of asbestos from 1940s which sustained till 1970. This put millions of people at a risk of exposure to asbestos. Throughout this time period, consequences of asbestos exposure came out dominantly, due to increasing reports of mesothelioma and related diseases. Even a limited amount of exposure was considered lethal leading to the diseases [Centre-Mosothelioma, 2006].

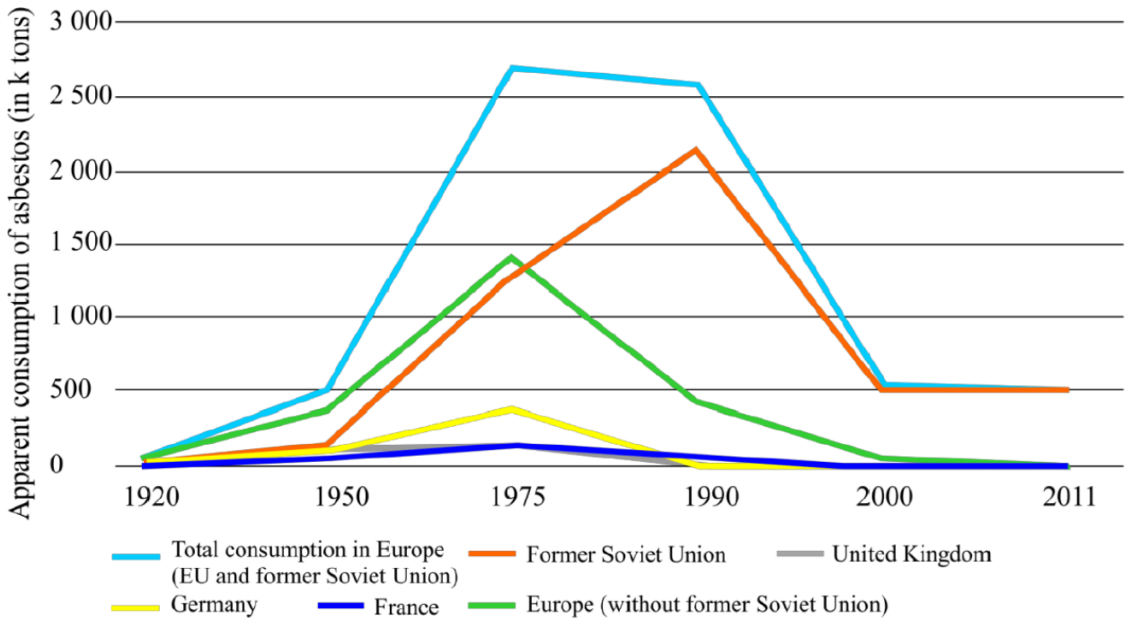

Figure 1.3: Apparent asbestos consumption in Europe in the last century (the apparent consumption is calculated on the basis of the national production of asbestos and imports and exports)

As the correlation between asbestos exposure and associated risks became evident, a ban on the products was introduced in more than 55 countries around the world that included Japan, Australia and countries from Europe. Iceland became the first one to ban asbestos imports in 1983, soon followed by Sweden.Total ban on asbestos was implemented by French government in 1997 [France-Goverment, 1996], by Germany in 1992 and by UK in 1999. However, certain parts of the world like Asia and Russia and USA continued to use asbestos [King, 2017]. Moreover, countries that banned the usage started providing detection and monitoring centers to inform occupants. The process started with identification of flocked asbestos surfaces, insulation and suspended ceilings and monitoring on a regular basis. Next, an assessment of the repairy state was performed by a technical inspector to evaluate physical protection, exposure to shocks and vibrations and air circulation. On the basis of results of this assessment (score 1, 2 or 3), it was required to :

- if the results is 1, conduct a periodic control on the state of repair within three years
- if the result is 2, monitor the level of dust accumulation
- if the result is 3, carry out suitable maintenance within 12 months

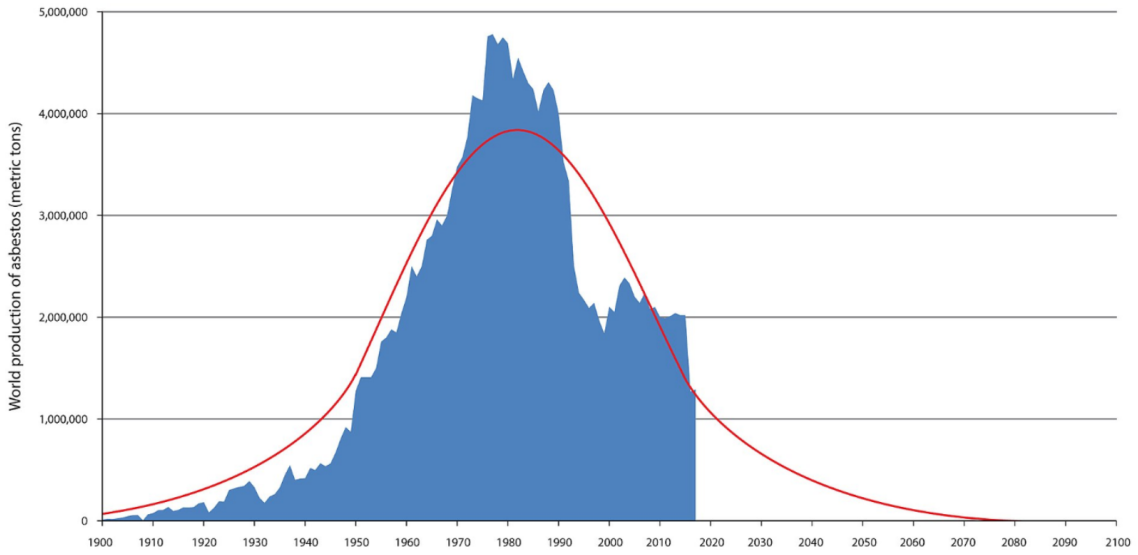

Figure 1.4: World production of asbestos (metric tons) from 1900 to the present (FutureTimeline [2018])

Since 2001, a program to identify materials containing asbestos such as floor tiles, coatings and asbestos-cement products, has also been in place since 2001. A regulatory threshold of 5 fibers per liter (f/l) was put for the level of dust accumulation inside buildings regardless of type of materials. Moreover, for buildings which were granted a permit before 1 July 1997, i.e. which is when asbestos was banned in France, the results of the identification was made mandatory to report in an asbestos technical file (DTA). The responsibility lied with the owner to update at each intervention (monitoring, removal, maintenance, etc.) [France-Goverment, 1996] (French Agency for Food, Environmental and Occupational Health and Safety [Anses, 2017] and French Ministry of Health [MSH, 2019]). Regarding workers at the risk of being asbestos exposure, specific regulatory provisions were applied to protect them in addition to general measures of prevention at work environment. To limit risks, French regulations made it mandatory to implement:

- common prevention measures for all activities with a risk of exposure to asbestos
- specific prevention measures for removal and encapsulation of asbestos or items containing asbestos, and for operations on materials, equipment, or articles that may cause release of asbestos fibers.

Common prevention measures included:

- assessing initial of the risk
- informing and training of staff
- controlling dust accumulation levels for asbestos fibers by analytical transmission electron microscopy (TEM) in order to guarantee compliance with limit values
- worker protection measures specifically focused on containment, techniques of operation and methods that limit release as much as possible, implementation of collective protection measures and PPE suitable for each operation

Depending on the magnitude of dust accumulation and the implemented processes, orders adopted by labor Ministry stipulate technical rules for companies including protection measures and use of personal protection equipment (PPE), measures for the protection of work site environments, and applicable provisions on completion of works. Certified companies carry out encapsulation activities and removal operations for asbestos containing materials. To protect damage at early age, young workers are prohibited from carrying out activities having risk of releasing asbestos fibers. The limit for the mean concentration of asbestos fibers, over a work shift of eight hours is 10 fibers per litre (French Ministry of Labor [FML, 2012]). Therefore, when performing refurbishment in the buildings contaminated with asbestos, intense safety measures should be taken to reduce the health risks for employees as Figure 1.3 shows. As can be seen in the figure, the workers are using heavy equipment and they are wearing special tight suits and masks to avoid exposing to the asbestos

(a) Floor cleaning (b) Wall cleaning (c) Ceiling cleaning

(d) Ceiling cleaning (e) Decontamination zone

Figure 1.5: Different scenarios of asbestos cleaning process

1.3 The Bots2ReC Project

Due to the extremely inefficient and restrictions on manual performance of removing asbestos, and the very tiring working conditions, automated solutions have emerged and started to be seen as a realistic alternative. Furthermore, in order to judge the impact of automating the asbestos removal tasks, a study regarding the situation of asbestos contamination in Europe was assigned. However, it is still quite difficult to evaluate the quantity of asbestos present in European buildings as there is no proper documentation for that. The situation is documented well for France and there are few legal dispositions or studies focused for certain other countries.

In France, according to the publication of the Social Union for Habitat (L'Union sociale pour l'habitat [USH, 2014]), more than 40% of the housing stock is contaminated by asbestos (around 15 million flats). An important study of the 'Centre Scientifique et Technique du Bâtiment' confirms these numbers and shows that 2 million out of 3,6

million non-residential buildings are contaminated [Chaventré and Cochet, 2005]. In Great Britain, the estimations are quite approximated, but 4,4 million buildings are said to need asbestos removal [BYG, 2015].

In Hungary, an isolated study of the NIOH detected presence of asbestos in 500 buildings of Budapest. Moreover, more than 4 million tons and 3 million tons of asbestos were imported in France and Great Britain respectively during the 20th century (Association Nationale de Défense des Victimes de l'Amiante [de Défense des Victimes de l'Amiante]. For Spain, the imports are around 2.6 million tons, and the German situation can be estimated to be similar to the Spanish one. In Italy, some studies announce very high amounts between 30 and 40 million tons of asbestos. For Belgium it was estimated that 800 thousand tons of asbestos were present in 2001.

Table 1.2: Asbestos consumption (in t) in the European community in 1973 (Asbestos Trade Association, France)

	Chrysotile	**Amosite**	**Crocidolite**	**Anthophyllite**	**TOTAL**
Ireland	6,400	600			7,000
France	150,000	2,800	3,100	100	15,600
Denmark	28,000	4,800			33,000
Netherlands	37,400		600		38,000
Belgium	76,000	5,000	5,000		86,000
Italy	130,600	2,200	6,200		139,000
United Kingdom	147,000	24,000		300	172,000
Germany	194,100	1,900	3,300	1,700	201,000
Total	770,400	41,300	18,200	2,100	832,000

These numbers from various European countries prove that asbestos contamination is present in millions of flats all over Europe, even if exact figures are limited. The asbestos exists in different forms: Chrysotile, Amosite, Crocidolite and Anthophyllite. Its consumption in the European Community in 1973 (when major amounts of asbestos were used) indicates that in Western Europe, the main countries probably present similar quantities of asbestos as France (see Table1.2), where the figures are well known. A peculiar case is Russia and the ex-Soviet union countries, where the asbestos market is still existing and the public institutions deny the danger linked to asbestos. There is potentially a very big quantity of asbestos in these countries, but no market for asbestos removal for the moment.

Few studies allow estimating the global costs of necessary refurbishment and clearance procedure for the European market. The publications concerning the French market indicate a total amount of 80 billion Euros [USH, 2014] to 200 billion Euros [Guérin and Joaun, 2014]) for private housing. For France, the most moderated sources announce 15 billion Euros needed to clean the polluted social housings only [Guérin and Joaun, 2014]. Taking into account the private housings and the non-residential sector, the total amount would exceed 100 billion Euros. In Great Britain the estimated costs are much lower: 15 billion Euros are estimated for the all buildings. It must be considered that in Great Britain, asbestos treatment is to keep the pollution in place, and cover it with some protection. This is far less expensive, and partly already done, which can explain the difference in the estimation compared to France [BYG, 2015]. Based on the data presented above, it can be estimated that the 5 to 6 biggest countries in Western Europe are in situation similar to France. Even if the cost of asbestos removal can be reduced in

future, it can be estimated that the total market of asbestos removal reaches several 100 billion Euros for these countries only.

Hence, the contamination clearance from European flats is expensive (11500 Euros per flat on average, according to Pertuy Construction's investigations) as the European asbestos removal market is very large. Moreover, the regulations mentioned in Section 1.2 should be respected, which means that the workers need to wear personal protective equipment complying with the highest technological standards and exchange it regularly. Thus, the automation of such kind of processes would allow the demolition and refurbishment industries in Europe to operate more efficiently [Detert et al., 2017]. In addition to that, automation will decrease the refurbishment costs and, at the same time, prevent the employees from being exposed to the asbestos microscopic fibers.

Motivated by the mentioned reasons, the "Robots to Re-Construction" Bots2ReC project was launched in February 2016. The project objectives include: "Introducing, testing and validating an operational process for the automated removal of asbestos contamination at a real world rehabilitation site using a robotic system."

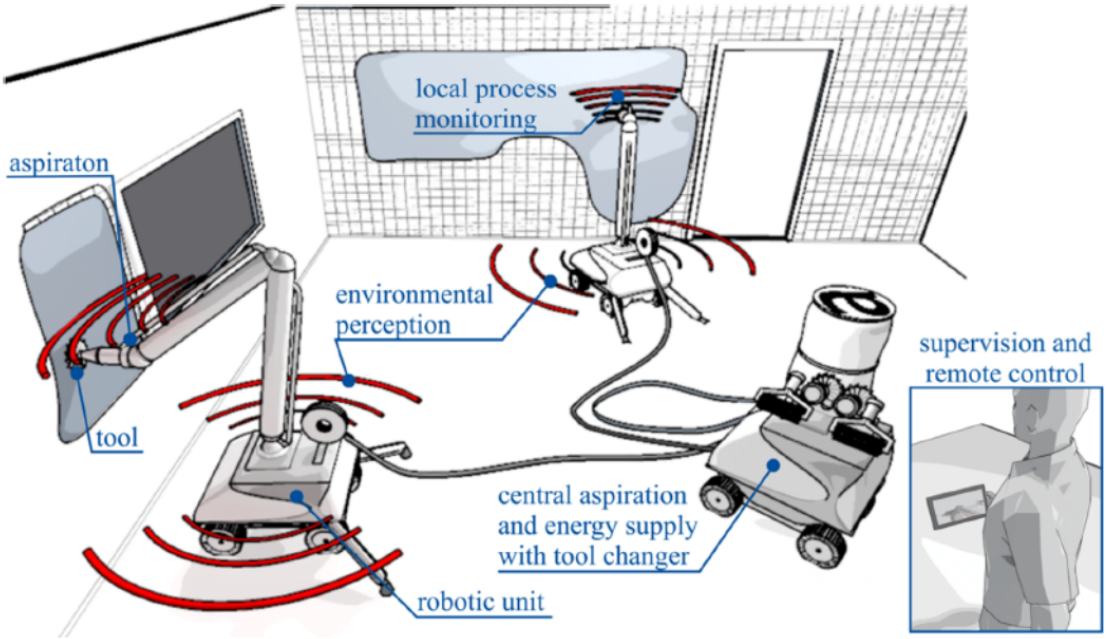

Figure 1.6: Conceptual sketch of the automated removal of asbestos contamination from rehabilitation sites using robotic units [Bots2ReC, 2016]

1.4 Bots2ReC Consortium

The Bots2ReC consortium consists of seven partners that are academic institutions, small-medium scale industries and a customer industry. Role of each partner in the project is described below.

1. **RWTH Aachen University** is a research institution that augments the state of the art technology in the areas of control, task planning and sensor data processing.

2. **SIGMA-Clermont** brings research expertise in mechatronic design, modeling, perception and collaborative control for simulating and piloting the robotic system in

its environment.

3. **Robotnik Automation** SLL develops and manufactures mobile platforms and manipulators for service robotics applications and unmanned ground vehicles. It develops the mobile base of the Bots2ReC robot.

4. **Telerobot Labs Srl** offers high level competences in design, development and production of robotic and mechatronic devices. It develops the robotic arm and tools for the Bots2ReC robot.

5. **Indurad** is a producer and integrator of optical and radar sensor technology with a unique data processing and visualization software framework. It develops sensors for single dimensional distance measurement and for localization of the Bots2ReC robot

6. **Fundacio Eurecat** is an experienced system integrator, that will integrate the robotic system including the developed operational process for the use case.

7. **Bouygues Construction** participates as the end-user and industrial partner. It is responsible for the clearance and refurbishment of a site and the system operation.

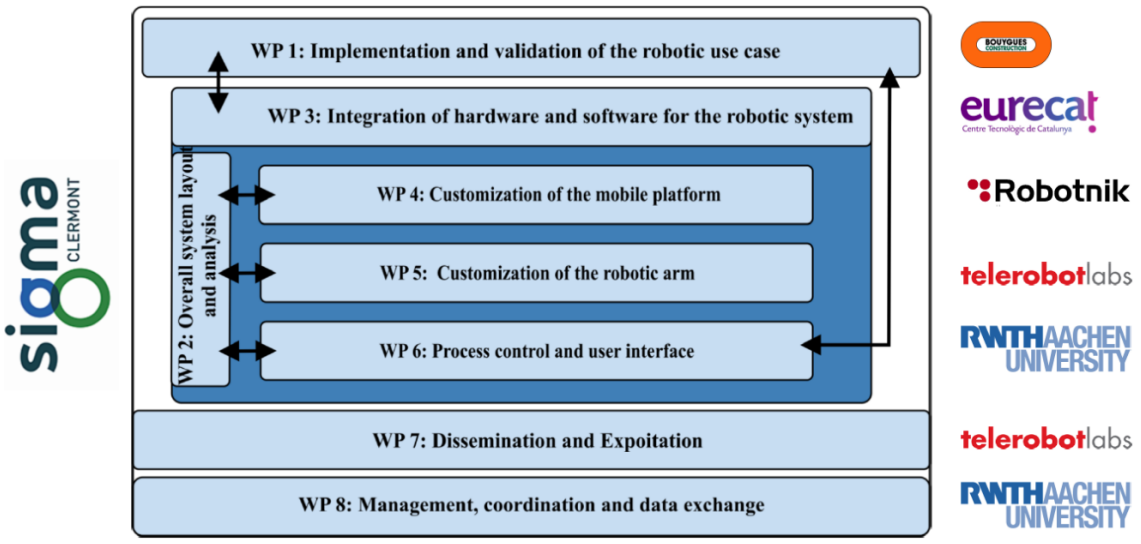

Figure 1.7: Work package management within consortium [Bots2ReC, 2016]

Conclusions

A detailed overview of usage of asbestos, its consequences and regulations were presented in the chapter. Data on the worldwide asbestos production was shown to highlight the extensive usage of asbestos throughout the first half of the 20^{th} century. Variety of products used in the construction of factories and residences (adhesives, connectors, gaskets, plastics, etc.) were based on asbestos that now poses health hazards to thousands of occupants.

In the context of refurbishment of sites, the process of manual asbestos removal alongside regulations was described to identify difficulties and health risks for human

(a) Prototype version 1 (b) Prototype version 2

Figure 1.8: Two prototypes developed by the consortium of Bots2ReC

operator that motivated the Bots2ReC project. The consortium of the project and respective roles were briefed to make the reader familiar with the sharing of responsibilities. Finally, main objectives of the thesis that is, structural selection of the arm kinematics, dynamic modeling of the robotic system and trajectory planning for efficient task planning were briefed.

A general overview of mobile manipulator research related to stability margins, dynamic modeling and path planning is performed in Chapter 2.

Chapter 2

Mobile manipulators and related research

Contents

This chapter presents a comprehensive review of the literature concerned with the stability management of mobile manipulator systems. Initially, different deigns and applications of mobile manipulators are recalled. Then a detailed study of existing stability margins is presented. Many works demonstrating stability analysis and management are put forth. Followed by is a brief review of planning, control and optimal base positioning techniques that play a key role in enhancing productivity of the mobile manipulator system.

2.1 General overview of Mobile manipulators

In the discipline of advanced robotics, mobile manipulators have earned continual attention among research as well as industrial community, the reason being coexistence of *mobility* and *manipulation* in them. Such a combination tends to yield a serious advantage of having *'large operational workspace'* over traditional (fixed-based) counterparts resulting into enhancement of utility. This has made mobile manipulators a preferred choice in number of applications like assembly tasks for manufacturing, logistics, home services, firefighting, military operations, disaster rescue, nuclear power station tasks, planetary exploration etc.

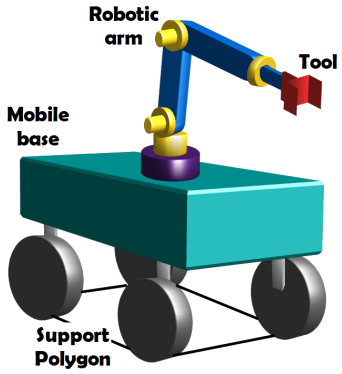

Figure 2.1: General schematic of mobile manipulator

Elementary components of a mobile manipulator system namely, a mobile base with locomotion system, one or several robotic arms and the corresponding end-effectors (tools) are shown in figure 2.1. Within the mobile base, ancillaries like electrical-electronic systems, aspiration unit etc. can also be found embodied within the base. Robotic arms, which come in variety of kinematics and desired end-effector. To achieve locomotion, different systems have been implemented, each offering particular advantage for a specific task. Figure 2.2a, 2.2b and 2.2c represent wheeled, caterpillar tracked and legged type of locomotion respectively. Wheeled locomotion is the most commonly used of them all. However, it has difficulties navigating stairs. This is overcome by the two other locomotion systems out of which caterpillars are suitable even for softer surfaces

(a) Husky
[Clearpath Robotics, 2017]

(b) Packbot
[FLIR Systems, 1998]

(c) Spot-*Boston Dynamics*
[Ackerman, 2016]

Figure 2.2: Mobile manipulators with different types of locomotion

since they distribute contact forces. Legged locomotion, even though complicated to control, allows base height adjustment and can navigate through extremely uneven surfaces thanks to intermittent contacts on the ground, that can be located at suitable places.

(a) Non-holonomic platform

(b) KMM-QUANTEC

(c) KMM-iiwa

(d) Wafer handling solutions

Figure 2.3: Mobile manipulators offered by KUKA Robotics [KUKA, 2015]

Mobile manipulators deployed in real world

A range of mobile manipulators offered by KUKA robotics is shown in figure 2.3. KMM-QUANTEC and non-holonomic platform are autonomously navigating mobile manipulators used in the machining of heavy components like big pipes, airplane parts etc. KMM-iiwa (figure 2.3) is a combination of a sensitive LBR-iiwa arm, that integrates torque sensors in all its joints sensitive LBR-iiwa [LBR-iiwa, 2013] and a mobile platform providing high degree of mobility and agility. It has utility in applications like material fetching and transportation, paint/glue applications, palletizing/packaging. Figure 2.3d shows a wafer handling mobile manipulator developed for semiconductor production application that has LBR-iiwa mounted on an automated guided vehicle (AGV). Sensitive LBR-iiwa enables safe and precise handling of wafer cassettes without subjecting to vibration. These examples demonstrate how different combinations of arm and mobile base result into systems suitable for variety of applications.

Figure 2.4 presents multiple operating domains of mobile manipulators. NASA has developed planetary exploration rovers like Opportunity mars rover (figure 2.4a) that carries on-board drilling arm for ground sampling with devices for environmental sensing and data acquisition. SpaceJustin is another robot developed by German Aerospace Centre (DLR-figure 2.4b) that has two arms DLR-HIT [Chen et al., 2014] and a torso

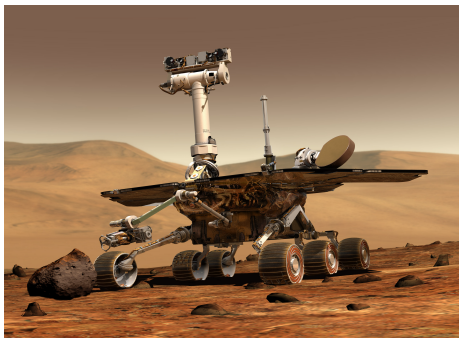

(a) Opportunity Rover
[NASA, 2003]

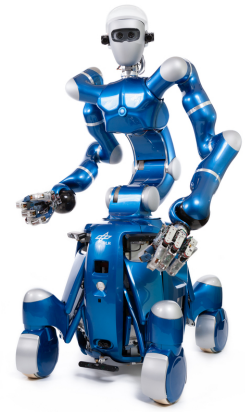

(b) SpaceJustin
[DLR, 2009]

(c) Flex robotic system
[Medrobotics, 2016]

(d) Mobile manipulator
[Fetch, 2016]

(e) TIAGo
[Pal-Robotics, 2016]

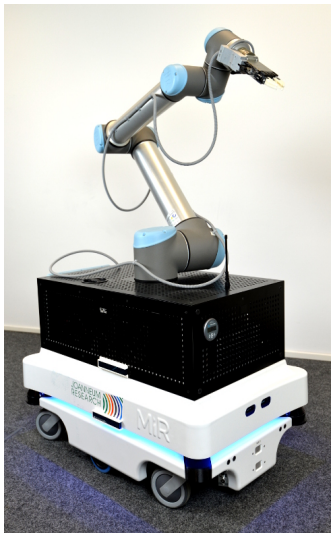

(f) CHIMERA
[Joanneum, 2016]

Figure 2.4: Mobile manipulators development for different applications

mounted on mobile base. More such applications are presented through- Medrobotics: Flex system for surgical applications (figure 2.4c), military application robot Packbot (figure 2.2b), household service robot Spot (figure 2.2c).

Research and development of mobile manipulators

Timeline of mobile manipulator development (figure 2.5) is traced in [Bøgh et al., 2011]. Moreover, in [Bostelman et al., 2017], an in-depth literature review on the mobile manipulators developed for different applications is presented. They mainly include 'peg-in-hole' insertion, shaft assembly, mobile manipulation in manufacturing, door opening, object fetching, book browsing, object handling, cooperative motion etc. Summary of this literature in debriefed in tables 2.1-2.2.

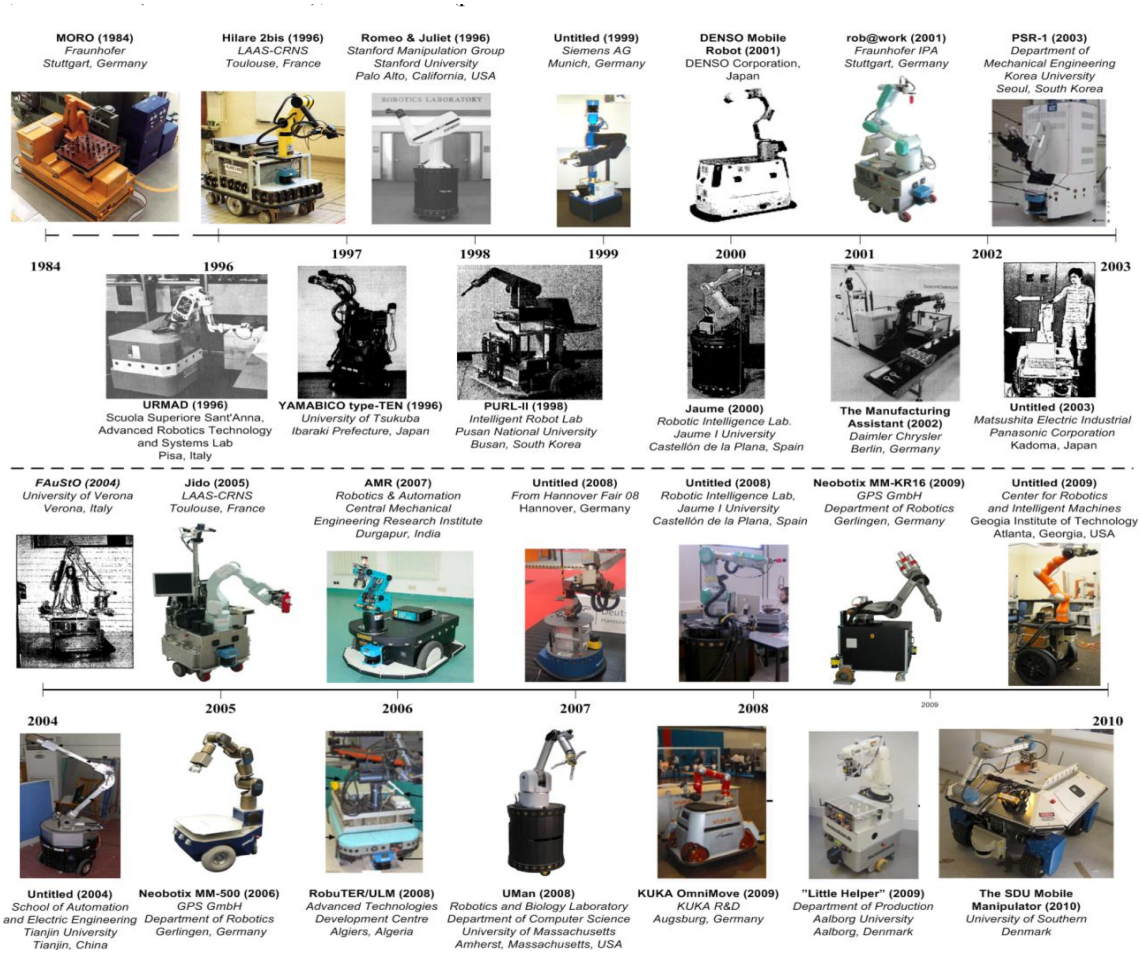

Figure 2.5: Timeline of mobile manipulator development. (Photo courtesy of MTECH, Aalborg University, Denmark [Bøgh et al., 2011])

Table 2.1: Applications of mobile manipulator - I

Work	Application Developed	Technique
[Pin and Culioli, 1992]	Optimal positioning for material handling in dynamic task environment	Multi-objective optimization under constraints of obstacle avoidance, maneuverability and torque
[Hvilshøj and Bøgh, 2011] [Car, 2012]	Peg-in-hole assembly : 'Little helper bot'	Prototype design with software and hardware integration, action based domain specific communication language
[Flannigan, 2012]	Long workspace operations e.g Fuselage	High accuracy remote position sensing of the end-effector,real-time tracking of multiple objects using metrology system
[Chen and Li, 2006]	Fixing leakage points of jugs filled with dangerous chemicals	3-Level (decision, processing and execution) Intelligent controller based o neural networkn neural network
[Petersson et al., 2000]	Door opening	Force/torque control algorithm, online estimation of door radius and axis or rotation
[Nagatani and Yuta, 1996]	Passing through Doorways	Design an implementation of action primitives to control robot according to planned motion primitives
[Chitta et al., 2010]	Door opening	Graph-search based efficient planning

Table 2.2: Applications of mobile manipulator - II

Work	Application Developed	Technique
[Tomizawa et al., 2003]	Book browsing in library	Control system for teleoperation via Ethernet, GUI for human operation
[Bort and del Pobil]	Object fetching	Human-robot verbal interaction with mobile manipulator
[Holmberg and Khatib, 2000]	Holonomic mobile manipulator for manipulation	Design and development of a powered caster vehicle (PCV) and its dynamically decoupled control
[Khatib et al., 1996a], [Khatib et al., 1996b]	Stanford Assistant Mobile Manipulators (SAMM)	Operational space formulation for motion and force control, dexterous dynamic coordination, augmented object model for multi-arm manipulation, virtual linkage model for control of internal forces
[Osumi and Terasawa]	Large object manipulation	Feedback control laws for cooperation of mobile platforms
[Sugar and Kumar, 1998]	Object manipulation and transportation	Novel fork-lift like arm, real time control system to control Cartesian stiffness or impedance
[Agah and Tanie, 1997]	Handling and delivering objects	Contention control architecture
[Jain and Kemp, 2010]	Object fetching	Directed segmentation-based perception, navigation to the user-selected location

2.2 Stability of mobile manipulators

In general, most of the mobile manipulators used in industry have a high base to manipulator ratio of mass. Thus, carrying a payload and maneuvering does not require consideration of tip-over phenomenon. However, there are number of applications (construction industry, spatial drilling etc.) where need of manipulator with low base to manipulator mass ratio can arise due to constraints on mass and dimensions of the base imparted by the working environment. Contrary to the heavy base mobile manipulators, use of top-heavy ones presents a distinct challenge of 'stability management' while carrying out intended tasks. Poor handling of the issue may seriously affect overall performance resulting in . Apart from being a constraint, stability can also compromise ' quality and safety of operation' putting the entire system and its surrounding in jeopardy. Hence, to ensure safe and productive functioning, it is necessary to integrate stability into task planning and control.

For mobile robots in general, including wheeled and legged ones, numerous attempts to accurately evaluate stability can be seen through the literature. A condition to determine the state of stability or instability is called a *criterion*, while a quantitative measure of stability is termed as *margin*. Review of static and dynamic margins was presented in [Armada et al., 2002]. In [Mahdi and Nestinger, 2012], based on stability metric, criteria were further classified into five types namely: distance, angle, force, moment and energy. This classification is adapted for presenting state of the art through following sections.

2.2.1 Distance based criteria

Distance based criteria use minimum distance between projection of center of gravity on the support polygon (CG) acting on the CG and an edge of the support polygon to define instantaneous stability. In [McGhee and Frank, 1968] and [Mcghee and Iswandhi, 1979] a static stability criterion based on the centre of gravity (C.G) was proposed. The claim was, a vehicle (wheeled or legged) is statically stable if '*the projection of its centre of mass lies within the supporting polygon*'. Support polygon of the footprint of the robot was defined as a convex polygon formed by connecting ground-wheel contact points.

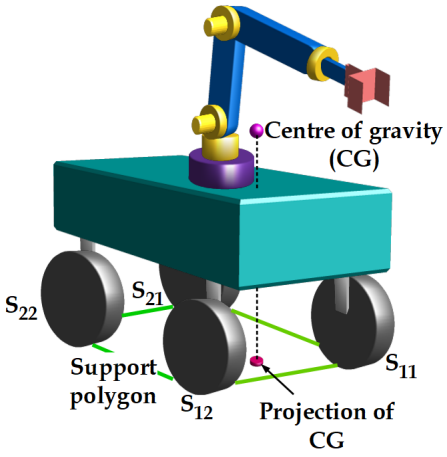

Figure 2.6: Statically stable pose

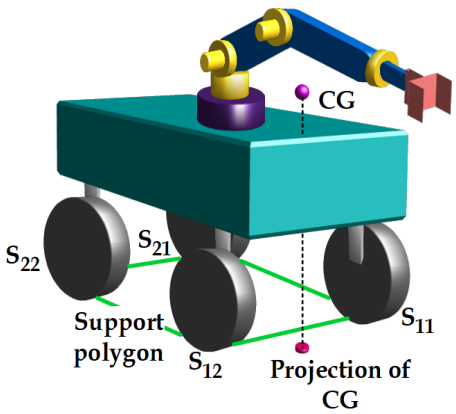

Figure 2.7: Statically unstable pose

Figures 2.6 and 2.7 respectively show statically stable and unstable poses of the mobile manipulator. Rectangular support polygon of the mobile manipulator defined

by points $S_{11}S_{12}S_{21}S_{22}$.

[Sreenivasan, 1994] proposed a distance based dynamic stability margin (figure 2.8). It projected the dynamic force F_g applied on the center of gravity CG of the robot to the ground and measured the distance d between line of action of the force and a parallel line passing thorough ground contact point. But this margin had a limitation of not being able to handle dynamic toques applied on the mobile platform.

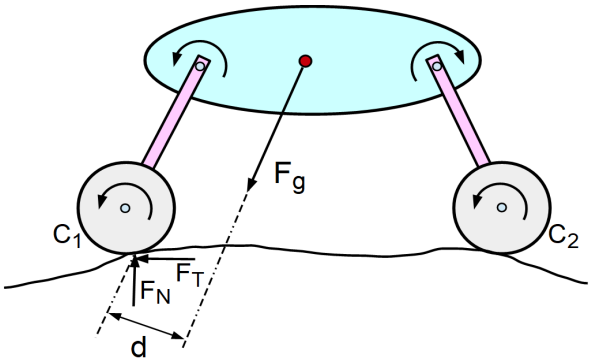

Figure 2.8: Distance based dynamic stability margin [Sreenivasan, 1994]

[Davidson and Schweitzer, 1990] proposed a static stability margin for four legged robots. In this method, external forces, force from a tethering cable-winch and inertial force were included in quasi-static manner as a wrench. Possible rotation of the vehicle around the axis defined by each edge of the support polygon is defined as a twist of zero pitch. Virtual power generated by resultant wrench and zero-pitch virtual twist was determined for all edges of the support polygon. Negative value of the virtual power was identified as a condition of instability. Minimum magnitude of this power was used as a value for stability margin.

2.2.2 Angle based criteria

In [Diaz-Calderon and Kelly, 2005], subtended angle (θ) between normal of the i^{th} tip-over axis and i^{th} resultant force is considered as a measure of stability about i^{th} tip-over axis. Minimum of all such angles calculated for respective axes is the stability margin of the entire system.

$$\theta = min(\theta_i) \tag{2.1a}$$

$$\theta > 0 \rightarrow stable; \;\; \theta = 0 \rightarrow marginally \;\; stable; \;\; \theta < 0 \rightarrow unstable \tag{2.1b}$$

Another tip over stability margin called force-angle stability measure (FASM) was proposed in [Papadopoulus and Rey, 1996]. The claim was easy calculation and sensitivity to top-heaviness. According to author- 'force-angle stability measure is based on the computation of *minimum of the angle between the net force vector and each of the tipover axis normal* (figure 2.9).

$$\beta = \theta_i.||d_i||.||f_r|| \tag{2.2}$$

Critical tipover instability occurs when β goes to zero, i.e., any θ_i becomes zero, or either of $||d_i||$ or the force f_r become zero.

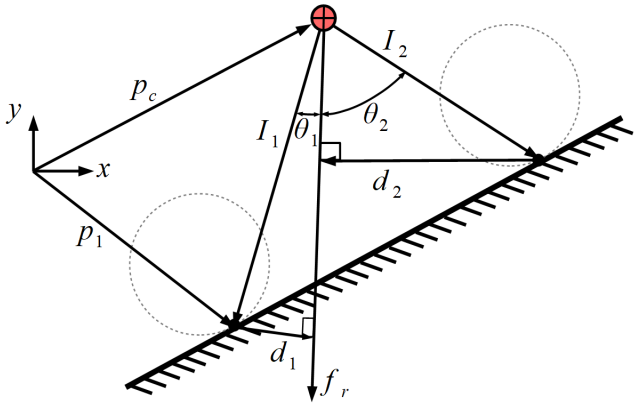

Figure 2.9: Concept of force angle stability margin [Papadopoulus and Rey, 1996]

2.2.3 Energy based criteria

[Messuri and Klein, 1985] proposed **energy stability margin** (ESM) as an improvement to the static stability margin. Energy stability level associated with a particular edge of a support polygon is equal to the mechanical work required to rotate body centre of gravity about an edge to a position where the vertical projection of CG lies along that edge of the support polygon (to the verge of instability). The energy stability margin is equal to the minimum of the energy stability levels associated of all the edges of the support polygon.

$$S_{ESM} = \min_{i=1}^{n_s}(mgh_i) \tag{2.3}$$

'i' is a vertex of the support polygon which form a rotational axis with $i+1$, n_s is the number of supporting legs and h_i is the elevation of CG during the tipover moment.

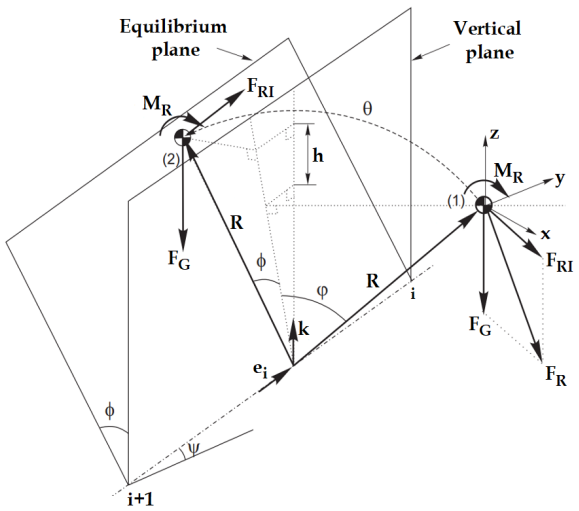

Figure 2.10: Equilibrium plane corresponding to the tipover edge [Ghasempoor and Sepehri, 1995], [Hirose et al., 2001]

[Ghasempoor and Sepehri, 1995] extended ESM for mobile manipulators by including other factors affecting stability - vehicle top-heaviness, uneven terrain conditions,

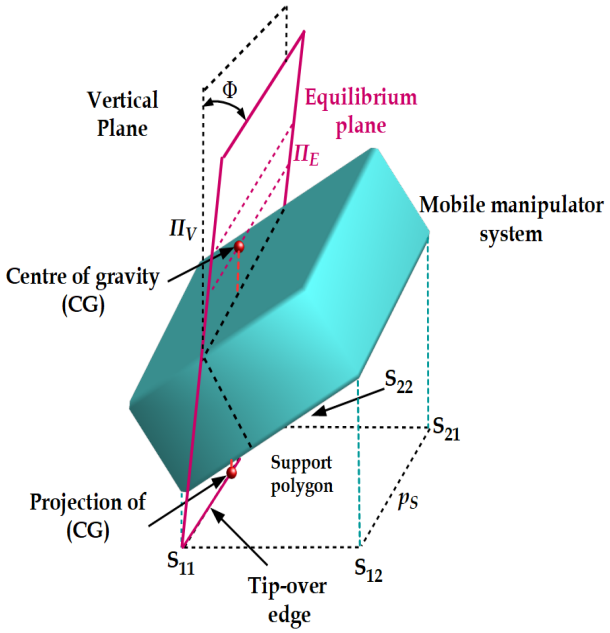

Figure 2.11: Hypothetical tipover of the robotic system

external forces arising from the manipulation of payload and inertial forces due to vehicle motions. ESM is intended to monitor the tipover potential of mobile manipulators. An *equilibrium plane* (π_s) associated with each edge of the support polygon was defined such that, the plane contains center of gravity at the hypothetical tilted position of the mobile manipulator system for which projection of center of gravity on p_S is on the respective edge. Figure 2.11 shows hypothetical tipover of the mobile robotic system. For this state of tilt, projection of center of gravity lies on the edge S_{11}-S_{22}. The equilibrium plane denoted by π_s is thus defined to pass through edge S_{11}-S_{22} and center of gravity.

The energy stability level associated with each edge was defined as the mechanical work required to rotate the system about respective edge till the centre of gravity lies in the equilibrium plane. Minimum of all the energy levels was regarded as dynamic energy stability margin (DESM). Energy associated with the supporting edge defined by points (i)-$(i+1)$ was calculated as,

$$Energy\ Stability\ Level_{(i,i+1)} = [W_1 - W_2]_{(i,i+1)}; \tag{2.4}$$

Here, W_1 is work done by stabilizing weight force and W_2 is work done by destabilizing forces and moments.

In [Hirose et al., 2001] normalized energy stability margin was proposed as the difference between the initial position of the center of gravity and its highest position in the process of tumbling.

$$S_{NESM} = \frac{S_{ESM}}{mg} = \min_{i=1}^{n_s}(h_i) \tag{2.5}$$

Here, n_s is number of edges of the support polygon, and h_i is the elevation of height of the CoM during tip-over. In Garcia and De Santos [2005] this concept was extended to walking machines considering leg dynamic effect an a disturbance. It was stated that, a walking machine is dynamically stable if every moment M_i around the edge i of the support polygon due to robot/ground forces moments is positive. Positive direction

was the clockwise direction of the force around the support polygon. Energy stability level for all the edges was calculated as a *difference of potential and kinetic energy*. Thus, the **normalised energy stability margin** (S_{NEDSM}) was defined as:

$$S_{NEDSM} = \frac{min(E_i)}{mg} \tag{2.6}$$

2.2.4 Moment based criteria

Dynamic stability margin was proposed in [Lin and Song, 1993] as the smallest of all moments M_i around the edges of the support polygon. This margin considered robot/ground interaction forces and was normalized by the weight of the system.

$$S_{DSM} = \min_{i=1}^{n} \frac{\boldsymbol{e_i}.\left(F_R \times \boldsymbol{P_i} + M_R\right)}{mg} \tag{2.7}$$

[Yoneda and Hirose, 1996] presented tumble stability criterion and introduced counter-force limit as an index to indicate manipulation capabilities. Concept of stability is based on ability of virtually lost wheel-ground contact points to generate support force required to suppress tumbling. Mathematical expression to calculate this margin is:

$$Tumble\ \ stability\ \ margin = \frac{min\left|\bar{M}.\frac{(p_a - p_b)}{|p_a - p_b|} + \bar{F}.\frac{(p_b \times p_a)}{|p_a - p_b|}\right|}{mg} \tag{2.8}$$

Here, $\bar{M}$ and $\bar{F}$ are net moment and force acting at CG, p_a and p_b are adjacent ground contact points that define axis of rotation.

[Sugano et al., 1993] was one of the initial works to introduce ZMP (zero moment point) as a stability criteria for mobile manipulators. It was identified that the stability of a mobile manipulator is closely related to motion of the mobile base, posture and motion of the on board manipulator and external forces on the end-effector. Based on ZMP, two concepts named *stability degree* and *valid stable region* are proposed. The former defined the stable limit while the later was used to discuss influence of disturbances in the task environment.

In this paper, support polygon of the mobile manipulator system was called *stable region*. A maximal stability curve (which is a straight line) was identified inside the stable region such that, stability is highest when ZMP lies on this curve. To ensure safety of the mobile manipulator under the influence of external forces or environmental disturbances, a valid stable region was defined such that, if ZMP lies within this region, stability is ensured. i.e ZMP lies within stable region (support polygon) after being displaced.

In [Moosavian and Alipour, 2006, 2007] Moment Height Tip-over Measure (MHS) was proposed. This index was proved to be computationally less expensive than energy and force based margins. The resultant of force and moments exerted by manipulator on the mobile base was calculated. Then the moment of this resultant about corner points of the support polygon was found. These moments were then projected on the respective edges of the support polygon. To make the criterion sensitive for the height of the COM, a multiplicative term h_{cm} was added to the MHS. In order to calculate the MHS, requirements are: all joint angles, velocities and accelerations of on board manipulator, linear and angular accelerations of mobile base, knowledge of external forces and torques exerted on the system.

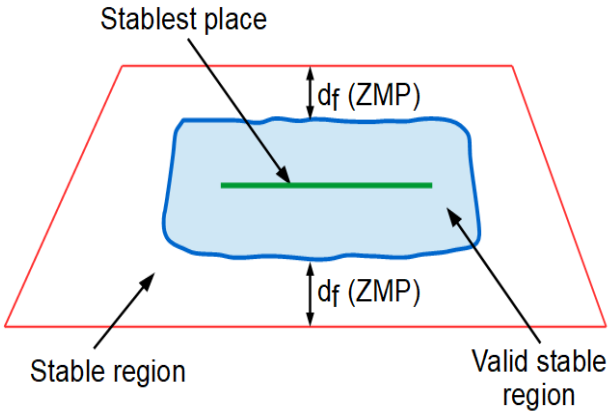

Figure 2.12: Concept of stable and valid stable region [Sugano et al., 1993]

MHS measure α is computed in 2.9,

$$\alpha = \min_{i}(\alpha_i) \quad i = \{1, 2, 3, 4...\} \tag{2.9}$$

Here, α_i denotes dynamic MHS measure about i^{th} edge which is given as,

$$\alpha_i = (I_i)^{\sigma} M_i \tag{2.10}$$

Here, I_i is the moment of inertia of mobile base about i^{th} axis, M_i is moment about i^{th} axis and $\sigma = 1$ if $M_i > 0$ else -1.

[Roan et al., 2010] presented a real-world validation of three tipover algorithms: Zero-Moment point (ZMP), Force-Angle stability measure (FA) and Moment-Height Stability (MHS). A scoring scheme was implemented to record value of criteria at actual time of tipover, to record lag/lead of criteria and to count false positives. FA and MHS are found to be quite identical except for negative values.

[Lee et al., 2009] proposed concept of a modified zero moment point for evaluating tip-over of mobile robots over uneven terrain. The turnover stability index for linear acceleration and rotational velocity are defined with the modified ZMP. The turnover stability space (TSS) with turnover stability indices is presented to control the mobile robot in order to avoid turnover effectively.

2.2.5 Force based criteria

[Mahdi and Nestinger, 2012] proposed a foot force criterion as an attempt to provide a quantitative measure to determine how far away the robot is from either instability or from maximum stable pose. Mathematically foot force stability criterion is expressed as

$$FFSM = \frac{f_1 f_2 .... f_n}{\bar{f}^n} \qquad 0 \leq FFSM \leq 1 \tag{2.11}$$

Here, n is the number of supporting legs with strictly positive foot force, f_i is the magnitude of i^{th} normal foot force and $\bar{f} = \frac{1}{n}\sum_{1=1}^{n} f_i$. Important feature of the stability margins that are based on foot forces is all the effects of gravity, external forces, inertial forces and disturbances are reflected in in foot forces [Papadopoulos and Poulakakis, 2000].

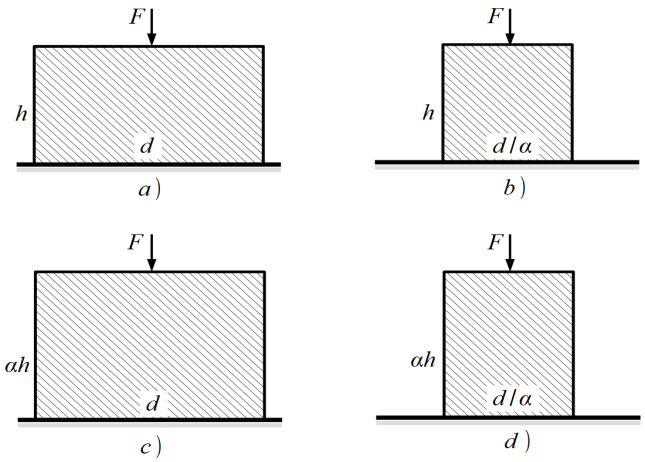

Figure 2.13: Effect of top-heaviness on stability [Mahdi and Nestinger, 2012]

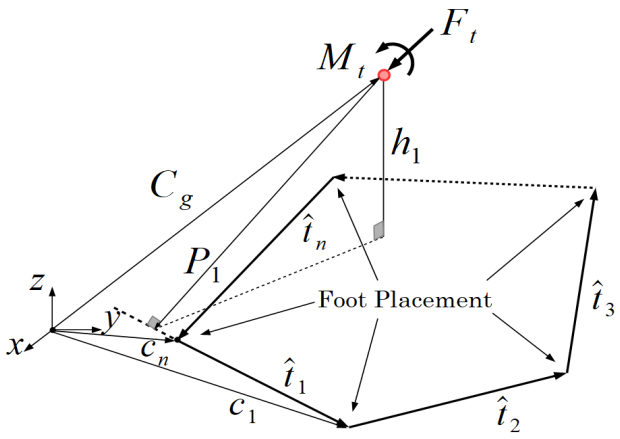

Figure 2.14: Schematic of general n-legged robot [Mahdi and Nestinger, 2012]

Figure 2.13 presents cross-sections of four different mobile bases with different aspect ratios. Considering lateral disturbances, these systems differ in terms of tip-over potential: Figure 2.13a) has the highest while 2.13d) has the lowest geometric tip-over potential. Depending on the magnitude of the force F, the potential changes for all cases. This is defined as a sensitivity to top-heaviness.

Modified foot force stability margin is given by following equation:

$$MFFSM = FFSM.\ \frac{(P_i)^j}{h_i}.f \tag{2.12}$$

Here, $j = 1$ if projection of CG is inside support polygon else, 1. h_i is height of the CG with respect to tip over axis and P_i is tip-over axis normal as shown in figure 2.14.

[Ding et al., 2019] presented an improved tip-over moment stability criterion taking into account wheel-ground and vehicle-manipulator interaction. Based on this criterion a real-time tip-over avoidance algorithm was proposed to minimize the tip-over moment transfer. It used two sets of corrective actions: adjusting the posture of the onboard manipulator or changing the running velocity of the vehicle.

Table 2.3: Stability margins: merits and limitations - I

Stability Margin	**Definition**	**Merits**	**Limitations**
Static stability margin [McGhee and Frank, 1968]	minimum distance between proj. of CG and support polygon	easy to compute	no consideration for reactions forces, dynamics absent
Dynamic stability margin [Sreenivasan, 1994]	minimum distance between net force vector and support polygon	consideration for forces	can't handle angular loads
Force angle stability margin (FASM) [Papadopoulos and Rey, 1996]	minimum of the angles between the net force vector and tip-over axis normal	easy calculation and sensitivity to top-heaviness	hard to use on uneven terrains
Stability Measure [Diaz-Calderon and Kelly, 2005]	angle between tip-over axis normal and resultant force	computation independent of altitude	dynamics absent
Energy Stability Margin [Messuri and Klein, 1985]	minimum of the energy stability levels of all support edges	effective, considers CG height	dynamics absent
Dynamic energy stability margin [Ghasempoor and Sepehri, 1995]	minimum of the differences in the work done by stabilizing and tumbling forces around all edges	includes top-heaviness, works on uneven terrains	all the external forces are considered to work on the CG
Normalized Energy Stability Margin [Hirose et al., 2001]	difference between initial and highest position of CG in the process of tumbling	easy computation	external forces are not included
New normalized Energy Stability Margin [Garcia and De Santos, 2005]	minimum of the energy levels of all edges of the support polygon	accurate measurement of stability among all ESMs	-

Table 2.4: Stability margins: merits and limitations - II

Stability Margin	Definition	Merits	Limitations
Foot force stability margin (FFSM) [Mahdi and Nestinger, 2012]	product of all normal forces normalized by the sum	all types forces are reflected in the margin	sensors are needed to estimate normal forces
Dynamic stability margin [Lin and Song, 1993]	smallest of all moments around the edges of the support polygon	easy to compute, considers ground interaction forces	performance and accuracy of the index are not demonstrated
ZMP based margin [Sugano et al., 1993]	minimum distance of the projection of ZMP from support polygon	real-time control, inertial forces are considered	computationally lengthy
Tumble stability criterion [Yoneda and Hirose, 1996]	absolute value of the moment divided by weight of the robot which generates around the line to avoid tumbling	can be used for irregular terrain	sensitivity to top-heaviness is not highlighted
Moment height tip-over measure [Moosavian and Alipour, 2006]	minimum product of moment of inertia and moment of all edges	computationally less expensive, sensitive to top-heaviness	-
Modified ZMP [Lee et al., 2009]	ZMP is modified to present constraints of linear acceleration and rotational velocity	enables mobile robot to prevent turning over	not applicable to different wheel types
Improved tip-over stability margin [Ding et al., 2019]	minimum of the tip-over moments of all edges	greater sensitivity to COM, smaller computations cost, and better real-time performance	not applicable to legged robot

2.3 Related research

Stability margins discussed in previous sections have formed a basis for research and development of top-heavy mobile manipulators. Several research works incorporating dynamic stability analysis of dynamic capabilities, algorithms for planning and control models are presented below.

2.3.1 Dynamic modeling and stability analysis

[Lin and Song, 1993] derived a dynamic model to study stability and energy efficiency of a quadrupedal walking machine. To perform dynamic stability analysis, the margin of stability used was the '*minimum resultant moment along boundaries of the supporting polygon normalized by the weight*'. Concept of specific resistance, defined as ratio of input power to the weight times velocity of the system, was used to determine energy efficiency. Stability analysis of the internal dynamics of mobile robot was demonstrated in [Yun and Yamamoto, 1997]. Authors claimed that since control model of the mobile manipulators doesn't include internal dynamics, its stability properties are neglected. Using Lyapunov function, it was shown that the internal dynamics of a two-wheel differential-drive mobile robot are unstable when commanded to move backwards.

In [Abo-Shanab and Sepehri, 2001], a method to analyze stability of the mobile platforms was proposed. This study considered *no impact* and *impact* phase of the mobile manipulator to assess stability. Dynamic model for both the cases were developed in order to separately analyze the behavior of the mobile manipulator. An equation to compute change in the joint velocities of the manipulator after impact with the ground was calculated. This model helped in predicting tip-over behavior of the base.

[Hatano and Obara, 2003] presented a new method for stability evaluation and a stabilization control based on reaction forces. Equations of motion were derived for three conditions namely: both edge contact, front or rear edge contact and the unconstrained model. Conditions for stable and unstable poses based on ground reaction forces were proposed. The control strategy proposed used a compensatory motion of the arm to regain the stability of the manipulator from a transition phase.

[Abo-Shanab and Sepehri, 2005] considered friction efforts while building dynamic modeling of the tip-over stability. They showed that, not considering friction efforts underestimates stability. Later, effect of variation of wheel-ground friction efforts on the dynamic tip over stability was studied. [Meghdari et al., 2006] developed an approach for achieving optimal stability using redundancy. Position, angular velocity and angular acceleration of the redundant link was formulated while end-effector and base trajectories were performed. Optimization problem was solved by the method of Genetic Algorithm (GA) such that ground reaction forces on wheels of the base are equalized.

Analysis of rollover stability margin was performed in [Peters and Iagnemma, 2006] for accuracy. They showed that factors like sensor placement, wheel dynamics and position estimation error of CG have significant effect on stability. [Lenain et al., 2007] made the dynamic analysis of an ATV (all terrain vehicle). Multibody model of a quad bike was made in ADAMS software. It was shown that sliding increased the dynamic stability of the ATVs. [Norouzi et al., 2013] demonstrated a statistical approach for uncertain stability analysis of mobile robots. Probability density function was assigned to the contact-points. Force angle stability margin and CG criteria were evaluated.

[Moosavian et al., 2007] proposed dynamics modeling of suspended wheeled mobile robots with multiple arms for tip-over stability. A general systematic process for developing dynamic model was presented based on Newton-Euler recursive formulation.

This approach was capable of determining the reaction wrench between the arm/dual arms and the mobile base. Authors also developed another dynamic model in ADAMS software to validate the analytical model. Later, the dynamic tip-over Moment Height Stability (MHS) measure was modified for suspended wheel. Effect of base compliance on the stability was studied by presenting simulations of two cases. It was shown that, *low stiffness coefficient yields into low stability of the system*.

In [Alipour et al., 2014] a real-time intelligent tip-over algorithm was proposed by taking into consideration, arm-base dynamic interactions. Moment height stability margin (MHS) was used to predict the tip-over. Once identified, tip-over prevention algorithm was activated to improve stability of the system. To achieve this, efficient system variable and their effect on system stability was determined through the concept of **Stability Margin Metric Increment Function** (SMMIF) as:

$$\Delta\hat{\alpha} = \sum_{i=}^{n} k_{q_i}(\Delta q_i) + \sum_{i=}^{n} k_{\dot{q}_i}(\Delta\dot{q}) + \sum_{i=}^{n} k_{\ddot{q}_i}(\Delta\ddot{q}) \tag{2.13}$$

where, $\hat{\alpha}$ in normalized MHS and $q = [q_1, q_2, ..., q_n]^T$ is vector of system generalized coordinates.

A fuzzy logic planner was then implemented to identify a primary motion variable. This motion variable was then given as a feedback into the robot controller as a new reference signal to be tracked. This approach was compared with the one presented in [Rey and Papadopoulos, 1997] and shown to be more efficient.

[Alipour et al., 2017] investigated capability of wheeled mobile manipulators for carrying heavy objects under the constraint of dynamic stability. Maximum mass manipulation problem was formulated in the form of Bolza problem of optimal control.

Figure 2.15: Mobile manipulator used for fuselage riveting [Guo et al., 2017]

[Guo et al., 2017] presented a method for tip-Over stability analysis of a wheeled mobile manipulator where Newton-Euler recursive formulation was applied to formulate reaction forces and moments exerted onto the mobile platform. Tip-over moment (TOM) criteria was derived to judge stability of the system. To compute this criterion, moment generated by the wrench vector (consisting of moments and forces on each joint of the manipulator) and gravity vector were computed along all tip-over axes, defined by any pair of two successive wheel-ground contact points. The maximum of all the moments was taken as the critical value which if comes out to be positive indicates tip-over. To perform stability analysis, three cases of force, one case of static loading condition

and two other cases including inertial forces generated due to motion of the arm were studied.

2.3.2 Motion planning and control

This section mainly focuses on the literature about motion planning, considering stability as a constraint while exploiting redundancy of the system to achieve the task.

In [Dubowsky and Vance, 1989], a planning method was proposed to permit efficient manipulator tasks whilenot compromising the dynamic stability of the overall system. This method incorporated constraints of forces and moments acting on the mobile base as well as constraints of joint actuators to plan manipulator motion such that the system is not destabilized. A path planning problem for a mobile manipulator performing sequence of tasks specified by locations and minimum force capabilities was studied in [Zhao et al., 1992]. Optimal sequencing of base positions and manipulator configurations was achieved through genetic algorithm. [Yamamoto and Yun, 1994] presented planning and control algorithm for coordinating locomotion and manipulation of the mobile manipulator. For energy efficient task execution and accuracy in end-effector positioning, platform must have a configuration that allows to achieve desired manipulability.

[Huang et al., 1994] demonstrated stability control using a potential field method. ZMP path planning was implemented to increase the degree of stability though concepts of goal state and prohibitive state. This included computing ZMP trajectory during vehicle motion, finding corrected ZMP trajectory for stability recovery using potential method and executing compensatory motion to recover the stability. This work was continued in [Huang et al., 1998] where stability compensation through static posture change was proposed. The feasibility of the mobile manipulator to compensate stability was studied and motion was planned using redundancy in the system. [Foulon et al., 1999] demonstrated a method of coordinating mobility and manipulation for nonholomic mobile manipulators executing complex tasks. A unified approach to motion control was developed by [Seraji, 1998]. Non-holonomy of the base and kinematic redundancy were treated in uniform manner to formulate task constraints. [Yamamoto and Yun, 1999] derived a kinematic and dynamic task space ellipsoids taking into account mobility and manipulation. Task execution was visualized through contribution of manipulator mobility and arm manipulability using these ellipsoids.

[Huang et al., 2000] studied motion of the mobile manipulator having small-sized platform. Manipulability and stability were simultaneously considered while coordinating vehicle and manipulator motions. This paper presented a concept of valid stable region to evaluate stability in the presence of disturbances followed by a method of planning motion of the mobile base.

Valid stable region was computed using following equations:

$$d_f(x_{zmp}) = \frac{\sum_{i=1}^{n} S_{zj}F_{xj} - S_{xj}F_{zj}}{\sum_{i=1}^{n} m_i(\ddot{z}_i + g) - \sum_{i=1}^{n} F_{zj}} \tag{2.14a}$$

$$d_f(y_{zmp}) = \frac{\sum_{i=1}^{n} S_{zj}F_{yj} - S_{yj}F_{zj}}{\sum_{i=1}^{n} m_i(\ddot{z}_i + g) - \sum_{i=1}^{n} F_{zj}} \tag{2.14b}$$

where 'j' represents force applied on the system, (S_{xj}, S_{yj}, S_{zj}) denote coordinates of the point of application of force.

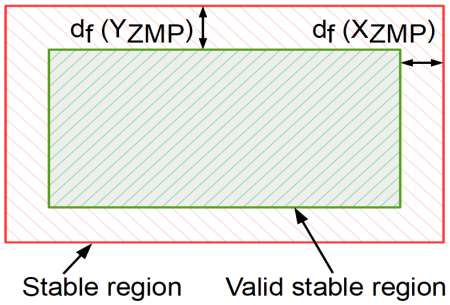

Figure 2.16: Concept of stable and valid stable region [Huang et al., 2000]

Similar to the concept in [Sugano et al., 1993], if ZMP lies in the green region-valid stable region, mobile manipulator will not tip-over due to disturbances and vice a versa. Thus is the region of dynamic stability. Here, red colored rectangle is the support polygon of the mobile base which also guarantees static stability.

A platform independent control approach for mobile manipulation and coordinated trajectory following was proposed in [Egerstedt and Hu, 2000]. While planning path of the end-effector, path of the base was planned in order to keep manipulability feasible. [Nagatani et al., 2002] proposed that implementation of a unified controller (locomotion and manipulation) was difficult due to difference in the characteristics of actuators. Thus, two controllers are kept separate and a coordinated motion is planned through their communication. The approach was to control the desired manipulability by adjusting the base pose. [Kim et al., 2002] proposed that offline planning is inefficient in overcoming disturbances and unexpected situations, hence highlighting the need of robust online approach. ZMP was derived using iterative Newton-Euler method to make it computationally efficient. Method of null-space control of redundant manipulators was used for implementing unified control approach. [Furuno et al., 2003] demonstrated trajectory planning with stability considerations using ZMP as a criterion. Trajectory planning problem was formulated as an optimal control problem. It was solved using a hierarchical gradient method which synthesizes the gradient function in a hierarchical manner based on the order of priority.

[Bayle et al., 2003] extended concept of manipulability of fixed based manipulators to the wheeled mobile manipulator. Initially, a generalized *instantaneous kinematic configuration model* (IKCM) of the mobile manipulator was derived. Then after an operational motion planning problem was defined to derive mobility control equation. Redundancy of the system was exploited to achieve internal motion by optimizing mobile manipulator manipulability measure which can be further useful for optimal positioning of the robotic arm, design of the system etc.

Optimization based path planning was developed in [Berenson et al., 2008] for pick and place tasks. Co-evolutionary algorithm was used to find optimal robot configurations. A path from initial to goal state was planned using rapidly-exploring random trees (RRTs). [Alipour and Moosavian, 2015] proposed a motion planning for heavy object manipulation considering dynamic stability. An initial and final pose of the payload with respect to the base and respective configurations of the arm were selected. This arm motion was planned by solving inverse kinematics and without considering stability of the system. Motion of the base was then planned to fulfill stability requirements.

2.3.3 Optimal positioning

This deals with finding a suitable placement for mobile base so as to result in safe and efficient task operation.

[Seraji, 1994] addressed the problem of base placement for mobile robots using reachability analysis. The goal was to automate base placement relieving operator from a tedious and repetitive process. A geometric solution was proposed to reach a vertical line, a square and a cube shape and was validated by two experimental studies: surface scanning and reaching inside an opening. In [Chen and Zalzala, 1997], multi-criteria motion planning was demonstrated using genetic algorithm approach. For position and configuration optimization constraints used were: least torque norm, manipulability, torque distribution and obstacle avoidance.

A new approach for optimal base placement and motion planning was proposed by [Du et al., 2012] using improved rapidly-exploring random tree (RRT) algorithm. Relative manipulability index (RMI) was proposed for this purpose, which was maximized based on joint self-motion using redundancy. Global manipulability map was plotted to analyze capabilities in the workspace. [Dharmawan et al., 2016] used expanded Lagrangian homotopy for simultaneous base placement and motion planning. Constrained optimization problem was formulated based on manipulability and kinematics which was soled by Newton-Raphson method.

Conclusions

This chapter presents literature review in the context of the topic of this dissertation, that is, 'the use of mobile manipulator for asbestos removal operation'. Important conclusions coming out of the review work are presented below.

In the literature, dynamic modeling of mobile manipulator system was mostly performed numerically. Various models took into account redundancies of the mobile manipulator system, elements like suspension system, internal dynamics in the system etc. Numerical models used Newton-Euler recursive method to compute join-velocities and joint accelerations. Factors like frictional force between wall-ground contact and wheel stiffness were also addressed to investigate their effect on the stability. This provided a detailed knowledge on the essential aspects to consider while developing the dynamic model.

A the application of asbestos removal demands mobile manipulator to operate dynamically, an appropriate stability margin must be integrated within the dynamic model. Review of stability margins is performed through the classification based on the parameter (distance, angle and energy) used to evaluated the margin. Some works evaluated accuracy and efficiency of margins to determine suitability in online planning applications. Approaches like defining valid stable regions, and statistical method for incorporating errors in CG estimation attempted to deal with uncertainties and disturbances. Asbestos removal requires robust stability margin that can also be used in the planning and control loop. After carefully reviewing stability margins, ZMP (zero moment point) is found as a suitable choice for the application under study. Zero moment point considers inertia forces, height of center of masses of the individual and capability of incorporating external forces. ZMP can also represent static margin if acceleration terms are zero. Thus, it will be used as a stability margin in this work.

To achieve efficient operation of the mobile manipulator, optimal motion of the arm as well as positioning of the base is necessary. Such problems were solved under con-

straints of joint torques, stability, obstacle avoidance. Control of mobile robots and walking machines for stability involved techniques like compensatory motion of the arm or base using redundancy, real time control using potential field, optimization of stability to determine amount of load to be carried out etc. To solve optimization problem methods like genetic algorithm, hierarchical gradient function, co-evolutionary algorithm etc. were used. Offline planning was suggested to be inefficient and hence online path planning was implemented using stability margins, fuzzy logic controllers and Lagrangian homotopy.

Chapter 3

Selection of suitable arm kinematics

Contents

This chapter presents a methodology for structural selection of the arm kinematics to be integrated with the robotic unit. The challenge in satisfying these requirements is overcoming constraints imposed by the interaction of the system with real world. All such requirements and constraints are taken into account for the synthesis of the arm architecture and dimensions. Workspace of the kinematics is analyzed to show the effectiveness of the methodology.

3.1 Asbestos removal use case

This section presents general process of asbestos removal and expectations from the robotic with customer's point of view. As described earlier, the robotic system is intended to be used in real world rehabilitation sites. Thus, an appropriate understanding of the cleaning environment as well as the restrictions put by the environment on the design of the robotic system is necessary.

3.1.1 Cleaning environment

The real world rehabilitation sites consists of rooms and corridors. Wall, ceiling, skirting and ground are the types of surfaces (figure 3.1) that must be cleaned. This order corresponds to the amount of area constituted by the surfaces in the cleaning environment. The ceiling has a height between 2.1 m and 3 m. The wall can have leaning angle of 0°-45° with the ground and radius between 1.5 m and 2.5 m.

3.1.2 Grinding process

Process of asbestos removal will be performed by grinding operation. This involves removing mixtures like plastering, spattling compound, glue and paint. Thus, the robotic system must be equipped with a suitable tool capable of performing the removal operation at a desired rate.

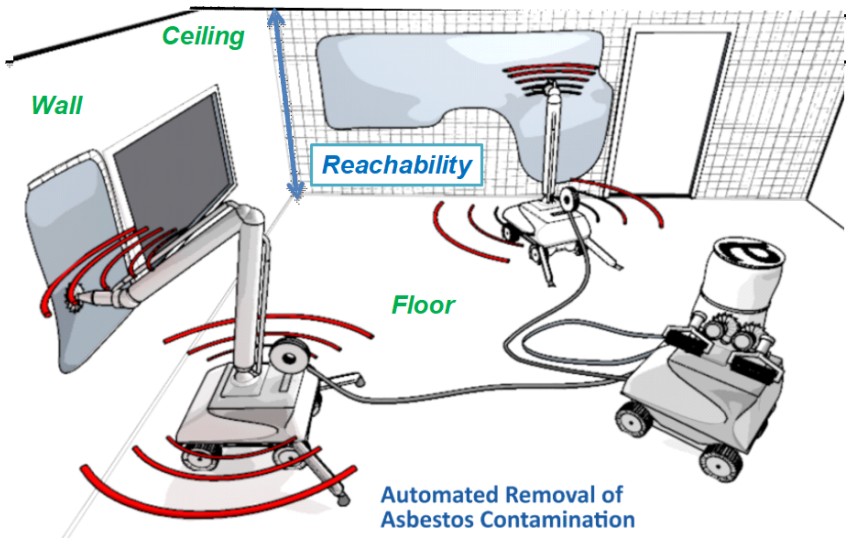

Figure 3.1: Requirements of Asbestos removal Process [Bots2ReC, 2016]

3.1.3 Safety

In order to ensure safe operation, the robotic system must be stable (statically and dynamically) while performing removal operation. Collision avoidance is another critical aspect of the safety process. Collisions are of several types: arm-environment, arm-mobile base, mobile base-environment.

The environment to be cleaned is secluded in order to avoid asbestos contamination being spit in outside atmosphere. While cleaning wall and ceiling surface, ground must be protected by plastic foil.

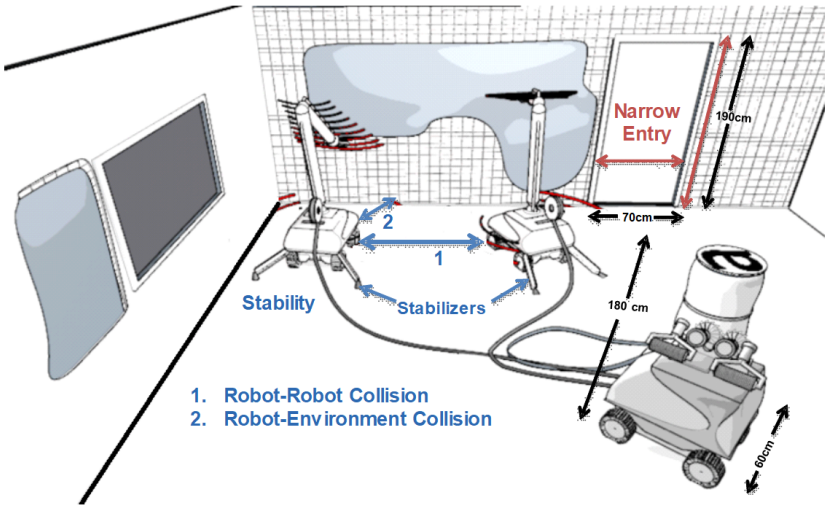

Figure 3.2: Requirements of Asbestos removal Process [Bots2ReC, 2016]

3.1.4 Navigation

Since rehabilitation sites can be located at higher stories, robotic unit would be carried through lifts to reach the targeted cleaning location. Thus, robotic unit must be able to fit within the dimensions of the lift. Reformulation : The robotic unit can also have maneuvering problems in narrow corridors. Consequently, it needs to have compact dimensions. Entry of the robotic unit into the cleaning site is facilitated through doors of dimension (80cm $\times$ 100cm) and robotic unit must fit through this.

3.1.5 Productivity

One of the main objectives of Bots2ReC project is to have a cleaning productivity better than that achieved by the human operators. Since the robotic system can work relentlessly, the target while designing the automatized operational process is to have a system that can do the job in the shortest possible time. Thus, to have optimal grinding speed design of the system must be robust.

3.2 Structural synthesis method

This section presents a methodology for synthesis of a suitable arm kinematics that was adapted from [Fauroux, 2015]. Figure 3.4 shows a the flowchart of the synthesis process that is explained below.

- **Complete design space:** It is the complete design space of 'n' dimensions presented by a sphere (top-left corner of figure 3.4) where the principal axes the space are features. The complete product is defined in this space, that is complex to represent.

- **Simplified design space:** The simplified design space has 's' dimensions such that $s < n$. In this space is defined a simplified representation of the product called "product skeleton" and integrating its main features.

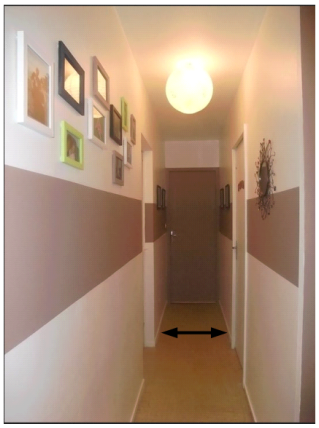

(a) Narrow corridors inside the site

(b) Limited dimensions of lift

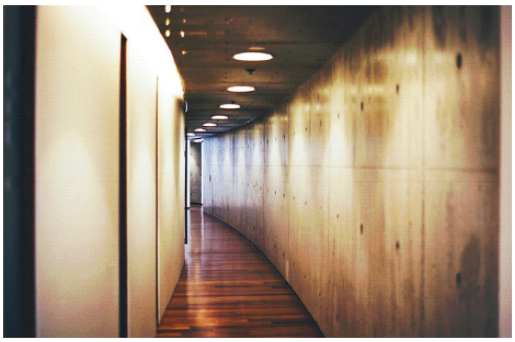

(c) Curved narrow corridor

Figure 3.3: Critical points inside rehabilitation sites

– **Design Rules:** Denoted by DR_i, they are abstract description of the expected behavior of the product. Specifications extracted from the requirements also a constitute pool of design rules. They serve as a starting point for reasoning. Design rules are created from inferences from premises supposed to be true. They can be inferred from external statements (denoted by ST_i) or even from other design rules. External information source, such as the knowledge-base or the experience of specialist design can contribute additional design rules (denoted DR^K_i) useful for the synthesis process. Design rules can lead to multiple choices out of which designer can select one based on simplicity or intuition. In case of dead-end, the method permits roll back to a suitable branching.

– **Skeleton features**: As design rules become explicit after certain level of inferencing, they can be embodied into skeleton features (denoted by FS_i). Skeleton features are general features of the skeleton that can be declined into more detailed product features when going back to the complete design space. For example, if a skeleton feature FS_1 consists in using a wheel, the detailed product features F_i to be defined when going back to the complete design space could be the wheel dimensions (rim diameter, wheel diameter, tire width), tire material, tire sculpture shape, reinforcement armature geometry, etc. This example also shows that preliminary synthesis must focus on a limited set of main features in order to keep a clear view of the objective. This is why a product skeleton is so useful.

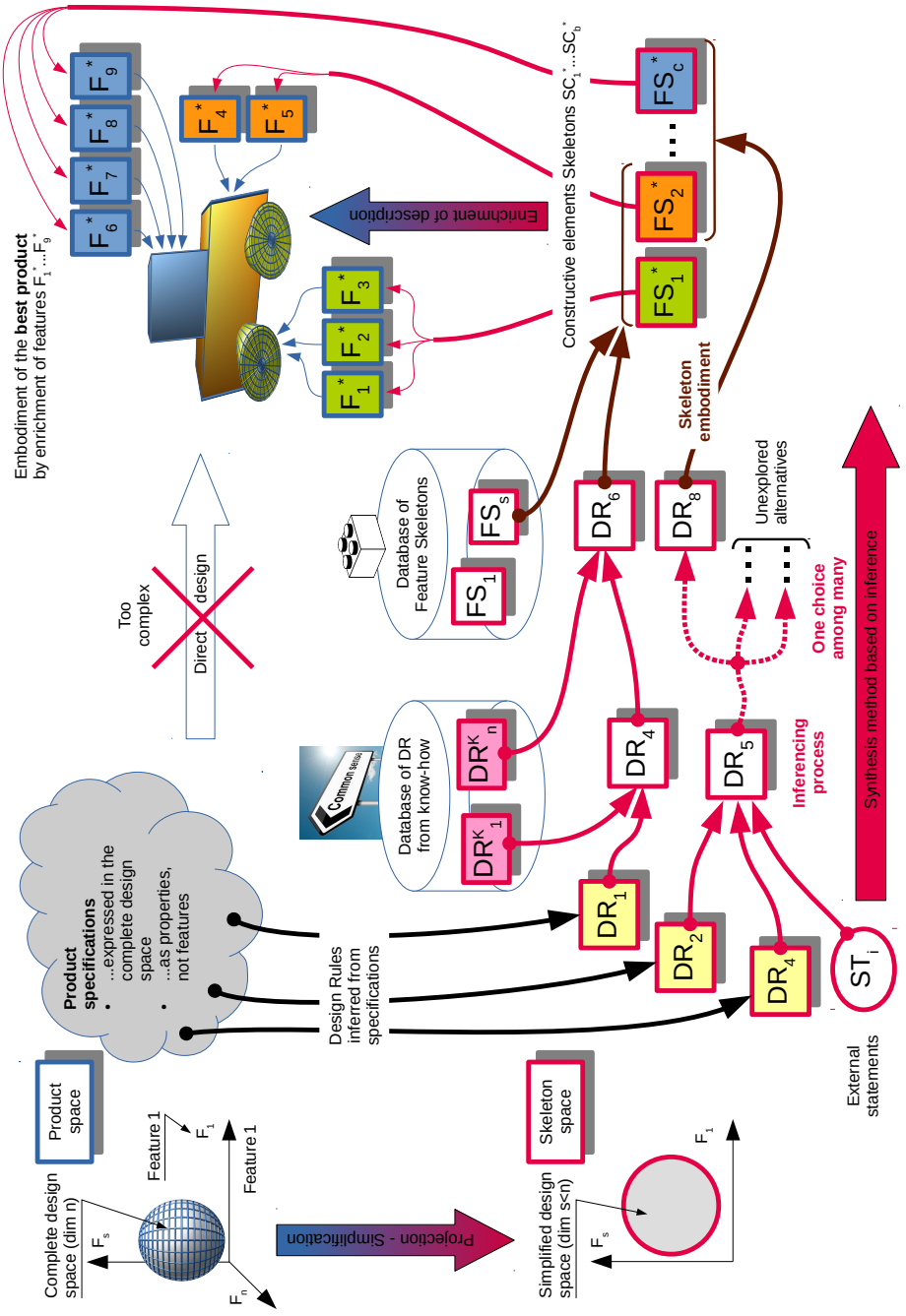

Figure 3.4: Synthesis based on inference of design rules [Fauroux, 2015]

Table 3.1: General requirements of asbestos removal use case

Type of requirement	Requirement name	Requirement formulation
Environment	Type of surfaces **(REQ_Surf)**	The surface to clean is a part of wall or ceiling or skirting-ground
	Reach **(REQ_Reach)**	The ceiling height is between 2.1 m and 3 m, wall leaning angle is $0^0/90^0$ with the ground and wall radius is between 1.5 m and 2.5 m (e.g spiral staircase walls)
Grinding process	Material **(REQ_mat)**	Ceramic tiles, glue and mixtures like plastering, spattling compound and paint
	Operation **(REQ_op)**	Grinding or scarification process will be used.
Safety	Stability **(REQ_stab)**	Static and dynamic stability is maintained within permissible limit.
	Collision avoidance **(REQ_noncollision)**	Operation of the robotic unit is free from collisions: Arm-Environment, Arm-Mobile base, Mobile base-Environment
	Contamination avoidance **(REQ_cont)**	Robotic unit must operate on ground protection plastic of thickness 150 μm without tearing
Navigation	Transport through elevators **(REQ_elevt)**	Robotic unit must fit into the elevator of dimensions 1 m$\times$0.8 m$\times$2 m
	Entry into sites **(REQ_entry)**	Robotic unit must fit through an entrance of dimensions 1 m$\times$0.7 m$\times$1.8 m
	Working and turning through narrow corridors **(REQ_corridor)**	Robotic unit must be able to operate and navigate through corridors of 0.7 m in width
Productivity	Optimal grinding parameters **(REQ_param)**	Robotic arm must operate at optimal feed, translational velocity etc.

3.3 Design rules

In order to satisfy each general requirement posed by the process of asbestos removal we generate a design rule. Design rules are constraints taken from engineering practices (know-how) or inferred from requirements. Table 3.1 summarizes general requirements and set of technical specifications.

- *Degrees of freedom: DR_DoF*
  Depending on the type of surfaces that are identified, task environment of asbestos cleaning is 5-dof in nature. Thus, to access all surfaces, the robotic arm must be able to provide 5-degrees of freedom which are three translations and two rotations (yaw and pitch).
- *Reachability: DR_Reach:*
  To reach the ceiling height as well as ground and skirting area, robotic arm must have suitable link lengths. This is achieved by dimensional synthesis that includes reachability analysis.
- *Grinding parametres DR_Param:*
  Materials to be ground require sufficient normal (upto 80N) grinding forces in order to perform the operation effectively. Thus, robotic arm must be equipped with suitable motors to generate a required tool force.
- *Stability DR_stab:*
  To satisfy the requirement of stability, robotic unit must satisfy static and dynamic stability margin throughout the process.
- *Collision avoidance DR_non_collision*
  To achieve collision free safe operation dimensional synthesis of link lengths must consider the constraint of self-collisions as well as well as collision with environment.
- *Mass: DR_Mass*
  Overall mass of the robotic unit is constrained by weight limit of the elevators as well as pressure handling capacity of the plastic sheets used to avoid ground surface from getting contaminated.
- *Navigation: DR_Nav*
  Robotic unit must follow dimensions of the entry points (doors) and other entry points like elevators.
- *Productivity: DR_Continuous_Trajectory* In order to ensure uninterrupted operation, a robotic arm must be able to execute continuous trajectories while performing grinding operation.

3.3.1 Design Features

Table 3.2 presents design rules inferred from requirements and design features to satisfy those design rules.

- *DF_Kinem*: To achieve the required degrees of freedom identified by DR_DoF, a suitable kinematics e.g classical anthropomorphic arm, must be adopted.

– *DF_LinkLengths*: To reach the required ceiling height, dimensional synthesis of the arm must include reachability analysis of the ceiling as suggested by DR_Reach. However, DR_Stab and DR_NonCollision tend to put restrictions on the link lengths. For constraints, shorter the link lengths, better the stability and collision avoidance. DR_Param identifies relation between link lengths and torques. With larger link lengths, torque requirements are higher. Thus, DF_LinkLength is associated with 4 design rules - DR_Reach, DR_Stab, DR_NonCollision and DR_Param.

– *DF_Dim*: Overall dimensions of the robotic unit must comply with the constraints put by DR_Dim on the length<(0.8 m), width<(0.6 m), and height (1.8 m).

3.3.2 Dimensional synthesis of the arm

For the dimensional synthesis of the robotic arm, a skeleton modeling approach is used through which, links are represented by lines and joints are reduced to points and/or motion axes [5,11]. Interactive geometric software (IGS) - **Geogebra** is used for this purpose. Geogebra allows construction of 2D and 3D graphics using simple geometric shapes. This feature is used to represent asbestos removal scenario.

Initial iteration

Using an existing commercial anthopomorphic arm with two segments doesn't satisfy the design rule DR_Mass was found because commercial arms+control box are too heavy. Thus, an in-house arm synthesis is adopted. A classical anthropomorphic kinematics '**Base-Shoulder-Elbow-wrist**' is chosen for an initial assessment of asbestos removal use case.

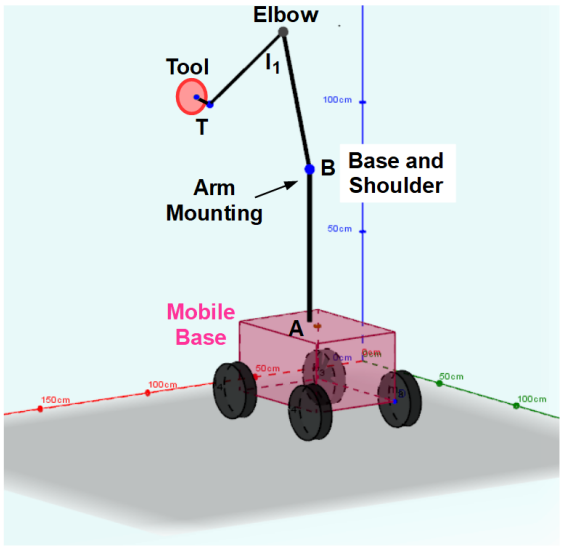

Figure 3.5: Geogebra model of the robotic unit

Base placement is the distance of the Robotic unit frame from the wall.

Base placement and link lengths

It is evident that base placement and link lengths are in direct relation. Thus, the following Design Rules will be used for converging to proper dimensions :

Table 3.2: Generation of design rules from design requirements

General requirement	Design rule	Design feature satisfying the design rule
Type of surfaces **REQ_Surf**	**Degrees of freedom:** Enough degrees of freedom are required reach aimed surfaces **DR_DoF**	Kinematic architecture that generates 3 translations and 2 rotations of the end-effector
Geometry **REQ_Reach**	**Reachability:** Sufficient link lengths to reach ceiling height in non-singular configuration **DR_Reach**	Dimensional synthesis considering reachability analysis
Asbestos removal process **REQ_Proc**	**Grinding parameters:** Apply enough cutting wrench (Normal and lateral force, cutting torque, feed, speed) **DR_Param**	Motors to generate joint torques (addition of mass)
Stability **REQ_Stab**	**Stability margin:** Satisfy stability margins for entire operation **DR_Stab**	Short link lengths for better stability **(Constraint)**
Collision avoidance **REQ_Noncollision**	**Collision constraint:** Link lengths must be designed for avoiding self collisions as well as with environment **DR_NonCollision**	Short link lengths for better collision avoidance **(Constraint)**
Contamination avoidance **REQ_Contm**	**Mass pressure:** To protect plastic sheets from getting damaged, mass pressure at the ground should be $< 300\ kg/m^2$ **DR_Mass**	Less overall mass for protecting plastic **(Constraint)**
Navigation **REQ_Nav**	Respect dimensions of elavators, doors and narrow corridors **DR_Dim**	Compact overall dimensions (Width <0.6 m, Length <0.8 m, Height <1.8 m) **(Constraint)**
Productivity **REQ_Prod**	**Cleaning time:** Robotic unit must perform the task in minimum possible time **DR_time**	Continuous trajectory with optimal feed and acceleration.

- *DR_Link_Dynam*: Dyanmic effects in the link We set down four new design rules to establish the relation between link lengths, mass, inertia and torque:
  - *DR_Length_Mass*: Longer link lengths add more mass in the system. Thus, joint torque required are higher which also adds mass of the motors used.
  - *DR_Length_Inertia*: Longer link lengths increase overall dimensions of the robotic unit and may exceed the criteria of being able to fold within maximum

Figure 3.6: Mounting of the robotic arm at a mid distance

dimensions.

  - *Inertia_Torque*: Moving a link with higher inertia require an actuator with higher torque.
  - *DR_Torque_Mass*: An actuator with higher torque will have a higher mass.

- *DR_Link_Length*: link length must be long enough to reach the ceiling (from REQ_Reach) and not too long so that the robot remains compact when folded (from REQ_Entry and REQ_Non_collision)

- *DR_Stab*: Stability is another constraint on link lengths. Longer link lengths may provide larger workspace. However, stability of the robotic unit is compromised due to overhanging of the links.

Thus, while performing dimensional synthesis, the attempt is to design shortest possible link lengths which provided a necessary reachability while satisfying constraints.

Preliminary Dimensional synthesis

Figure 3.7 shows robotic unit placed laterally in front of (A). Links BI_1 and I_1T are the principal links contributing to reachability. Figure 3.7.b shows intersection of the 3D-workspace (W) with the wall. This intersection is the circle '(C)'. Plane (π) is a lateral plane passing through points A and T. It is this plane where, elbow of the robotic arm has maximum chance of colliding with the wall since the base angle is 0^0. If collisions of the robotic arm are avoided in this plane, the arm doesn't collide with the wall for any other lateral position. Thus, reachability analysis can be then restricted to 2D (in plane (π)) by fixing the base revolute joint. Ignoring one wrist joint, kinematics is reduced to RRR i.e Shoulder-Elbow-Wrist pitch.

Moreover, narrow corridors is a critical factor affecting design of link lengths. Thus, *DR_Narrow_Corridor* must be satisfied. Considering the most critical case, dimensional synthesis is performed for cleaning inside narrow corridors.

Mounting of the Robotic arm

DR_Mass puts a constraint on the overall mass of the robotic unit. Combining this with DR_Reach, base mounting can be done at the mid distance between the ground and the ceiling.

- *DR_Mid_Dist*: The arm base should be located at mid-distance between the ground and ceiling and with a reach superior or equal to this mid-distance.

Locating the arm base at mid-distance between ground and 3 m high ceiling and provide arm ream superior to 1.5 m as shown in figure **??**. A center position is chosen on the top of the mobile base (pink box).

Arm analyses

A narrow corridor is represented in cross-section by the rectangle $C_1C_2C_3C_4$. The parameterization feature of Geogebra is used to move the base and adjust link lengths.

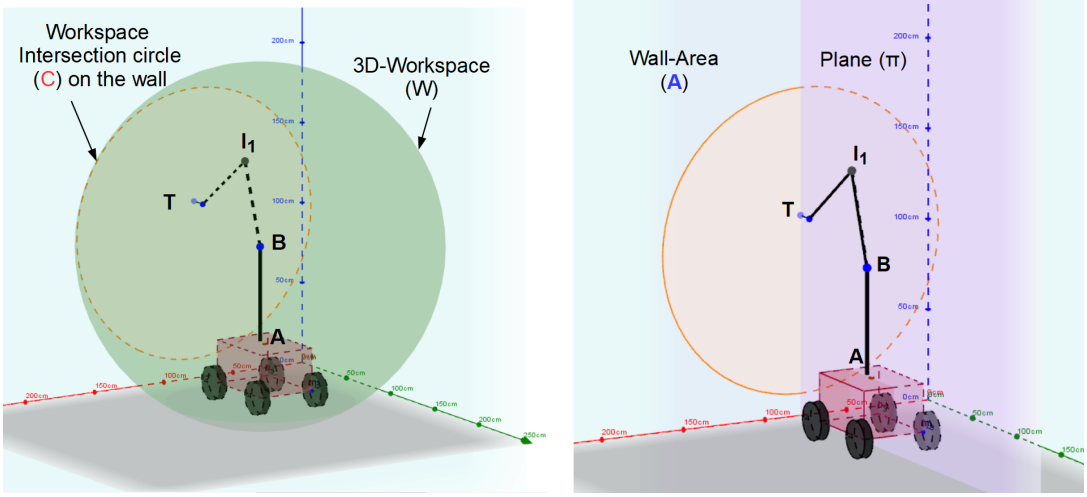

(a) Lateral plane π passing through robotic unit

(b) Intersection of 3D workspace with cleaning wall

Figure 3.7: Arm link length design process

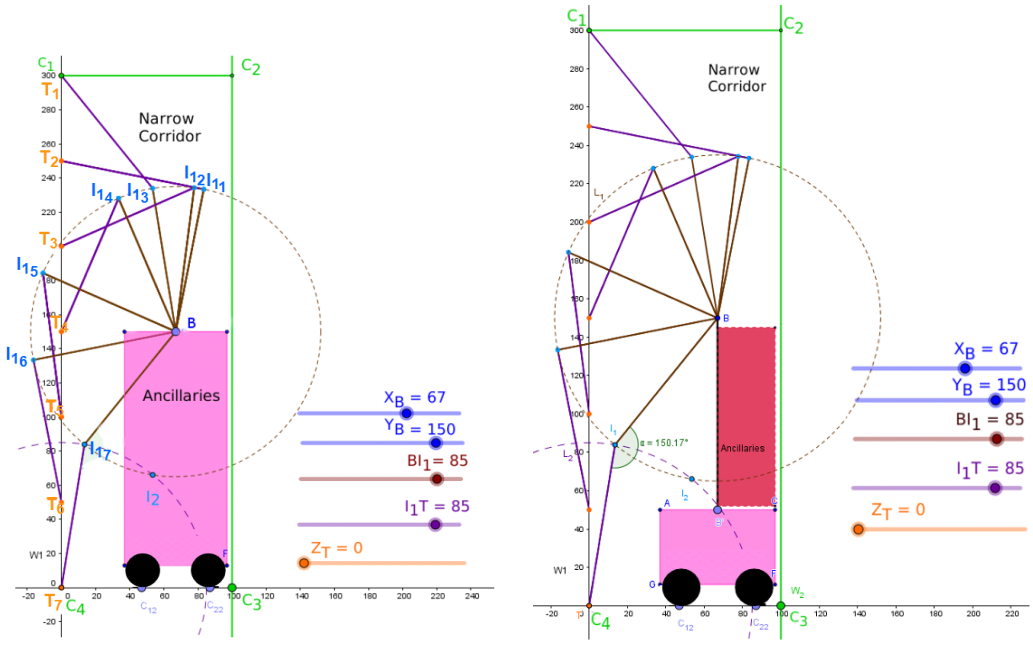

(a) Robotic unit with long link lengths: self collisions

(b) Robotic unit with long link lengths: wall-arm collisions

Figure 3.8: Collisions while performing vertical trajectory in a corridor

Point B represents the base of the arm and is adjusted at 150 cm height with the Y_B slider, according to *DR_Mid_Dist*. By fixing the base B, circle (L_1) that characterizes the first link is (parameterized by slider BI_1). For constructing the second link, the end-effector point T is first fixed at a position on the wall represented by the Y-axis. Another circle (L_2) that characterizes the length of second link is parameterized by slider I_1T. Two intersection points I_1 and I_2 are obtained that are the two possible elbow points. Point I_1 (elbow-up) configuration is chosen. A vertical trajectory is traced along line

C_1C_2 and intermediate positions of the arm are shown in Figure 3.8.a. It can be seen that, for the choice of given link lengths, the issue of collisions of the elbow joint with the wall as well as Link 1 with the mobile platform while performing vertical trajectory are inevitable.

Figure 3.8.b proposes an alternate design of the mobile platform to avoid arm-platform collision. In this design, the red box indicating ancillaries is mounted behind the working plane of the arm and hence does not interfere within the workspace. However, arm-wall collisions can't be avoided. Thus, *DR_Non_collision* is not satisfied.

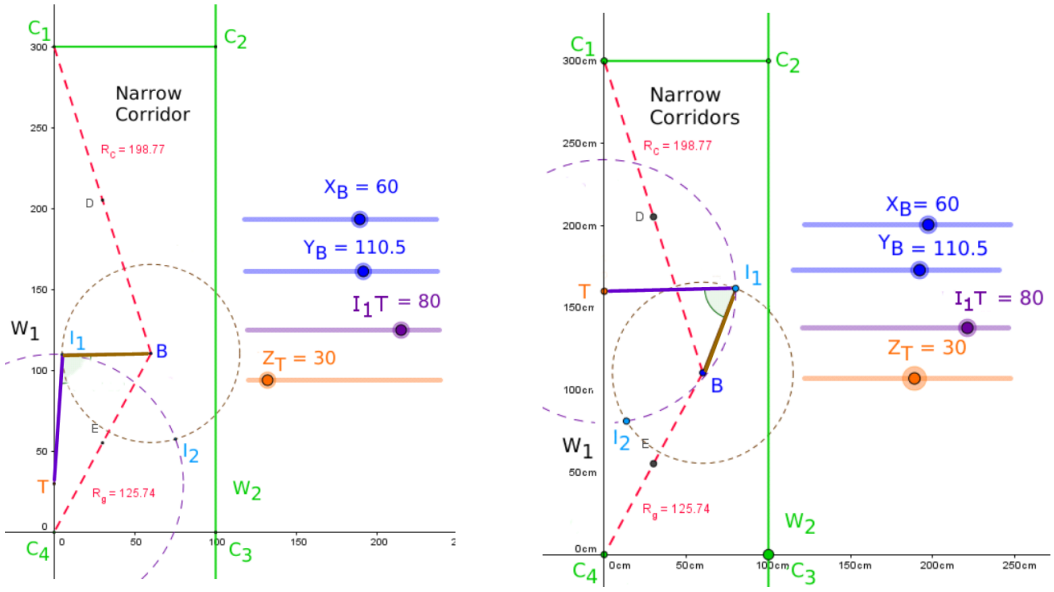

(a) First arm link BI_1 is chosen short enough to avoid wall-collision when horizontal

(b) Second arm link I_1T is chosen short enough to avoid wall-collision when horizontal

Figure 3.9: Arm link length design process in the (%π) plane

New design rules

A solution to satisfy the design rule *DR_non_collision* is to infer the new following design rules as follows:

- *DR_Link_1*: For avoiding collision, the link length of the first link must not exceed the distance between the base position, B and the front wall. Thus, the input radius for circle L_1 (which controls the link length L_1) is given adjusted to make link BL_1 not collide with the wall when it is perpendicular to the wall.
- *DR_Link_2*: Similarly, to avoid the collision of elbow with wall C_2C_3, a design rule for second link can be obtained as: length of link 2 (I_1T) should be less that the width of the width of the corridor" as shown in figure 3.9.b

However, for link lengths obtained by following these two rules, it is impossible to reach both ceiling and ground points by keeping the base position fixed (figure 3.10. Another design rule can be generated to solve this issue.

- *DR_Arm_Base_Motion*: To achieve reachability, need of a vertical shift in the base point B is identified. The arm can be fixed on the slider so that

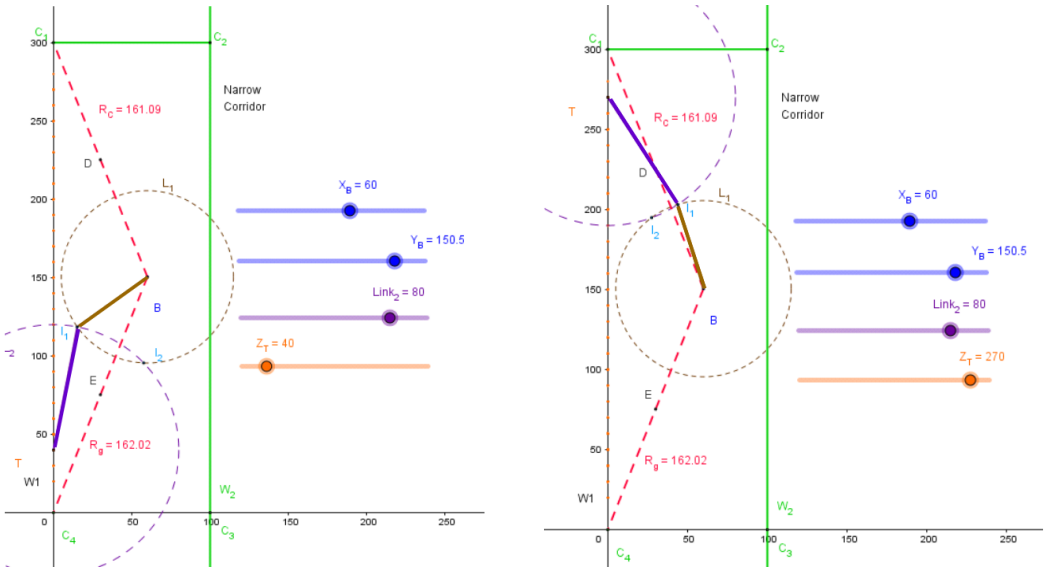

(a) Attempt to reach ground point (b) Attempt to reach ceiling point

Figure 3.10: Reachability assessment with new link lengths

By adding an extra joint redundancy is introduced in the kinematics. Therefore, the result is *DR_non_collision* is satisfied. This can be seen through figures 3.11. Vertical displacement of the prismatic joints is shown by dotted trace of point *B*. In this case, the arm base B elevates from 100cm to 180cm.

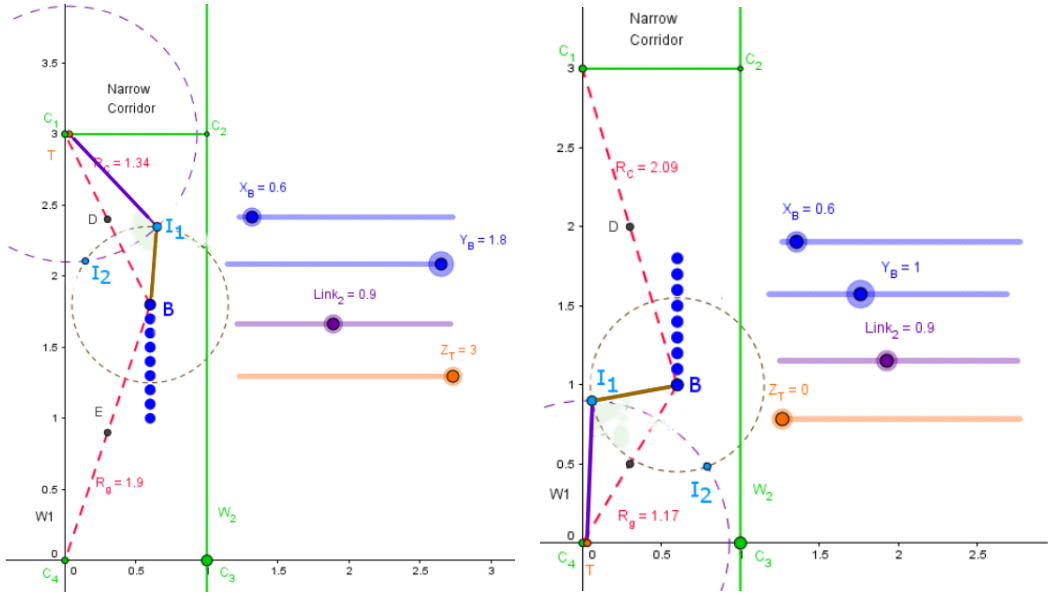

(a) Slider position to reach ceiling point (b) Slider position to reach ground point

Figure 3.11: Arm link length design process

3.3.3 Workspace of the Robotic Unit

Intersection of the 3-Dimensional workspace of the arm with walls of the narrow corridor are shown in figure 3.12. Intersection circle of the wall and ceiling are different due to the position of the prismatic joints not being at the equidistant from ceiling and ground on the slider position.

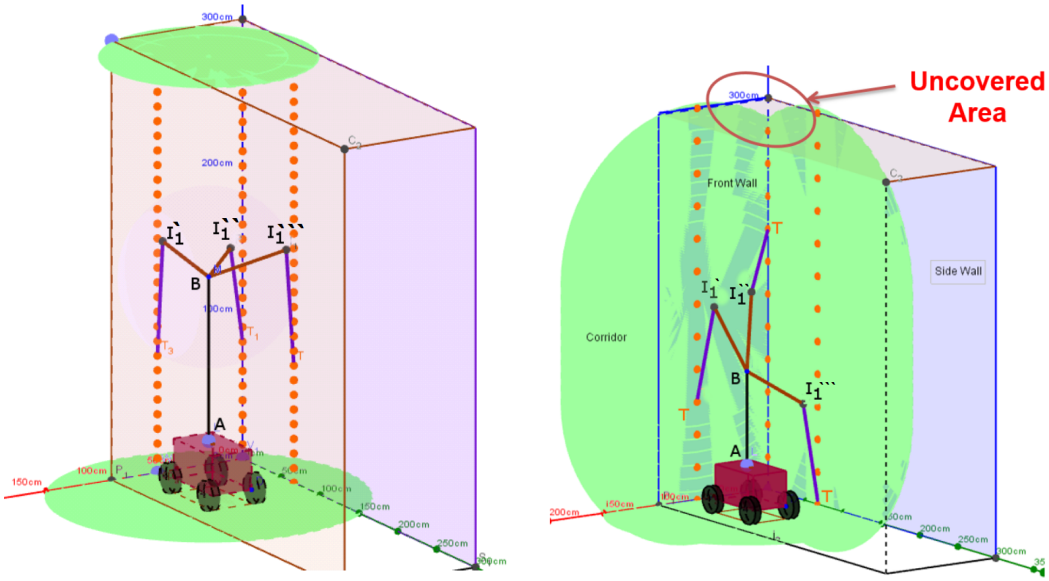

(a) Three arm positions to show accessibility to front wall, lateral wall and the corner

(b) Intersection of 3D workspace with wall, ceiling and ground

Figure 3.12: Arm link length design process

3.4 DH parameters of the robotic arm

Robotic arm to be integrated with mobile base has an architecture 'P-6R' i.e an anthropomorphic '6R' arm mounted on a 'vertical axis slider'.

- P_1: Prismatic joint as a consequence of DR_Arm_Base_Motion
- R_2: Allows to rotate the plane (π) with respect to the (A,z)
- R_3: Completes the shoulder mobility
- R_4: Elbow
- R_5: R_6, R_7: Wrist R_6 and R_7 maintain the tool disk in the plane of the wall when R_1 is actuated. The consortium chose a 3 DoF wrist.

Such architecture is redundant in terms of task requirement since in task space we need 5 d.o.f and the architecture has 7 d.o.f in total. In Fig.3.13, XYZ is a global frame of reference. Vertical axis of the slider is along 'Z'-direction. Frames (i) are attached to each joints as per modified DH conventions [Khalil, 2002]. Table 3.3 presents architecture of the robotic arm in terms of modified Denavit-Hartenberg parameters.

Table 3.3: MDH parameters

(i)	σ	θ	d	α	r
1	1	0	0	0	r_1^*
2	0	q_2	0	0	0.1
3	0	q_3	0.1	$\frac{pi}{2}$	0.9
4	0	q_4	0.6	0	0
5	0	q_5	0.6	$-\frac{pi}{2}$	0
6	0	q_6	0.13	$-\frac{pi}{2}$	0.13
7	0	q_7	0	0	0

$^*r_1 = h = (0.5, 1.8)\, m$

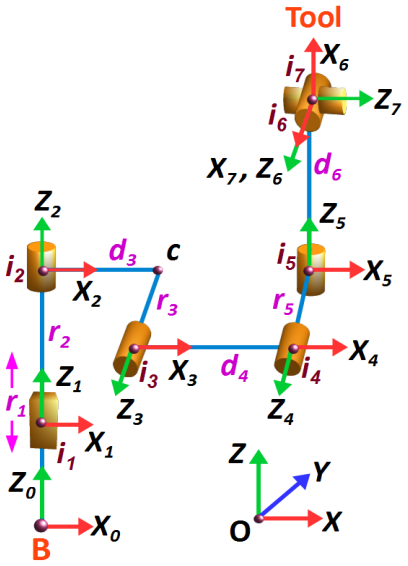

Figure 3.13: Visualization of the P-6R architecture

Conclusions

In this chapter, a methodology of selecting a kinematic architecture is demonstrated. An anthropomorphic arm structure is synthesized using inference of design rules and 2D parametrized models in an Interactive Geometric Software (IGS). The synthesis method is based on a loop of series of three stages:

- Inference of design rules that determine geometrical properties represented in simplified models.
- The geometric model is simulated. If the design rule is seen to be violated (e.g. collision, singularity...), a better restrictive design rule is inferred and the loop continues.
- If violation of constraints can't be avoided, a new kinematic architecture is adapted.

The workspace of the kinematics designed is sufficient and can perform a 3 m high continuous trajectory while avoiding singularities. The width of the workspace is constrained in the narrow corridor scenario: the most critical pose is when the arm is located on the lateral plane (BYZ) passing through the arm base point. As the RR arm architecture generates too many collisions a redundant PRR kinematics was proposed. Adding redundancy to the originally considered architecture was proved to generate a better compact design avoiding collisions and allowing singularity-free continuous vertical trajectories. This work proved the interest of combining design rule inference and skeleton modelling using IGS in order to perform dimensional synthesis of an arm for mobile manipulator. The design rules are helpful for converting requirements into geometrical constraints. The IGS is powerful software for expressing design constraints in the Cartesian space and exploring the design space through parametrization. The IGS permitted to extract new design rules that allow local geometrical optimization of the mechanism in the design space.

Chapter 4

Dynamic Modeling of the Robotic Unit: Stability Evaluation

Contents

Dynamic nature of the asbestos removal process generates the need of setting up a simulation model for assessing behavior of the robotic unit while performing removal operation. Primary objective of this assessment is stability evaluation of the robotic unit to ensure safe and stable operation. In this context, the chapter presents a methodology adapted to study dynamic behavior of the robotic unit. Initially, environment to be cleaned and its key components are presented. Thereafter, cleaning scenarios arising due to the presence of different entities like wall, ceiling and ground are analysed to identify reaction wrench and its effect on the stability of the robotic unit. Finally, two methods of stability evaluation, numerical and co-simulation, are explained in detail.

4.1 Need of dynamic modeling

Process of asbestos removal involves dynamic interaction between cleaning environment and robotic unit. This interaction occurs at two levels. Firstly, a grinding tool mounted on the robotic arm interacts with the cleaning surface and generate reaction forces. Secondly, wheels of the mobile base are subjected to ground reaction forces due to:

- weight of the robotic unit
- grinding forces (normal and tangential reaction forces, three reaction wrenches)
- inertia forces generated due to the motion of robotic arm and tool rotation

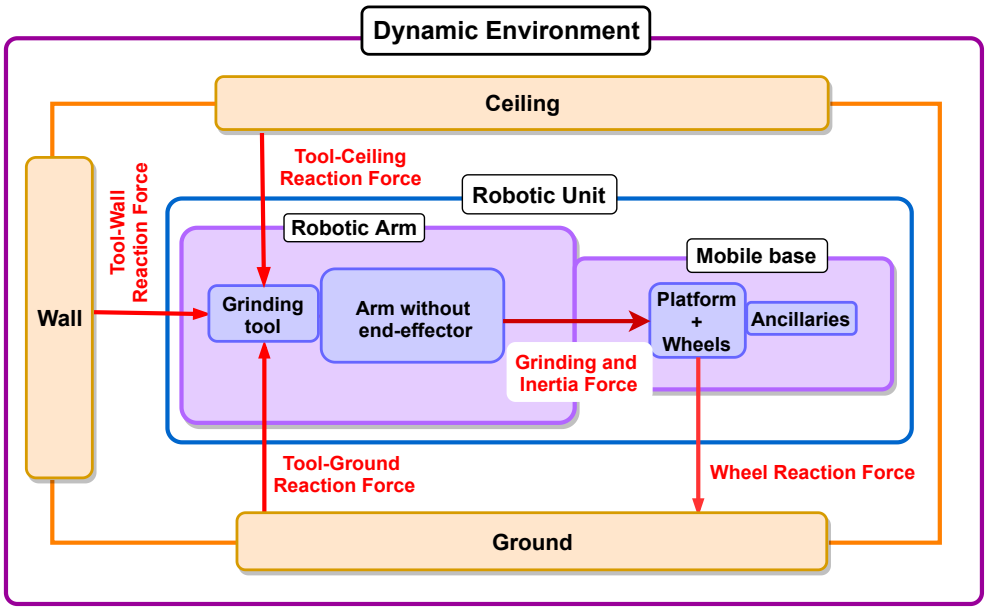

Figure 4.1: Interaction model of asbestos removal use case

In figure 4.1 a typical interaction model existing within the process of asbestos removal is detailed. Reaction forces generated by tool-surface interaction (ground, wall and ceiling) are transmitted to the arm through tool-arm connection. Since, arm performs accelerated motions, varying inertial forces are generated in addition to grinding reaction forces. Connection of arm to the mobile base transmits these forces to the mobile base which are further passed on to the ground surface through wheels. Due to these transmissions, stability of the robotic unit is significantly affected. Therefore, in order to study effects of arm motion and grinding reaction forces on the stability of robotic unit, a dynamic simulation model capable of simulating realistic asbestos removal scenario must be constructed.

For realistic simulation of the process, intended dynamic model should incorporate following components:

- Cleaning environment consisting of elements like wall, ground and ceiling.
- Multi-body dynamic model of the robotic unit localized inside cleaning environment (with inertial parameters: mass, center of mass, inertia).
- Geometric and kinematic models (direct and inverse) of the robotic arm for motion generation.

- Tool-wall and wheel-ground contacts to simulate robot-environment dynamic interaction.
- Control scheme to govern motion of the robotic arm.
- Formulation for dynamic stability of the robotic unit.

In the following sections, components of dynamic model are explained in detail.

4.2 Cleaning Environment

Cleaning environment is typically a rehabitation site located in a residency building. The site consists of rooms like bedroom, office/study room, living room, kitchen, dining room, front entrance, garden, laundry room, etc. They vary in terms of dimensions (ceiling height, room width and length) as well as materials used for construction (resurfacing concrete, plaster, bricks, tiles etc). However, one obvious commonality for all the rooms is that the surfaces to clean can be on the ground, the walls or the ceiling.

4.3 Description of representative frames

To represent the environment as well as the robotic unit, coordinate frames are defined for individual entities (figure 4.2). Here, we consider surfaces of the room are perfectly planar and perpendicular to each other. Also, an important assumption for the placement of the robotic unit through out the cleaning operation is to have length of the robotic unit perpendicular to the wall. Let, **w** and **h** be the width and The frames consist of three mutually perpendicular unit vectors. Detailed description of these frames goes below:

Environment frame ($\mathcal{F}_\mathcal{E}$)

Environment mainly consists of three surfaces i.e wall, ceiling and ground. In most of the cases where walls are planar (i.e without curvatures), these three surfaces can help defining the global environment frame of reference. The origin of the frame is named as O_E. Position of O_E can be assumed at a convenient location e.g center of the room, corner of the room etc. Axis $\mathbf{x_E}$ is defined as normal to plane (P_G) point inside the room. Then, axes $\mathbf{x_E}$ and $\mathbf{y_E}$ can be defined as mutually perpendicular axes that lie in the ground plane P_G. Axis Y_E is selected along the line of intersection of planes (P_W) and (P_G) and its direction is shown in figure 4.2. According to general conventions, $\mathbf{x_E} = \mathbf{y_E} \times \mathbf{z_E}$.

Ground frame ($\mathcal{F}_\mathcal{G}$)

Ground frame $\mathcal{F}_\mathcal{G}$ is assumed to be oriented parallel the frame $\mathcal{F}_\mathcal{E}$. So the axis $\mathbf{z_E}$ is normal to the plane P_G. Position of the origin O_G can be assumed at any convenient on the plane P_G. Here, assumption is that, the room is parallelepipedic in shape.

Ceiling frame ($\mathcal{F}_\mathcal{C}$)

Ceiling plane P_C is parallel to the ground plane P_G and is separated by height h and located on the ceiling. Thus, orientation of the ceiling frame ($\mathcal{F}_\mathcal{C}$) is parallel to that of the ground frame ($\mathcal{F}_\mathcal{G}$).

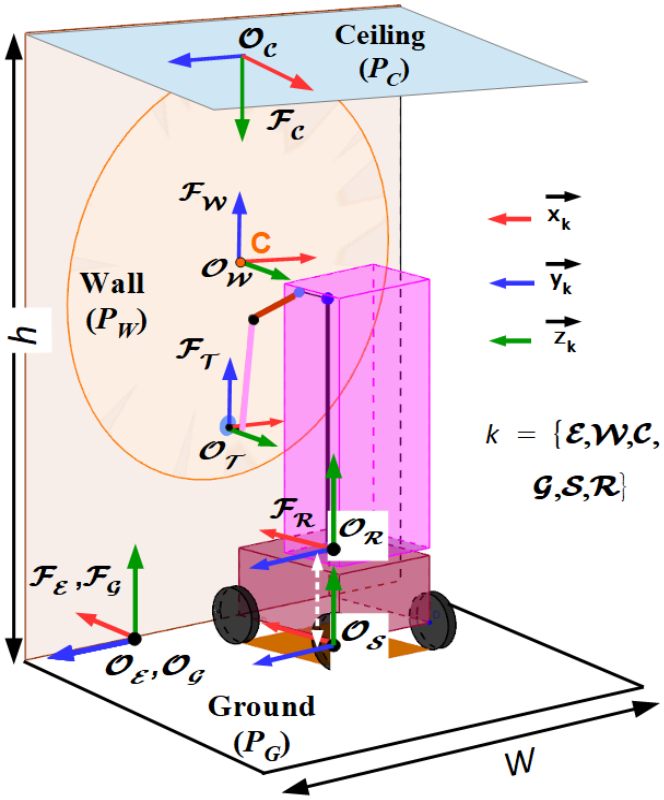

Figure 4.2: Description of cleaning environment and frames

Wall frame ($\mathcal{F}_\mathcal{W}$)

Origin of the front wall frame O_W is fixed on the wall surface. Z-axis $\mathbf{z_W}$ is normal to the wall plane P_W. Axes $\mathbf{x_W}$ and $\mathbf{y_W}$ are mutually perpendicular and lie in plane P_W. Also, $\mathbf{z_W} = \mathbf{x_W} \times \mathbf{y_W}$. Thus, w.r.t the frame $\mathcal{F}_\mathcal{E}$, $\mathbf{z_W}$ is parallel to $\mathbf{x_E}$, $\mathbf{x_W}$ is parallel to $\mathbf{y_E}$ and $\mathbf{y_W}$ is parallel to $\mathbf{x_E}$.

Frame of the Robotic Unit ($\mathcal{F}_\mathcal{R}$)

Frame of the robotic unit with origin O_R is attached on the center of the top face of the mobile base. Axes $\mathbf{x_R}$ and $\mathbf{y_R}$ are directed along the length and the width of the mobile base and are parallel to plane (P_G). Thus on a flat standard ground, orientation of axis $\mathbf{z_R}$ is parallel to axis $\mathbf{z_E}$.

Frame of the support polygon ($\mathcal{F}_\mathcal{S}$)

Frame of the support polygon with origin O_S is attached on the center of the support polygon of the mobile base. Axes $\mathbf{x_R}$ and $\mathbf{y_R}$ are directed along the length and the width of the mobile base and are parallel to axes $\mathbf{x_R}$ and $\mathbf{y_R}$ respectively. Naturally, orientation of axis $\mathbf{z_R}$ is parallel to axis $\mathbf{z_E}$.

Table 4.1: Description of Frames

Frame ($\mathcal{F}$)	Position ($\mathcal{P}$)	Orientation ($\mathcal{O}$)
Environment ($\mathcal{F_E}$)	At a convenient position on P_G	$\mathbf{z_E} \perp (\mathrm{P}_G)$
		$\mathbf{y_E}$ = any of the two directions along $(P_G) \cap (P_W)$
		$\mathbf{x_E} = \mathbf{y_E} \times \mathbf{z_E}$
Ground ($\mathcal{F_G}$)	At a convenient position on P_G	$\mathbf{z_G} \perp \mathrm{P}_G$
		$\mathbf{y_G} = \mathbf{y_E}$
		$\mathbf{x_G} = \mathbf{x_E}$
Wall ($\mathcal{F_W}$)	At a convenient position on P_W	$\mathbf{z_W} \perp \mathrm{P}_W$
		$\mathbf{y_W} = \mathbf{h}$, $\mathbf{y_W} \ \epsilon \ (P_W)$
		$\mathbf{x_W} = \mathbf{w}$, $\mathbf{x_W} \ \epsilon \ (P_W)$
Ceiling ($\mathcal{F_C}$)	At a convenient position on P_C	$\mathbf{z_C} \perp \mathrm{P}_C$
		$\mathbf{y_C} = \mathbf{y_E}$
		$\mathbf{x_C} = \mathbf{x_E}$, $\mathbf{x_W} \ \epsilon \ \mathrm{P}_W$
Robotic Unit ($\mathcal{F_R}$)	Center of the top face of the mobile base	$\mathbf{z_R} \perp \mathrm{P}_G$
		$\mathbf{y_R} = \mathbf{y_G}$
		$\mathbf{x_R} = \mathbf{X_G}$
Support Polygon ($\mathcal{F_S}$)	Geometric centre of the support polygon	$\mathbf{z_S} \perp \mathrm{P}_G$
		$\mathbf{y_S} = \mathbf{y_G}$ P_G
		$\mathbf{x_S} = \mathbf{X_G}$

Transformation between frames

There exists a fixed transformation between environment frame ($\mathcal{F_E}$) and frames representing components of the environment. i.e. wall frame ($\mathcal{F_W}$), ground frame ($\mathcal{F_G}$) and ceiling frame ($\mathcal{F_C}$). These transformations are summarized in the Table 4.2.

Table 4.2: Transformation of frames w.r.t environment frame

Frame	Position w.r.t $\mathcal{F_E}$	Orientation w.r.t $\mathcal{F_E}$
Wall frame ($\mathcal{F}_w$)	${}^E[o_{w_x} \ o_{w_y} \ o_{w_z}]$	$[R_{z_E}(\text{-}\frac{\pi}{2}).R_{x_E}(\text{-}\frac{\pi}{2})]$
Ground frame ($\mathcal{F_G}$)	${}^E[o_{g_x} \ o_{g_y} \ 0]$	
Ceiling frame ($\mathcal{F_C}$)	${}^E[o_{c_x} \ o_{c_y} \ o_{c_z}]$	$[R_{y_E}(\text{-}\pi)]$
Support polygon ($\mathcal{F_S}$)	${}^E[o_{s_x} \ o_{s_y} \ 0]$	$[R_{z_E}]$
Robotic unit ($\mathcal{F_R}$)	${}^E[o_{r_x} \ o_{r_y} \ H_b.\hat{k}]$	$[R_{z_E}]$

R_{k_E} denotes a rotation matrix around axis k_E where, $k = x, y, z$

4.4 Representation of asbestos removal use case

Process of asbestos removal involves positioning the mobile platform base in the cleaning environment at a suitable distance so as to access maximum possible area at a given base position and be able to grind the surfaces with optimal grinding parameters while maintaining stability of the overall robotic unit.

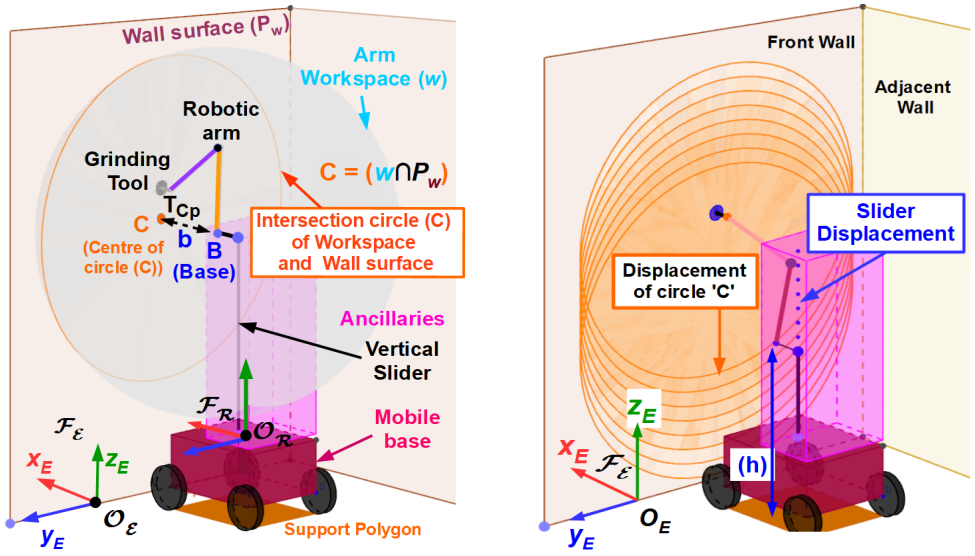

(a) Representation of workspace

(b) Extension of workspace

Figure 4.3: Representation of asbestos use case scenario using Geogebra [geo, 2016]

Figure 4.3a shows robotic unit placed at a distance 'b'from wall surface (P_W). At this distance, the 3D workspace (W_A) of the robotic arm intersects with surface (P_W) for giving circle (C). The area of (C) is the area available for cleaning at a given base placement such that collision free (arm-cleaning environment) continuous trajectories are feasible. However, since the robotic arm is mounted on a vertical slider figure 4.3b, circle (C) can move along a vertical axis to sweep a surface with a geometric shape called 'stadium' (rectangle with semicircles on either of the opposite sides). Thus, even at fixed base position, the workspace of the robotic arm is extended due to presence of architectural redundancy (P-joint).

4.5 Identification of reaction wrench

While realizing robotized grinding operation, it is inevitable to consider the difference in the geometry of the cleaning environment for precise modelling and simulation of the process. Moreover, grinding operation generates reaction wrench being applied on the end-effector. Since, the end-effector while cleaning different surfaces, takes different orientations, it is quite intuitive to conclude that the reaction wrenches acting on the robotic unit while cleaning these surfaces have different positions and orientations. Thus, stability of the robotic unit is affected differently while performing grinding operation of these surfaces.

4.5.1 Frontal wall

Figure 4.4.a shows reaction wrench being applied on the end-effector (tool) during the grinding operation while $\mathcal{F}_w : \{x_w, y_w, z_w\}$ indicates wall frame. Reaction wrench consists of normal reaction forces $[(F_{NZ})_w]$, tangential reaction forces $[(F_{TY})_w]$, $[(F_{TX})_w]$ and reaction torque $[(T_Z)_w]$. Here, subscript 'w' indicates that components of the reaction wrench are expressed in wall frame ($\mathcal{F}_w$). Normal and tangential reaction forces are responsible in producing moments which act on the robotic unit through end-effector. These moments, and the distances responsible for creating them are summerized in table 4.3. Also, effect of these forces on stability are identified.

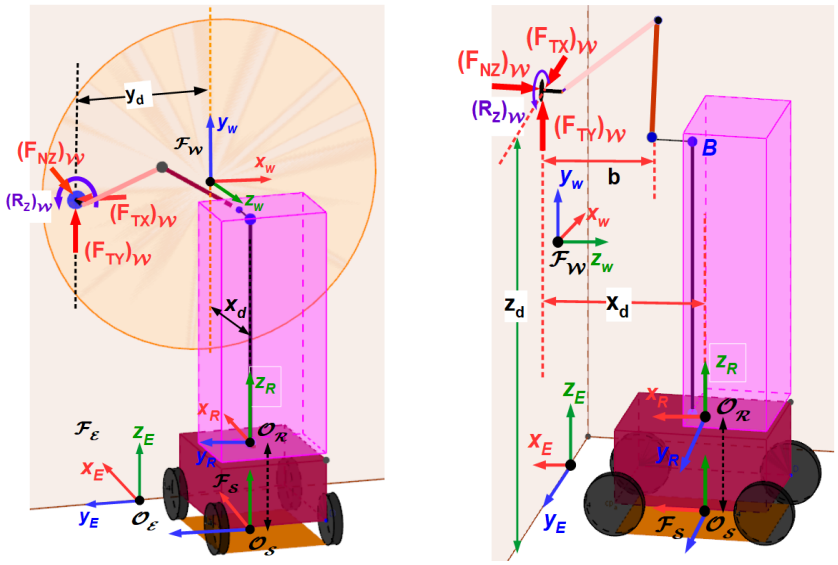

(a) Rear view (b) Side view

Figure 4.4: Forces and moments acting during wall scenario

4.5.2 Ceiling

For cleaning the ceiling portion of the environment, the directions of reaction forces differ from those during cleaning frontal walls. Reaction wrench consists of normal reaction force $[(F_{NZ})_c]$, tangential reaction forces $[(F_{NY})_c]$, $[(F_{NT})_c]$ (figure 4.5). Subscript 'c'indicates ceiling frame $\mathcal{F}_c$.

4.5.3 Ground

Ground cleaning is a scenario, as shown in figure 4.6 where the cleaning surface plane P_G and the plane defined by axes $x_E - y_E$ of the environment frame are same. Reaction wrench consists of normal reaction force $[(F_{NZ})_G]$, tangential reaction forces $[(F_{TX})_G]$, $[(F_{TY})_G]$ and reaction torque $[(R_Z)_G]$. Here, subscript 'G' indicates ground frame of reference $\mathcal{F}_\mathcal{G}$. Since, tangential reaction forces lie in the plane of the support polygon, moments produced by these forces are zero in the ground plane. Thus, normal reaction force and reaction torque are the two entities which affect stability of the robotic unit.

Table 4.3: Generation of moments in wall scenario

Reaction force	Normal distance	Resulting moment	Probable Effect on the robotic unit
$(\mathbf{F_{NZ}})_{\mathbf{w}}$	y_d	$\vec{M}_{z_S}$ (Moment around $\mathbf{z_S}$)	**Yaw** motion of the robotic unit
	z_d	$\vec{M}_{y_S}$ (Moment around $\mathbf{y_S}$)	**Pitch** motion affecting longitudinal stability
$(\mathbf{F_{TY}})_{\mathbf{w}}$	x_d	$\vec{M}_{z_S}$ (Moment around $\vec{z}_S$)	**Yaw** motion causing rotation of the platform
	z_d	$\vec{M}_{x_S}$ (Moment around $\mathbf{x_S}$)	**Roll** motion affecting lateral stability
$(\mathbf{F_{TX}})_{\mathbf{w}}$	x_d	$\vec{M}_{y_S}$ (Moment around $\mathbf{y_S}$)	**Pitch** motion affecting longitudinal stability
	y_d	$\vec{M}_{x_S}$ (Moments around $\mathbf{x_S}$)	**Roll** motion affecting lateral stability
		$(R)_w.\mathbf{x_S}$ (Reaction moment around $\mathbf{x_S}$)	Roll motion affecting lateral stability

Table 4.4: Generation of moments in ceiling scenario

Reaction component	Normal distance	Resulting moment	Probable Effect on the robotic unit
$(\mathbf{F_{NZ}})_{\mathbf{C}}$	x_d	$\vec{M}_{y_S}$ (Motion around $\mathbf{y_S}$)	**Pitch** motion affecting longitudinal stability
	y_d	$\vec{M}_{x_S}$ (Moment around $\mathbf{x_S}$)	**Roll** motion affecting lateral stability
$(\mathbf{F_{TY}})_{\mathbf{C}}$	y_d	$\vec{M}_{z_S}$ (Moment around $\vec{z}_S$)	**Yaw** motion of the robotic unit
	z_d	$\vec{M}_{y_S}$ (Moment around $\mathbf{y_S}$)	**Pitch** motion affecting longitudinal stability
$(\mathbf{F_{TX}})_{\mathbf{C}}$	z_d	$\vec{M}_{x_S}$ (Moment around $\mathbf{x_S}$)	**Roll** moment affecting lateral stability
	x_d	$\vec{M}_{z_S}$ (Moment around $\mathbf{z_S}$)	**Yaw** motion of the robotic unit
		$(R_Z)_C.\mathbf{z_S}$ (Reaction moment around $\mathbf{z_S}$)	Yaw motion of the robotic unit

4.6 Stability criteria based on Zero Moment Point

Issues regarding stability of the robotic unit during grinding operation are already discussed in previous sections. In order to ensure safe and stable operation, a suitable

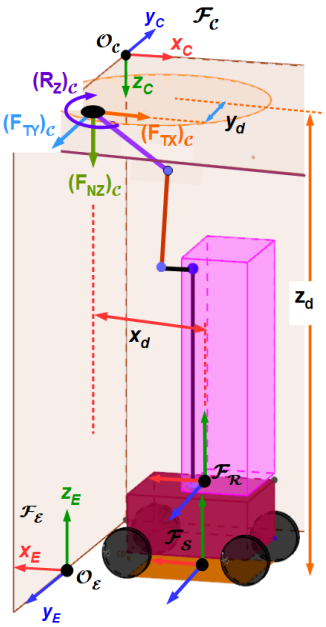

Figure 4.5: Forces while cleaning ceiling

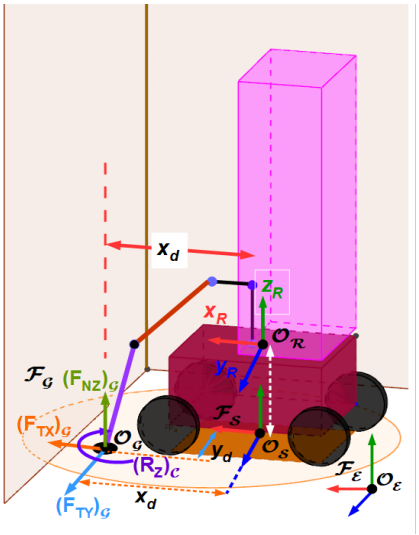

Figure 4.6: Forces while cleaning ground

Table 4.5: Generation of moments in ground scenario

Reaction force	Normal distance	Resulting moment	Effect on the robotic unit
$(F_{NZ})_G.(\vec{z}_S)$	z_d	$\vec{M}_{y_S}$ (Moment around $\mathbf{y_S}$)	Pitch moment affecting longitudinal stability
	y_d	M_{x_S} (Moment around $\mathbf{x_S}$)	Roll motion affecting lateral stability
		$(R_z)_G.\mathbf{z_S}$ (Reaction moment around $\mathbf{z_S}$)	Yaw motion of the platform

stability margin, must be defined. For a dynamically operating system, a well known stability criteria called Zero moment point (ZMP) is widely used in the filed of biped locomotion. ZMP (zero moment point) is defined as a point on the ground at which the net moment of the inertial forces and the gravity forces has no component along the horizontal axes [Vukobratovic and Juricic, 1971]. The two components of ZMP are presented as:

$$x_{zmp} = \frac{\sum_{i=1}^{n} m_i(\ddot{z}_i + g)x_i - \sum_{i=1}^{n}(m_i\ddot{x}_i)z_i - \sum_{i=1}^{n}(\mathcal{L}_y)_i}{\sum_{i=1}^{n} m_i(\ddot{z}_i + g)} \tag{4.1a}$$

$$y_{zmp} = \frac{\sum_{i=1}^{n} m_i(\ddot{z}_i + g)y_i - \sum_{i=1}^{n}(m_i\ddot{y}_i)z_i - \sum_{i=1}^{n}(\mathcal{L}_x)_i}{\sum_{i=1}^{n} m_i(\ddot{z}_i + g)} \tag{4.1b}$$

where, i indicates number of rigid bodies, (x_i, y_i, z_i) indicate coordinates of the CoM of the i^{th} body and $(\mathcal{L}_x, \mathcal{L}_y)$ indicate components of derivatives of angular momentum, where, $\mathcal{L}_i = I_i\dot{\omega} + \omega_i \times I_i\omega_i$; ω_i is angular velocity of link i and I_i is its mass moment of

inertia matrix.

From the definition of ZMP, we see that each term in the numerator represents a moment acting on the system. Thus, to integrate grinding reaction forces in ZMP, moments produced by normal and tangential reaction forces must be taken into account. These moments are already identified in the section (4.5).

$$x_{zmp} = \frac{\sum_{i=1}^{n} m_i(\ddot{z}_i + g)x_i - \sum_{i=1}^{n} (m_i\ddot{x}_i)z_i - \sum_{i=1}^{n} (\mathcal{L}_y)_i - \vec{M}_{y_S}}{\sum_{i=1}^{n} m_i(\ddot{z}_i + g)} \tag{4.2a}$$

$$y_{zmp} = \frac{\sum_{i=1}^{n} m_i(\ddot{z}_i + g)y_i - \sum_{i=1}^{n} (m_i\ddot{y}_i)z_i - \sum_{i=1}^{n} (\mathcal{L}_x)_i - \vec{M}_{x_S}}{\sum_{i=1}^{n} m_i(\ddot{z}_i + g)} \tag{4.2b}$$

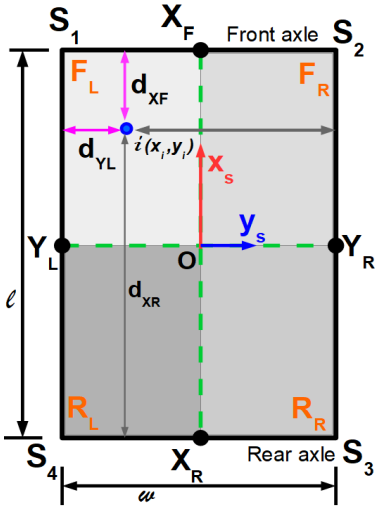

Figure 4.7: Notations for stability in the support polygon

Stability criteria

In our case, mobile base has a support polygon '$S_1S_2S_3S_4$'of dimensions $(l \times w)\ mm$ with lateral and longitudinal axes 'Y_LY_R'and 'X_FX_R'respectively (see Figure 4.7). The polygon is divided in four quadrants namely, front-left (F_L), front-right (F_R), rear-left (R_R) and rear-right (R_R). Longitudinal (S_{long}) and lateral (S_{lat}) percentage stability of point *'i'* having ZMP coordinates (x_i, y_i) is calculated as,

$$S_{long} = \left(\frac{min(d_{XF}, d_{XR})}{0.5 \times l}\right) \times 100, \quad S_{lat} = \left(\frac{min(d_{YR}, d_{YL})}{0.5 \times w}\right) \times 100 \tag{4.3}$$

where, $d_{XF} = \left|\frac{l}{2} - x_{zmp}\right|$, $d_{XR} = \left|\frac{l}{2} + x_{zmp}\right|$, $d_{YL} = \left|\frac{w}{2} - y_{zmp}\right|$, $d_{YR} = \left|\frac{w}{2} + y_{zmp}\right|$

4.7 Numerical evaluation of stability

An algorithm to carry out numerical evaluation of stability is implemented using MATLAB computing software (figure 4.8). The main objective of developing numerical

method is to exploit computational efficiency of MATLAB script execution, which is much higher than that of the co-simulation with a black-box dynamic model in ADAMS. Numerical simulation is a fast way to simulate the simplified dynamics of the robot as it simplifies the process of simulation by avoiding repetitive steps like modifying initial posture of the arm for different trajectories.

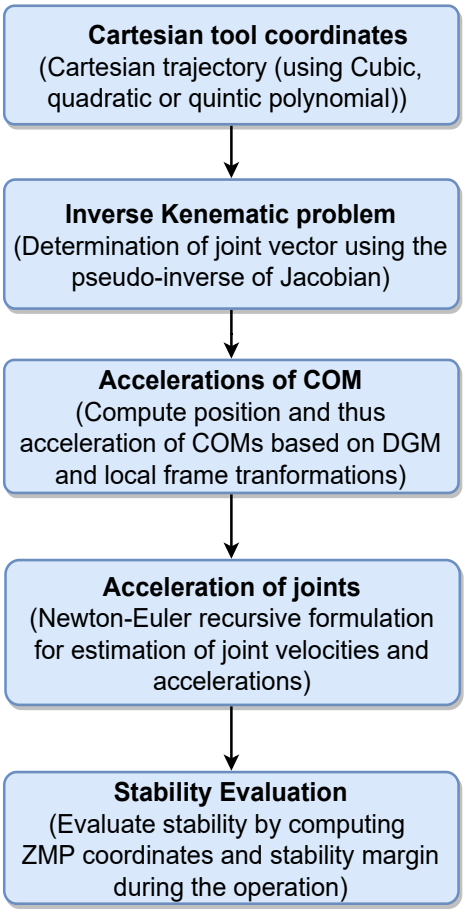

Figure 4.8: Numerical evaluation of stability

Numerical algorithm of stability evaluation

General approach adapted in defining the algorithm is explained below :

- *Cartesian trajectory input* : Targeted operational surfaces in construction applications can be 3-dimensional in nature (curved walls, ceiling or ground). However, in thesis, focus is limited to non-curved surfaces. Thus, 2-D Cartesian trajectories are defined while performing simulations. Cartesian poses of the end-effector frame corresponding to trajectory coordinates serves as an input to the algorithm.
- *IKS* : Inverse kinematics solution is needed to generate arm motion. Since arm is kinematically redundant, IKS is determined using redundancy resolution method that uses pseudo-inverse of the kinematic Jacobian matrix.
- *Recursive computation of link accelerations* : Angular velocities and accelerations of moving links contribute in generating dynamic effects on the robotic unit.

Newton-Euler recursive algorithm is used to compute these entities.

– *Stability Evaluation* : Zero moment point for the instantaneous dynamic state of the robotic unit is computed using equations 4.2a and 4.2b. Stability is then evaluated as per equation 4.3.

For evaluating stability during a continuous trajectory, the algorithm runs in loops defined by end positions of the trajectory. To provide readers with details on execution of each step, the algorithm is elaborated through following subsections.

4.7.1 Modeling of the robotic arm

Since, the mobile platform is steady during the operation, the geometric model of the robotic arm is sufficient for stability evaluation. SYMORO (**Sy**mbolic **Mo**deling of **Ro**bots) developed by [Khalil and Creusot, 1997] is used to model the robot. In SYMORO, robotic arm is described using MDH parameters. It then generates analytical expressions for :

– Homogeneous transformation matrices of joint frames (DGM)
– Kinematic Jacobian matrix
– Inverse kinematic solution (for non-redundant manipulators)
– Inverse dynamic solution

4.7.2 Cartesian trajectory

Cartesian pose of the tool (X) is given as an input for motion generation. A desired tool velocity (v_t) or acceleration (a_t) can be generated by providing time dependent values of pose. This can be achieved by different types of trajectory generating polynomials [Khalil, 2002]. Table 4.6 summarizes properties and minimum time takes by different polynomials for generating trajectories.

Trajectory Generation

For the three Cartesian coordinates of the tool, three trapezoidal profiled velocity trajectories can be planned. By keeping one of the coordinates constant, a planar trapezoidal trajectory (on a wall, ceiling or ground) can be generated. To perform vertical or horizontal wig-wag trajectory, one of the two changing coordinates can be varied reciprocally between fixed limits and the other one would undergo periodic increment or decrement for tool to make horizontal advancement.

Figure 4.10 shows a vertical wig-wag trajectory such that y_w coordinate varies from y_{min} to y_{max} while x_w periodic increment or decrement by Δx_w. A simulink model for generating trapezoidal trajectory of the z-coordinate is shown in figure 4.10. q_i and q_f are two pulse generating blocks 180° out of phase. The two pulse generators revere system inputs (from y_{min} to y_{max}) periodically. t_{repeat} produces a repetitive linear time input trajectory that varies from 0 to t_f. $vmax$ and $amax$ are values of maximum velocity and acceleration allowed during the trajectory.

Table 4.6: Polynomials for trajectory generation

Interpolation function	**Minimum time**	**Properties**
Linear interpolation	$t_{f_j} = \frac{\lvert D_j \rvert}{k_{vj}}$	Position is continuous, velocity is non-continuous
Cubic polynomial	$t_{f_j} = \max\left[\frac{3\lvert D_j \rvert}{2k_{vj}}, \sqrt{\frac{6\lvert D_j \rvert}{k_{aj}}}\right]$	Position and velocity are continuous, acceleration is non-continuous
Quintic polynomial	$t_{f_j} = \max\left[\frac{15\lvert D_j \rvert}{8k_{vj}}, \sqrt{\frac{10\lvert D_j \rvert}{\sqrt{3}k_{aj}}}\right]$	Position, velocity and acceleration are continuous
Bang-bang profile	$t_{f_j} = \max\left[\frac{2\lvert D_j \rvert}{k_{vj}}, 2\sqrt{\frac{\lvert D_j \rvert}{k_{aj}}}\right]$	Position and velocity are continuous, acceleration is non-continuous

where, j= joint number, k_{vj} = coefficient of velocity polynomial, k_{aj} = coefficient of velocity polynomial

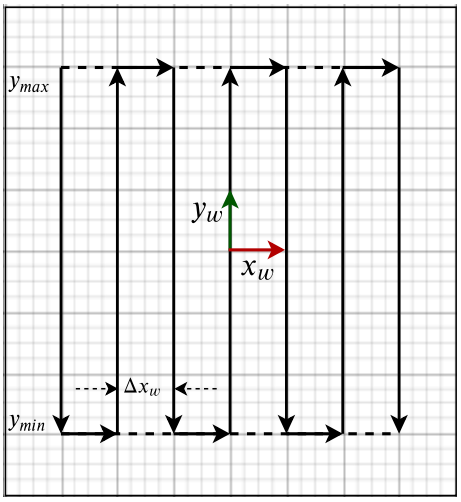

Figure 4.10: Vertical wig-wag trajectory

Where,

qi :	initial pulse generator for input.
q_f :	final pulse generator for output.
t_{repeat} :	repeating sequence block.
v_{max}	Maximum velocity of the trajectory.
a_{max} :	Maximum acceleration of the trajectory.

General algorithm for trapezoidal trajectory goes as below :

Input: Define : g, v_{max}, a_{max}
initialization: Start point ;
if $(0 \leq t \ \&\& \ t \leq \tau)$ **then**
  $y_t = y_0 + (0.5 \times t^2).a_{max}.\text{sign}(y_d)$
else if $(\tau \leq t \ \&\& \ t \leq t_f - \tau)$ **then**
  $y_t = y_0 + v_{max}.\text{sign}(y_d).(t - \frac{\tau}{2})$
else if $(\tau - t_f \leq t \ \&\& \ t \leq t_f)$ **then**
  $y_t = y_f - 0.5 \times (t_f - t)^2.a_{max}.\text{sign}(y_d)$
else
  $y_t = z_f$
end

Algorithm 1: Algorithm for trapezoidal trajectory generation

4.7.3 Inverse Kinematics Problem

Inverse kinematic problem deals with identifying vector of joint velocities ($\dot{q}$) for given pose ($\dot{X}$) of the end-effector. Method of pseudo-inverse J^+ of the Jacobian matrix is proposed in [Whitney, 1969] to obtain IKS of kinematically redundant manipulator.

$$\dot{q} = J_e^+ \dot{X} \tag{4.4}$$

However, for tasks requiring accurate end-effector position, desired pose vector (X_d) has to be the input for controlling motion of the manipulator. Mathematically, problem to find the joint position vector (q) that yields the desired end-effector pose can be expressed as

$$X_d = f(q) \tag{4.5}$$

This is called *redundancy resolution at the position level*.

Trajectory is nothing but a sequence of end-effector poses w.r.t time. In a continuous trajectory, successive points can be regarded as new desired point and motion of the manipulator can be planned to go from point to point. An algorithm to plan each individual point-to-point motion goes below [Fahimi, 2009].

– *Discretization of line segment* :
  Let, X_1 and X_2 be the two successive points on the trajectory. Let, X_1 be the initial position of the manipulator. Line between the two points is divided into N smaller line segments for numerical integration (figure A.7). Points $x_1, x_2 ... x_{N+1}$ represent intermediate positions of the end-effector during iterations.

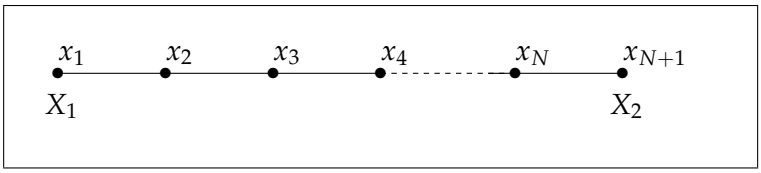

Figure 4.11: Discretization of line segment into N intervals

– *Computing initial pose* :
Initial pose can be computed using equation 4.5

$$x_0 = f(q_0) \tag{4.6}$$

– *Planning velocity of motion* :
For i^{th} interval, calculate velocity $\dot{x}_i$ to drive manipulator towards the desired pose.

$$\dot{x}_i = \alpha \frac{X_2 - x_i}{(N+1-i)\Delta t} \quad , \quad \Delta t = \frac{t}{N} \tag{4.7}$$

– *Computing joint rates* :
Based on cartesian velocity, joint velocities are calculated using the pseudo-inverse of Jacobian.

$$\dot{q}_i = J_e^+(q_i)\dot{x}_i \tag{4.8}$$

– *Computing joint positions* :
Joint positions for $(i+1)^{th}$ iteration is

$$q_{i+1} = q_i + \dot{q}_i.\Delta t \tag{4.9}$$

– *New end-effector position* :
Hence, end-effector pose for $(i+1)^{th}$ iteration

$$x_{i+1} = f(q_{i+1}) \tag{4.10}$$

– *Iterations* :
Repeat equations 4.7 - 4.10 for N iterations.

4.7.4 Estimation of COMs

Evaluation of ZMP requires position, instantaneous velocity and instantaneous acceleration of C.o.Ms of all the individual components. To compute COMs,

– Using homogeneous transformation, position of the each joint frame F_{q_i} is determined with respect to global frame of reference
– Fixed transformation between centre of the i^{th} joint C_{q_i} and COM of the i^{th} link is identified
– COM, R of i^{th} link in environment frame of reference is computed as

$${}^{E}R_i = {}^{E}T_{F_{q_i}}.{}^{F_{q_i}}T_{C_{q_i}} \tag{4.11}$$

4.7.5 Recursive formulation of velocities and accelerations

Newton-Euler recursive formulation is used to compute joint velocities (ω) and accelerations ($\dot{\omega}$) of moving bodies. Velocities of link $(i+1)$ with respect to link i is given as:

$$^{i+1}\omega_{i+1} = {}^{i}_{i+1}R\ {}^{i}\omega_i \tag{4.12a}$$

$$^{i+1}v_{i+1} = {}^{i+1}_{i}R({}^{i}v_i + {}^{i}\omega_i \times {}^{i}P_{i+1}) + \dot{d}_{i+1}\ {}^{i+1}\hat{Z}_{i+1} \tag{4.12b}$$

Angular momentum of the each link can now be calculated using ω calculated above.

Thus, all the entities required to calculated ZMP are obtained using analytical approach. Cartesian co-ordinates of the end-effector are input to the algorithm. Calculating ZMP requires

- Inertial parameters of individual links - mass (m), moment of inertia (I)
- Angular velocity and angular acceleration of moving links
- Angular acceleration of COM of each link

4.8 Stability evaluation using Co-simulation

Cooperation of dynamic modeling and simulation tool - ADAMS (Automated Dynamic Analysis of Mechanical Systems) with the computing software MATLAB (Matrix Laboratory) is a known methodology in robotics research community. In [Angel et al., 2012], importance of co-simulation is highlighted for robotics domain by simulating 2-link planar robot. Several other notable works are also mentioned. Co-simulation combines features of both software and provides a robust and efficient tool for dynamic system analysis.

Table 4.7: Features of ADAMS and MATLAB

ADAMS	MATLAB/SIMULINK
-Modeling of Mechanical system -Importing CAD parts (e.g. CATIA) -Parameterization of design -Modeling contacts (with friction) -Applying External force -Defining input-output variables control variables -Robust Dynamic solver -Measuring output variables	-Designing control architecture using block diagrams Predefined blocks -Defining MATLAB function blocks within control model -Data logging and processing

4.8.1 Procedure of creating co-simulation model

In this section, procedure of constructing ADAMS-MATLAB co-simulation described in detail.

1. Parameterized multibody ADAMS model of the robotic unit

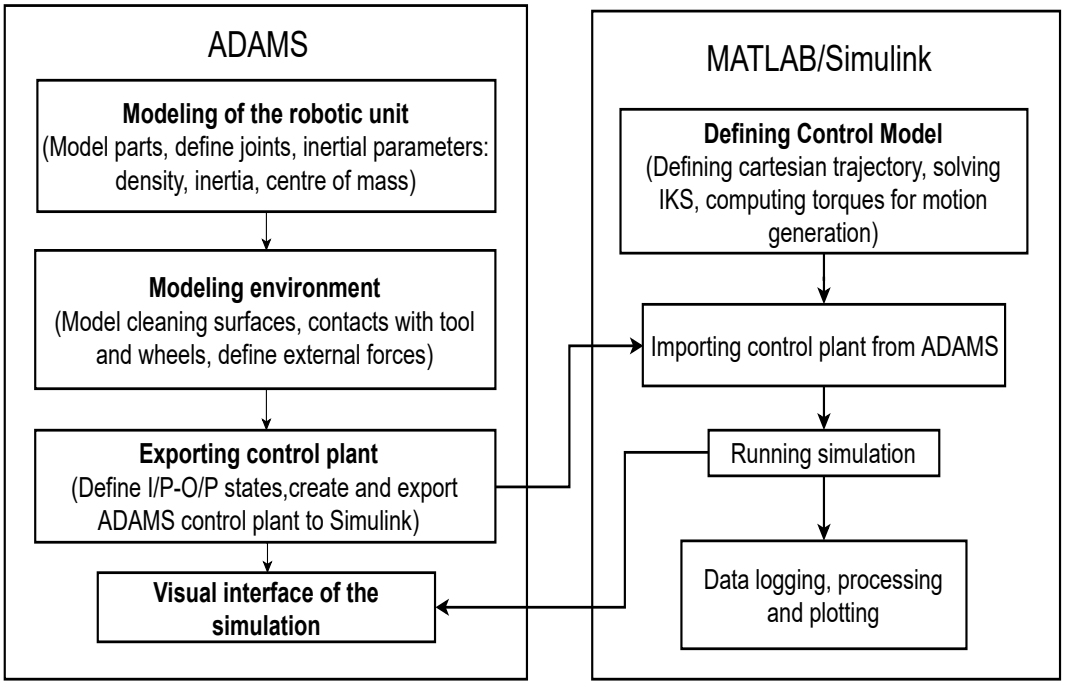

Figure 4.12: Flow-chart of ADAMS-Matlab co-simulation

(a) Direct geometric model (DGM) of the robotic arm is found using SYMORO. DGM provides pose of the each joint frame in cartesian space coordinates

(b) Using these co-ordinates, construction points are created in ADAMS environment

(c) Individual links are then built with the help of these construction points

2. Input-Output control plant

(a) State variables are assigned to each joint angle as well as CoM of the each link to track position, velocity and acceleration.These are output variables of the control scheme.

(b) Input variables consist of torques given to the joints of the robotic arm

(c) ADAMS control plant is created which is then exported to Simulink environment co-simulation purpose.

3. Control Scheme in simulink environment

(a) PID controllers are implemented at each joint angles to compute required input torques for desired motion

(b) Gravity compensation torques are added to PID generated torques to account for the effect of gravity

(c) Output coming from ADAMS i.e. joint velocities and accelerations are used for PID feedback

4. Estimation of ZMP

(a) All the necessary components to calculate ZMP are obtained in runtime through ADAMS output. While angular moments can be calculated from information available

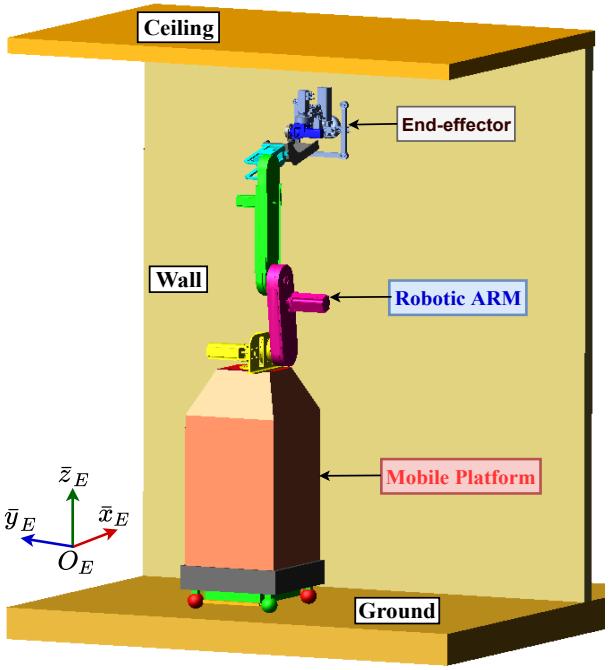

Figure 4.13: Multibody dynamic model of the Robotic Unit - V2

(b) ZMP criteria is then implemented to compute stability at each pose while performing desired motion

4.8.2 ADAMS model of the Robotic unit

It is a multi-body dynamic model positioned inside cleaning environment consisting of ground, ceiling and frontal wall (figure 4.13). Peculiarities of the model are enlisted below :

- *Part modeling* : Simple geometric shapes like sphere, cylinder, cuboid etc. are used to create multi-body model of the robotic unit. These are solid rigid bodies that can mutually interact to generate displacement, reaction forces etc. Construction of robotic arm is performed by importing parts from CATIA as .stl files (figure 4.14).

- *Parameterization* : It can be achieved through design variables (DV). They are used as an input (length, width etc.) to the geometric shapes. On changing value assigned to the DVs, geometries can be quickly modified or re-positioned in the environment.

- *Joints/motion constriants* : Prismatic and revolute joints are added to create suitable joint angles between bodies. Static components are connected using fixed joints. Joints can also be parameterized to change posture of the arm (or individual link). This is helpful in achieving suitable initial posture during co-simulation.

- *Contact modeling* : Contacts between grinding tool and cleaning surface is created to generate reaction forces. Similarly contacts between wheels of the mobile manipulator and ground surface are created to restrict motion of the robotic unit in

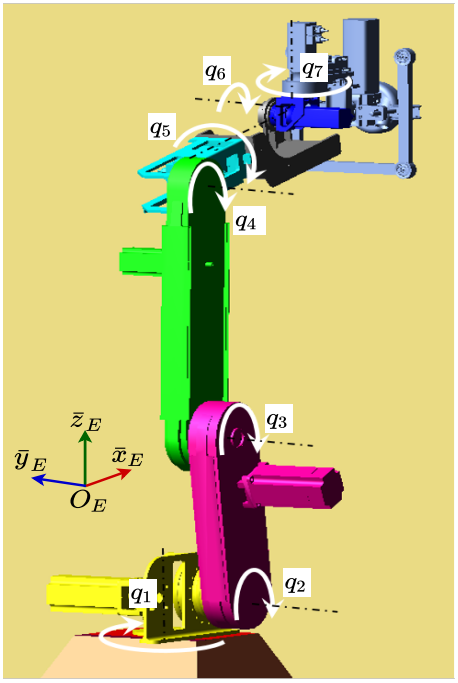

Figure 4.14: Multibody dynamic model of the Robotic Arm - V2

the plane and record ground reaction forces. Contact feature in ADAMS allows to select coefficients of static and dynamic friction.

- *Inertia parameters:* Values of mass, inertia matrix and position of COM are determined through CAD models and are added to the components.

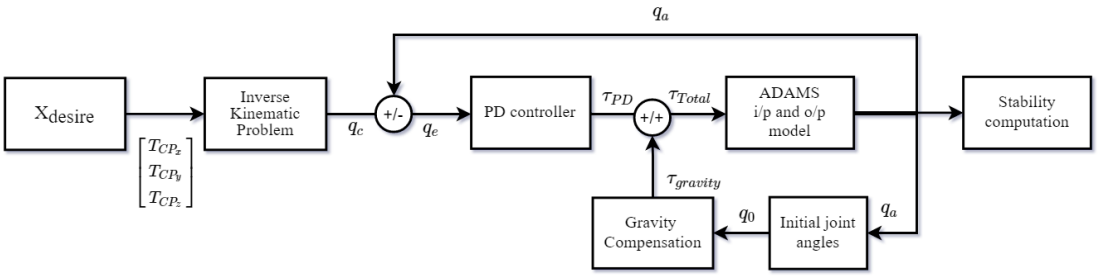

Figure 4.15: ADAMS-Simulink Control model for stability evaluation

q_c : command joint position.
q_a : actual joint position.
q_e : $(q_c - q_a)$ i.e. error in the joint position.
τ_{PD} torque generated by PD-controller.
$\tau_{Gravity}$: torque input for gravity compensation.
τ_{Total} : total torque input for joint.
T_{CP_x} : x-coordinate of the tool.
T_{CP_y} : y-coordinate of the tool.
T_{CP_z} : z-coordinate of the tool.
X_{desire} : desired Cartesian coordinates of tool centre point.

For the sake of simplification of analysis and computations conducted in the paper, following assumptions are made:

1. the ground is even and no surface shrinkage is considered;
2. the center of mass (CoM) of the platform is coincides with its center of geometry
3. all wheels are always in contact with the ground. i.e., no slippage of the wheels occurs;
4. the onboard manipulator is rigidly connected with the platform, and the links of the onboard manipulator are rigid

Conclusion

This chapter detailed the dynamic modeling of the robotic unit for stability evaluation. Initially, the robot-environment interaction model was presented to highlight the need of developing the dynamic model. Thereafter, cleaning environment and the robotic unit were described through representative frames. This representation provided a base for developing the numerical model. Using Geogebra illustrations, process of asbestos removal was analyzed to identify reaction wrench acting on the robotic unit during different cleaning scenarios namely wall, ceiling and ground.

Further, the approach for numerical evaluation of dynamic stability based on zero moment point (ZMP) was elaborated. Steps of this approach that are, kinematic modeling of the robotic unit, trajectory generation and solving inverse kinematic problem have been explained in detail. Method of co-simulation for evaluating stability was developed so as to validate the results to be obtained by the numerical approach. Multibody dynamic model of the robotic unit was developed in MSC ADAMS software which provides information on the behavior of the system (joint velocities, accelerations etc.). Control commands of this model were fed in the Simulink environment.

In the next chapter, stability evaluation approaches are utilized to investigate static and dynamic behavior of the two versions of the robotic unit.

Chapter 5

Tool path planning based on stability evaluation

Contents

This Chapter presents static and dynamic stability analyses of the two versions of the robotic unit. For Version-1, analysis is made for the two positions of the slider height to identify stability behavior for cleaning wall surface. For Version-2 three cleaning scenarios (wall, ground and ceiling) are investigated to evaluate static and dynamic stabilities. Based on this, a stable grinding trajectory for cleaning wall surface is demonstrated.

5.1 Stability conditions of the robotic unit

The arm of the robotic unit (mobile manipulator) executes several sub-tasks like end-effector positioning, aerial path traversing and/or a process like grinding, in order to perform grinding operation. These sub-tasks affect static, quasi-static or dynamic stability of the robotic. The stability conditions of robotic unit and the associated tasks are described below:

1. **Static stability condition** : Pose of the robotic unit consists of pose of the mobile base and the robotic arm integrated on the top. Since manipulator, while performing any operation undergoes significant change in pose, static stability of the mobile manipulator is majorly governed by pose of the robotic arm. Robotic unit encounters static condition in following situations during the operation :

   (a) At the start of trajectory: End-effector positioning at the starting point of the trajectory when the arm motion is about to begin.

   (b) At the end of trajectory: Trajectory is completely executed (for contact operation: the end-effector is about to be detached from the wall).

   (c) At emergency stop: In this scenario, arm is stopped suddenly and a pose that can not be predicted in prior.

   From these scenarios, it is quite clear that, robotic unit must be statically stable for all poses of the arm required to perform the operation. This underlines the important **constraint** of **static stability** to be followed at each instance during the operation.

2. **Quasi-static stability condition** : Whenever arm has low translational velocity, motion of the links in joint space can be regarded of uniform angular velocity. During such motion, stability condition of the robotic unit is quasi-static.

3. **Dynamic stability condition** : Dynamic stability condition of the robotic unit occurs during two types of operations:

   (a) **Non-contact :** When the arm is moving in air, i.e. there is no contact between end-effector and environment. However, accelerated motions of the arm generate inertial effects which affects the dynamic stability of the robotic unit.

   (b) **Contact:** In operations like grinding, end-effector (grinding tool) interacts dynamically with the environment. Reactions forces generated in the process act on the robotic unit to make is dynamically unstable. Along with, reaction forces, angular accelerations of the links during accelerated motion of the arm also contributes to dynamic effects.

5.2 Evaluation of Static stability of V1-prototype

For analysis of static stability, 25% is considered as a safe limit. This value was chosen based on the preliminary co-simulation of the robotized asbestos removal. A sample cleaning trajectory was performed to observe that below 25% the fall of stability was rapid and unrecoverable. Static longitudinal and lateral stability behavior of the V1 prototype at slider position $d = 0.9\,\text{m}$ is shown in figures 5.1 and 5.2.

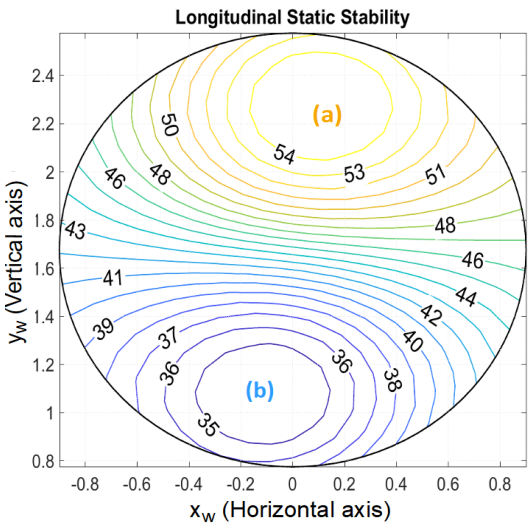

Figure 5.1: Contour: Static longitudinal stability in (%)

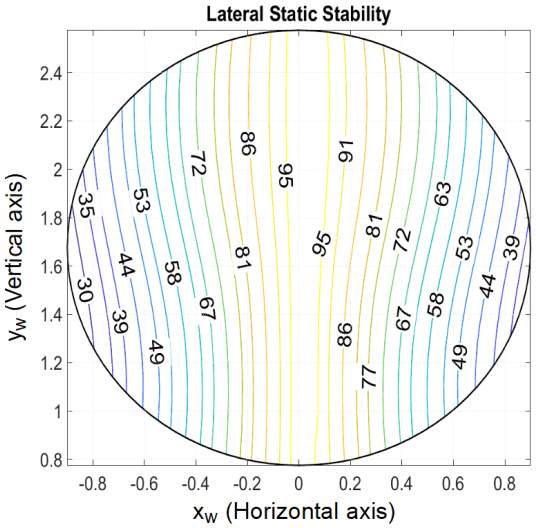

Figure 5.2: Contour: Static lateral stability in (%)

Static longitudinal stability - Figure 5.1

,Stability always stays above 25%. It is highest (54%) in the region (a) - [$y_w > 2.2\,\text{m}$ and x_w =(1.2 m, 0.8 m)]. On the other hand it is lowest (35%) at the bottom part of the map in the region (b) - [$y_w < 1.2\,\text{m}$ and x_w =($-0.4\,\text{m}, 0.2\,\text{m}$)]. Top to bottom along Y_w axis, static longitudinal stability shows a decreasing trend. Figure 5.3, shows three poses of the robotic arm at a fixed position of the mobile base. For pose (a), tool altitude is 2.45 m while for (b) it is 1 m. Table 5.1 summarizes CoMs of two long links which contribute the most in deciding overall CoM of the robotic unit. CoM projections of both links of pose (a) are less than those for link (b). Thus, longitudinal static stability of the pose (a) is higher than the that of pose (b). Here, an important conclusion is stability at a pose with higher altitude (2.4 m) of the end effector is lower than that of the lower altitude (1 m). This could appear as a counter intuitive phenomenon.

Static lateral stability - Figure 5.2

- Lateral stability has a symmetric variation about vertical axis passing through $y_w = -0.05\,\text{m}$ (see figure 5.2).

- Except for axis of symmetry (LL'), along any vertical line inside circle (C), lateral stability decreases from top to bottom. This is the result of increase in the overhanging distances of arm links from top to bottom.

- Near y_w = 0.9 m and -0.9 m blue zones indicate decrease in stability close to 40% and as low as 30%.

For accessible wall area, both the stabilities are above a critical limit.

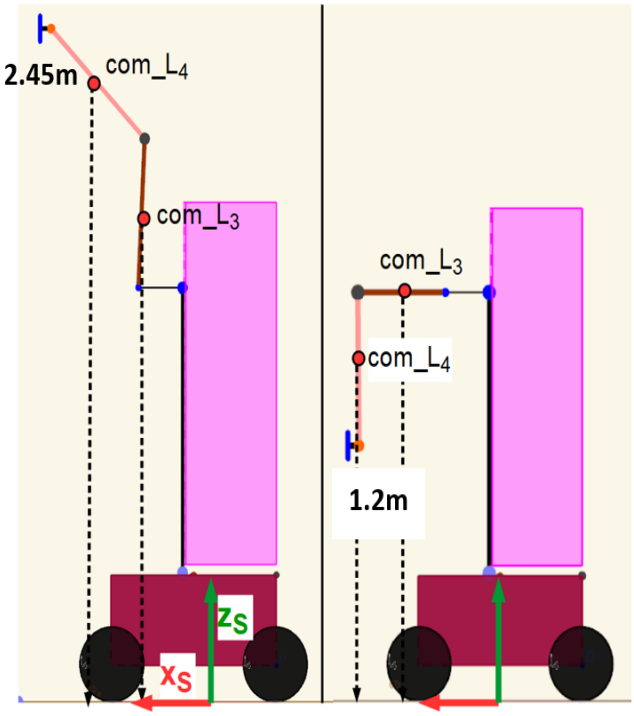

Figure 5.3: Side view: Robotic unit equipped with P-6R architecture

Table 5.1: Arm poses and corresponding stabilities

Pose	**COM**	**Coordinate (x_s in m)**	**Longitudinal Static stability (%)**
(a)	com_{L_3}	0.244	72
	com_{L_4}	0.455	
(b)	com_{L_3}	0.455	36
	com_{L_4}	0.67	

5.3 Evaluation of Static stability of V2-prototype

This section presents numerical evaluation of two static stabilities namely: static longitudinal stability (S_{Lo_s}) and static lateral stability (S_{La_s}). Method of numerical evaluation is detailed in chapter 4. It was shown that, 3D workspace of the robotic arm intersects cleaning surface in the circle (C). Thus, grid-points on the circle of intersection (wall-workspace) are input end-effector positions to the stability evaluation algorithm. Also, while computing static stability, the arm is not in the contact of environment.

Let, x_{m_k} and y_{m_k} be a points on the circle (C) which can be parameterized using polar coordinates (r, θ) as:

$$\begin{aligned} x_{m_k} &= r_m.cos(\theta_m) + x_{O_k} \\ y_{m_k} &= r_m.sin(\theta_m) + y_{O_k} \end{aligned} \tag{5.1}$$

where, $k = \{w, c, g\}$ i.e. wall, ceiling or ground (depending on surface being cleaned).

Variation of $r\epsilon[0\ , r_{max}]$ and $\theta\epsilon[0\ , 2\pi]$ with yield end-effector positions $(x_{m_k}, y_{m_k})\epsilon C$ and each of the position corresponds to a pose of the robotic arm. Here, r_{max} is the radius of circle (C) and its value depends the dimension of link lengths.

5.3.1 Wall scenario

This section identifies static stability behavior of the V2 prototype for wall scenario. For given (x_{m_k}, y_{m_k}), the arm is actually not in the contact with the wall but has the pose that will be acquired by the arm while performing cleaning operation.

Figure 5.4 shows three different poses of the robotic arm at constant elevation (Y_w) through sub-figures (a)-(f). Figures (a)-(c) show front-top isometric view whereas figures (d)-(f) show top views. Figure (a) shows robotic arm at co-ordinates (-1.38, 2.45) in wall frame of reference. Pose of the Links L_1-L_6 determine CoM of the arm.

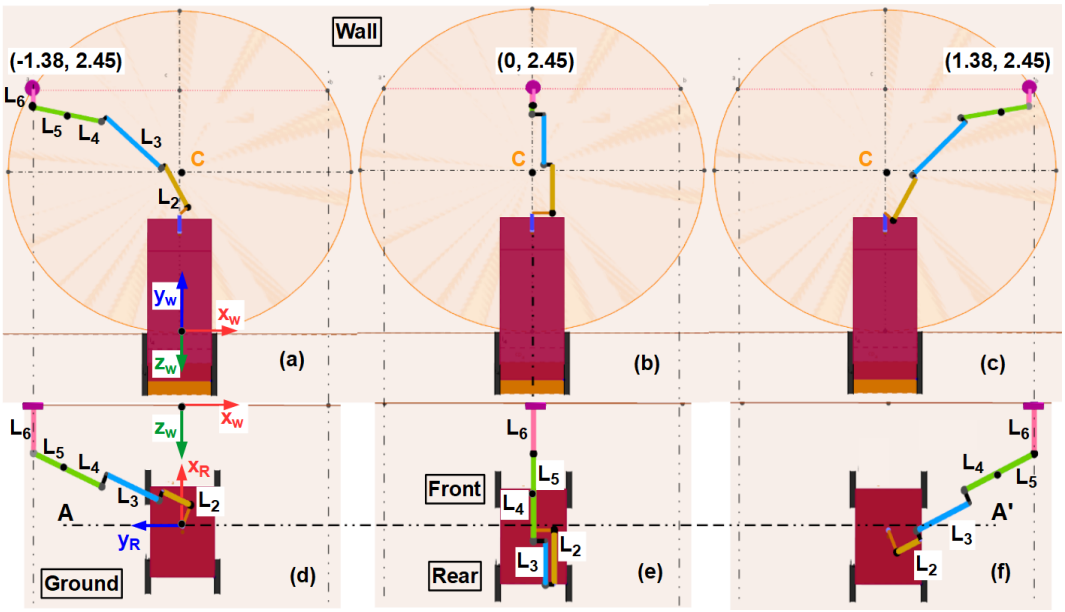

Figure 5.4: Three poses of the mobile manipulator at constant $y_w = 2.45\,\text{m}$

Comparison of poses shown in (d)-(f) reveals why longitudinal stability is affected for laterally varying poses. In figure (e), links L_2 and L_2 lie below axis AA'. Stability at this place is 84%. On the other hand, pose shown in (f) is symmetric to pose (d) around $y_w = 0$. However, static longitudinal stabilities for these symmetric poses are not equal. Poses (f) and (d) have stabilities (46%) and (72%) respectively. The reason for difference in the stability of two poses is the difference in the position of links with respect to axis AA'. For the pose (d) all the links lie above AA' while in the case of (f), link L_2 lies on the below AA'. The arm is more extended longitudinally in pose (d) that (f). Thus, it can be concluded that, closer the links to axis AA', better is the longitudinal stability.

Figures 5.5 and 5.6 present contour maps of the static longitudinal and lateral stabilities.

Static longitudinal stability - Figure 5.5

Numerical evaluation of static longitudinal stability for wall cleaning scenario is plotted in figure 5.5. x_w and y_w are axes of the wall frame of reference. Important observations of the contour plot are detailed below:

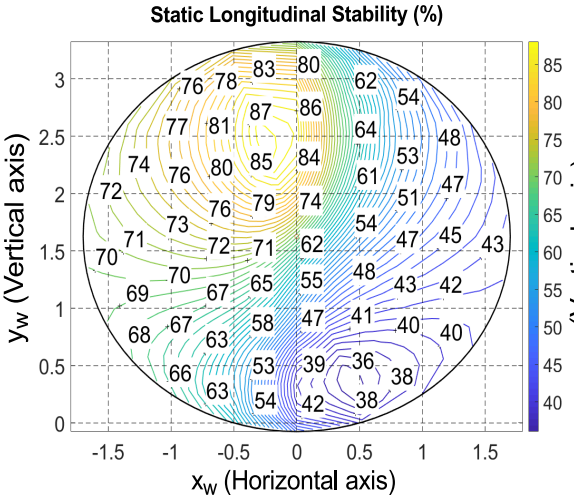

Figure 5.5: Contour: Static longitudinal stability - Wall scenario

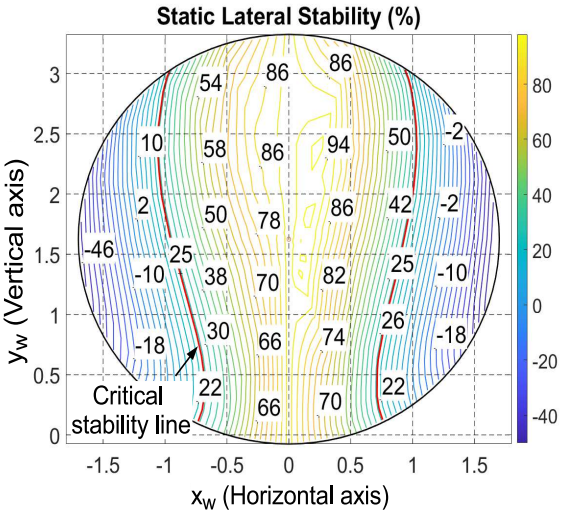

Figure 5.6: Contour: Static lateral stability - Wall scenario

– Static longitudinal stability is dependent on the position of CoM of the each link with respect to the robot frame of reference ($\mathcal{F}_R$)

– A maximum value of (84%) of static longitudinal stability occurs in the vicinity of x_{m_w} =-0.25, y_{m_w} = 2.5. while the minimum (35%) occurs around x_{m_w} = 0.5, y_{m_w} = 0.5.

– At a given y_w, on both sides of $x_w = 0$, S_{Lo_s} shows a decreasing trend. This happens due to the extension of arm links along longitudinal axis while reaching lateral distances.

Static lateral stability - Figure 5.6

– Maximum static lateral stability (S_{La_s}) is highest near to axis $y_w = 0$ line.

– It decreases along both sides of this axis due to lateral extension of the arm. Since poses of the robotic arm are not symmetric around this axis while reaching equidistant points, variation of stability is not symmetric either.

– Further, away from both sides of axis, it decreases to reach zero making those areas unsuitable for cleaning.

– Lateral stability is higher when y_{m_w} is higher. This behavior is a results of higher lateral extension of arm at lower y_{m_w}.

5.3.2 Ceiling scenario

Ceiling forms the second most frequent area to be cleaned inside the cleaning environment. Figures 5.7 and 5.8 present contour plots of static longitudinal and lateral stabilities respectively.

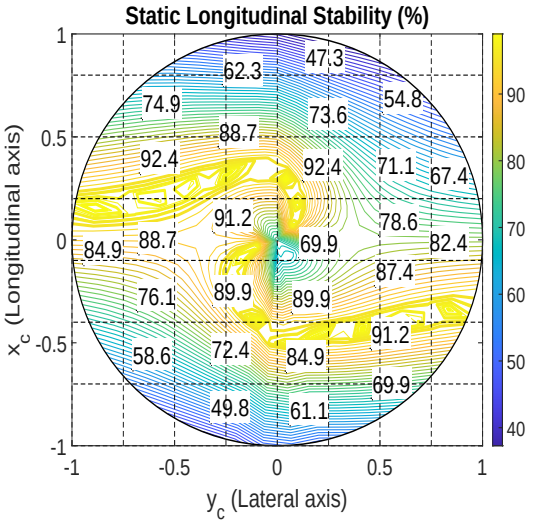

Figure 5.7: Contour: Static longitudinal stability - Ceiling

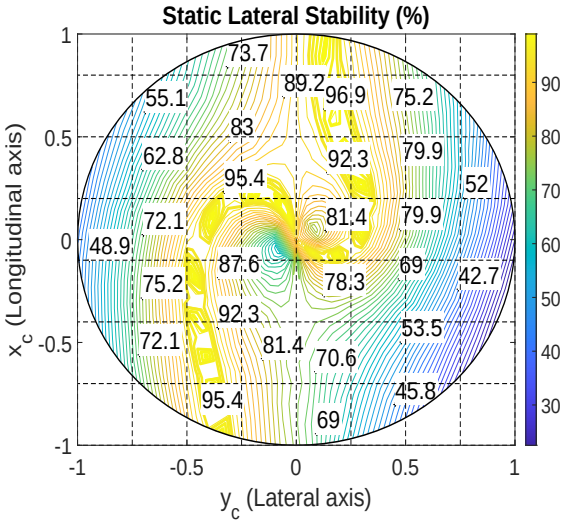

Figure 5.8: Contour: Static lateral stability - Ceiling

Static longitudinal stability - Figure 5.7

- Figure 5.7 shows contour plot of static longitudinal stability in percentage for ceiling scenario. Radius of the ceiling accessed is 1m.
- Static longitudinal stability is above the critical limit of 25% all over the accessed area.
- Maximum stability zones are highlighted in respective figures for both lateral and longitudinal stabilities.
- In case of longitudinal stability, maximum stability zone is a s-shaped curve with axis indicated in figure 5.7.

Static lateral stability - Figure 5.8

- Static lateral stability too shows a stable behavior over the area accessed as shown in figure 5.8.
- Maximum lateral stability zone is a s-shaped curve highlighted in figure 5.8 .

Thus, it can be concluded that in case of ceiling scenario, robotic unit is always stable.

5.3.3 Ground scenario

Cleaning ground surface is a special case where the accessible workspace is limited by the presence of mobile base. Since, rear side of the robotic unit has a power supply cable and other ancillaries, is not entirely safe to access rear area.

Static longitudinal stability - Figure 5.9

- Figure 5.9 presents static longitudinal stability for ground cleaning scenario. For cleaning at front and rear sides of the mobile base, stability is minimum since pose of the arm is extended in longitudinal direction.

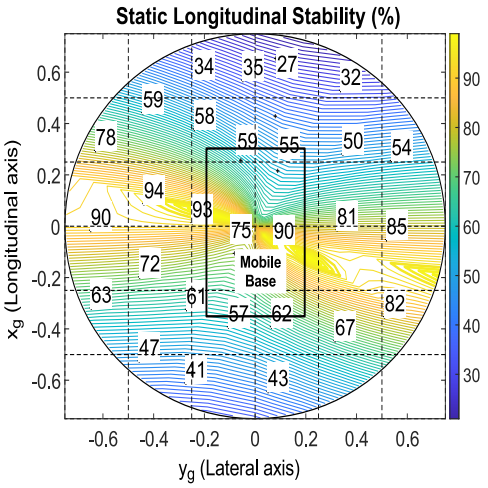

Figure 5.9: Contour: Static longitudinal stability - Ground

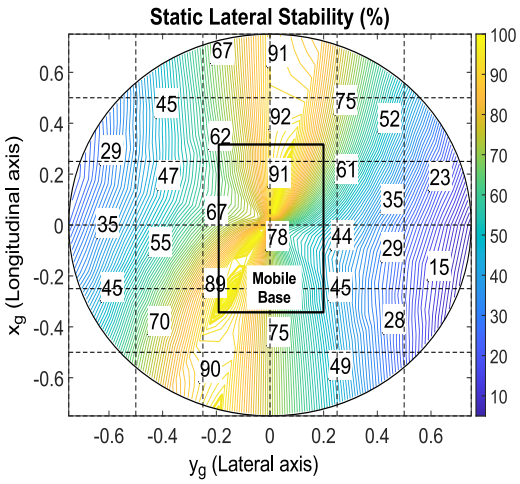

Figure 5.10: Contour: Static lateral stability - Ground

– However, along lateral axis ($x_c = 0$) this behavior is mostly stable.

– The arm poses required to clean ground surface are close to singularity. Also, availability of better machines weakens the case of using this arm for ground cleaning.

Static lateral stability - Figure 5.10

– Figure 5.10 shows static lateral stability. Contrary to longitudinal stability, lateral stability is higher while for front and rear poses.

– Inclined zone of cleaning occurs due to offset of arm link-1.

5.3.4 Statically stable task workspace

To satisfy the constraint of static stability throughout the operation, a region must be identified on the cleaning surface where both, lateral and longitudinal static stabilities are above critical limit. Since static longitudinal stability always stays above the critical limit, stable task workspace is determined by looking at the static lateral stability map. Area beyond zero lateral stability is unsuitable for cleaning.

From figure 5.11, a stable zone having lateral and longitudinal stability margin greater than zero percent is highlighted in figure 5.11. Here, the line $y_w = 3$ indicates ceiling height and hence the stable zone is clipped at this height. Even though stability of robotic unit is ensured above zero inside this region, it is important to note that, CoM is quite close to the edge of the support polygon when stability is near zero and hence a safety margin is necessary. **Area inside the statically stable task workspace does not ensure stability while performing the operation. It ensures for any pose of the arm that the robotics unit takes up inside this workspace, it will always be statically stable (if operation is stopped in the middle of the process)**

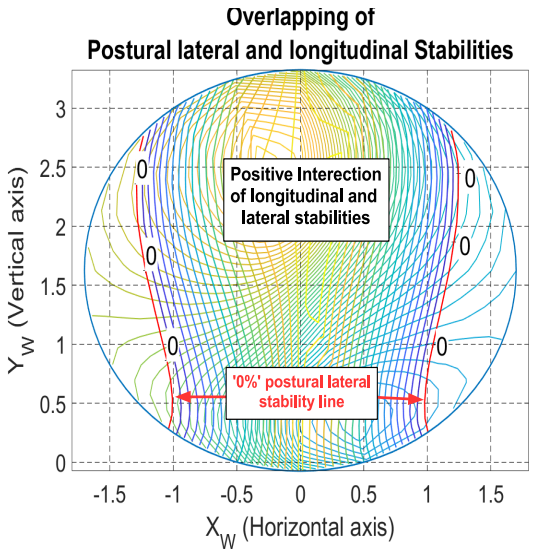

Figure 5.11: Contour: Postural longitudinal stability

5.4 Evaluation of dynamic stability of V1-prototype

For P-6R architecture, slider height (h) plays a role in governing altitude of the cleaning tool. It governs normal distance z_d between tool center point and origin of reference frame F_s that is responsible for pitch and roll motions of the robotic unit. Here we evaluate longitudinal and lateral stabilities at two different slider heights h = 1.075 m and 1.675 m. By applying accelerations in $\pm x_w$ and $\pm y_w$ directions following results are obtained.

Dynamic longitudinal stability for grinding motion

Longitudinal stability maps are shown through figures (5.12 - 5.15).

- **Motion in $+y_w$, $h = 1.675$ m:** Here, tangential reaction force acts along -y_w. Moment $+M_{y_s}$ responsible for longitudinal stability decreases from top to bottom due to decrease in distance z_d (figure 5.12) decreasing the stability. Maximum stability is 57% at $y_w = 2.2$ m and minimum stability is 29% below $y_w = 1.2$ m.

- **Motion in $-y_w$, $h = 1.675$ m:** Tangential reaction force acts along $+y_w$ and moment $-M_{y_s}$ now pushes ZMP along $-x_E$, that is towards center of the support polygon. Thus, longitudinal stability at respective points for motion along $-y_w$ is greater than that for motion along $+y_w$ (see figure 5.13).

- **Motion in $+y_w$, $h = 1.075$ m:** From the two slider heights, $y_w = [1.8\,\text{m}, 0.8\,\text{m}]$ is a common accessible area. However, static stabilities of the arm poses from h = 1.075 m (see figure 5.14) to access this common area are less stable than those from h = 1.675 m (see figure 5.12). Thus, even the disturbing moment M_{y_s} is lower in case of 1.075 m than h = 1.675 m, longitudinal stabilities are respectively lower while accessed from h = 1.075 m. Red contour in the figure (5.14) shows 25% stability line below which stability is critical.

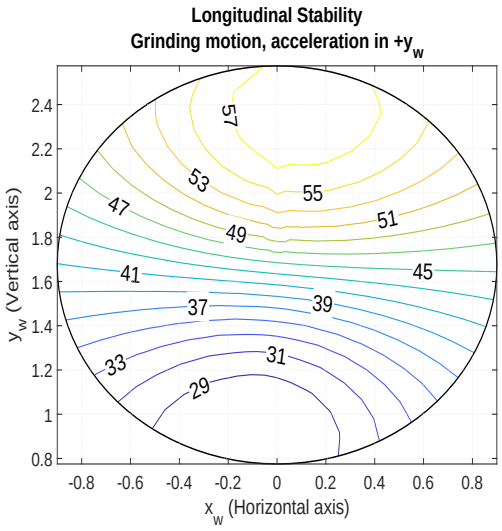

Figure 5.12: Dynamic longitudinal stability of prototype V1 when tool grinds towards $+y_w$, h = 1.675 m

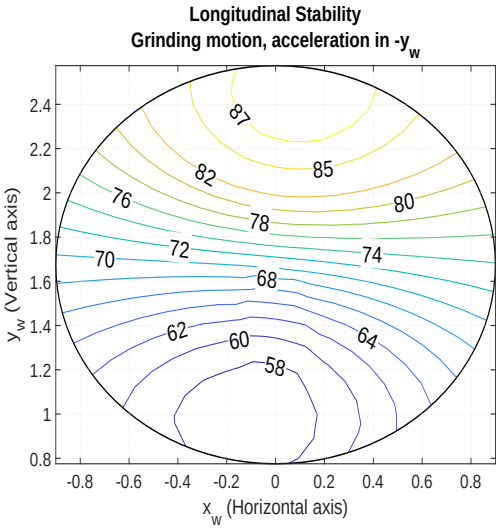

Figure 5.13: Dynamic longitudinal stability of prototype V1 when tool grinds towards $-y_w$, h = 1.675 m

– **Motion in** $-y_w$**,** $h = 1.075$ m**:** In this case, tangential reaction force acting along $+y_w$ generates a supporting moment $-M_{y_s}$. Thus the stability is higher than the case before (see figure 5.15)

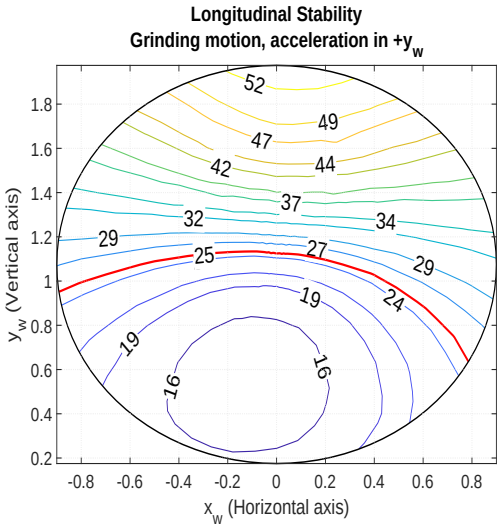

Figure 5.14: Dynamic longitudinal stability of prototype V1 when tool grinds towards $+y_w$, h = 1.075 m

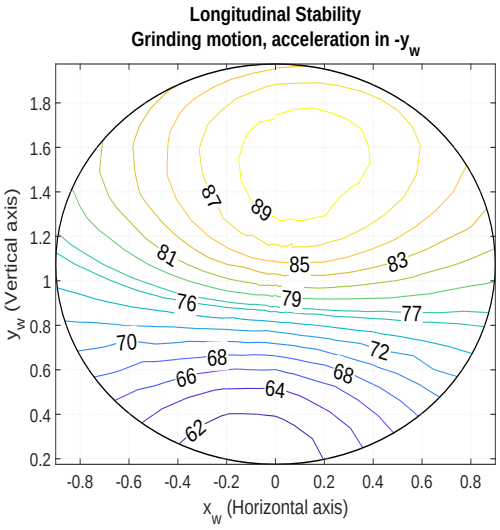

Figure 5.15: Dynamic longitudinal stability of prototype V1 when tool grinds towards $-y_w$, h = 1.075 m

Dynamic lateral stability for grinding motion

Lateral stability is plotted for two slider configurations i.e h = 1.675 m and h = 1.075 m. Differences in the stability maps are analyzed below:

- **Motion in $+x_w$, $h = 1.675\,\text{m}$:** Tangential force acts along $-x_w$ pushing ZMP towards edge S_1S_2 of the polygon. Thus, area on the right of $x_w = 0$ line is stable. However area on the left contains a red line that defines 25% stability limits. In the region $x_w < 0$, ZMP is pushed towards S_1S_4, decreasing the later stability below 25% as shown in figure 5.16.

- **Motion in $-x_w$, $h = 1.075\,\text{m}$:** Similar pattern of lateral stability is observed as earlier case. However, since distance y_E is lower due to lower h, unstable area is reduced as indicated by red contour in figure 5.17.

- **Motion in $+x_w$, $h = 1.675\,\text{m}$:** Tangential force acts along $+y_w$ direction creating moment M_{x_s} that tends to move ZMP towards edge S_1S_2 of the support polygon. Figures (5.18) and (5.19) show lateral stability maps at two different slider heights. opposite to what observed in the case of motion along x_w, at slider height h = 1.675 m, stable area available for cleaning are larger than for this slider height.

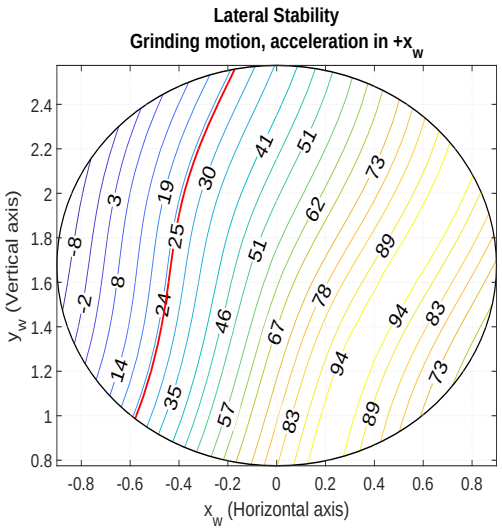

Figure 5.16: Dynamic lateral stability of prototype V1 when tool grinds towards x_w, h = 1.675 m

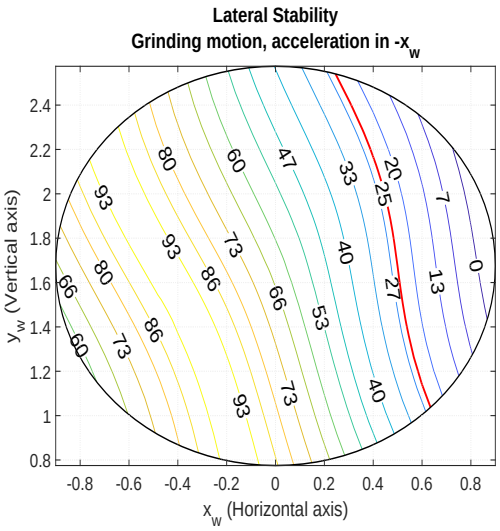

Figure 5.17: Dynamic lateral stability of prototype V1 when tool grinds towards $-x_w$, h = 1.675 m

5.5 Evaluation of dynamic stability of V2-prototype

Evaluation of dynamic stability aims to ensure not only safety but also operational productivity of the robotic unit which can be quantified in terms of time taken to complete the operation. It is positively affected by translational and rotational velocities of the end-effector. However, higher values of $v_{t_{max}}$ tend to largely affect stability. Thus, association of stability and operational efficiency must be studied while performing task planning.

5.5.1 Stability for accelerated motions without contact - wall scenario

This is a scenario where robotic unit is performing an application of spray painting, or watering walls etc. In such applications, robotic arm performs accelerated motions

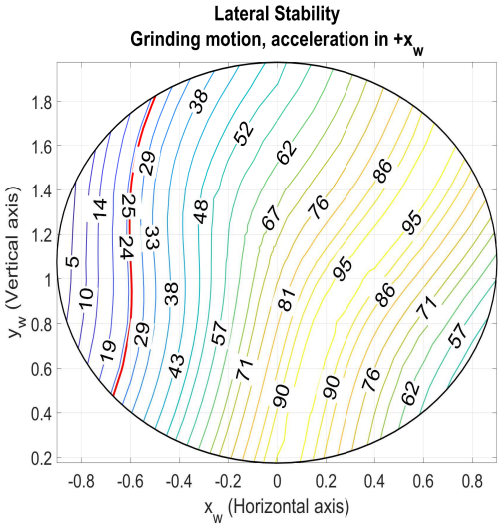

Figure 5.18: Dynamic lateral stability of prototype V1 when tool grinds towards x_w, h = 1.075 m

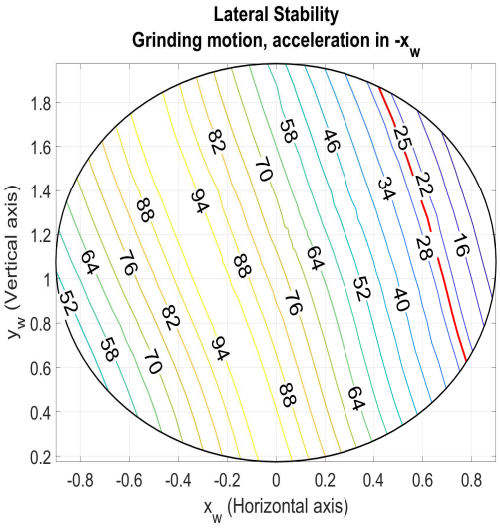

Figure 5.19: Dynamic lateral stability of prototype V1 when tool grinds towards $-x_w$, h = 1.075 m

without touching the wall (environment). Thus, grinding like reaction wrench is absent and the dynamic effect due to accelerated motion and pose of the robotic arm play role in deciding stability.

- **Motion along $+y_w$:** Longitudinal stability is above a critical value of %25 over entire area. Decreasing trend from top to bottom along tilted axis is observed (figure 5.20).
- **Motion along $-y_w$:** Longitudinal stability is above a critical value of %25 over entire area but has lower values compared to the case above. This is due to inertial force creating destabilizing force while tool accelerates along -y_w (figure 5.21).
- **Motion along $+x_w$:** Lateral stability is approximately symmetric about $x_w = 0$. For $x_w < 1.5$ m, the value drops below critical value of 25% when $x_w < -0.7$ or $x_w > 0.7$ (figure 5.22).
- **Motion along $-x_w$:** Similar trends are observed for this motion as for the above case (see figure 5.23).

5.5.2 Stability for accelerated motions with contact

To generate these maps, each point inside the safe static zone is accelerated along two principle axes: y_w, x_w. The two axes are chosen by keeping in mind directions required to generate horizontal and vertical zigzag trajectories. These maps are intended to identify dynamic behavior of the robotic unit for accelerations in the principal axes.

Dynamicstability for grinding motion

Longitudinal stability is largely affected by motion of the tool in $\pm y_w$ direction. As described in chapter 3, tangential reaction force acting in the opposite direction of the tool motion.

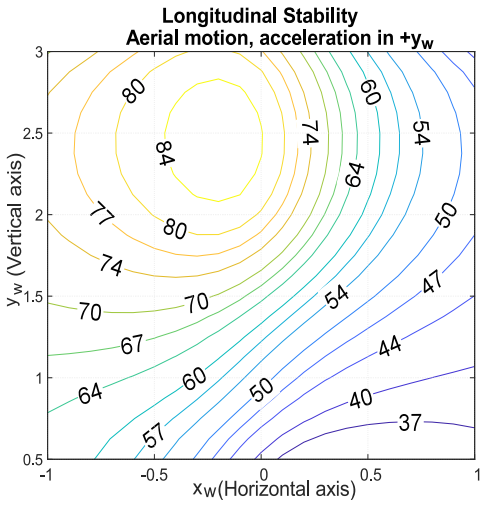

Figure 5.20: Dynamic longitudinal stability of prototype V2 for tool motion in the air along $+y_w$

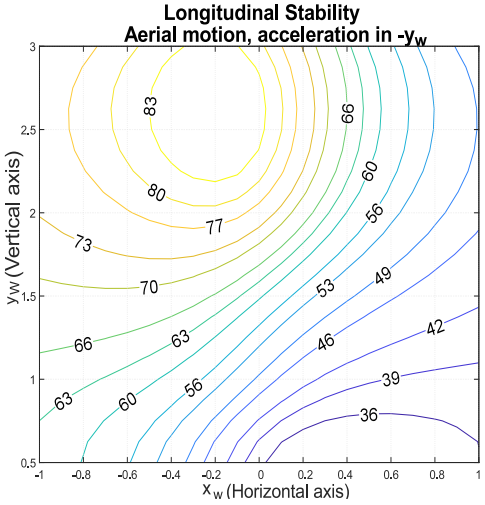

Figure 5.21: Dynamic longitudinal stability of prototype V2 for tool motion in the air along $-y_w$

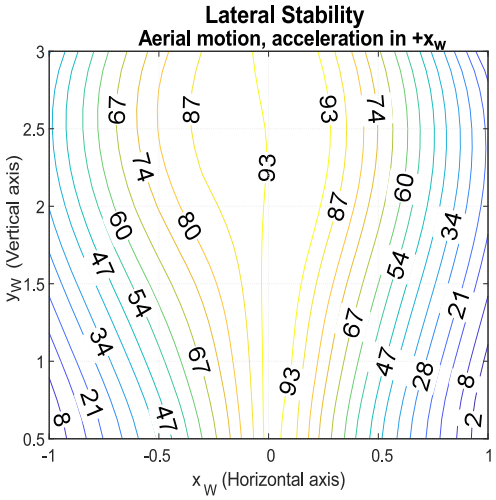

Figure 5.22: Dynamic lateral stability of prototype V2 for tool motion in the air along $+x_w$

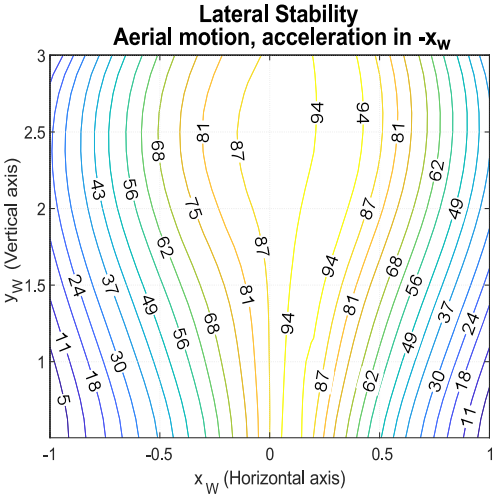

Figure 5.23: Dynamic lateral stability of prototype V2 for tool motion in the air along $-x_w$

– **Motion along** $+y_w$: For motion in $+y_w$ direction, tangential reaction force is in $-y_w$ direction. Figure 5.24 shows, at higher values of y_w, longitudinal stability is higher and vice a versa. This forces ZMP to move towards front edge of the support polygon reducing stability.

– **Motion along** $-y_w$: For motion in -y_w direction, tangential reaction force is in $+y_w$. direction and the resulting moment pushes ZMP to move towards center of the support polygon. Hence a stability as high as 96% observed in figure 5.25.

– **Motion along** $+x_w$: For this motion, tangential forces are along $-x_w$. The two red lines denoted in 5.26 define the critical limit. of 25%. The lines are not parallel to

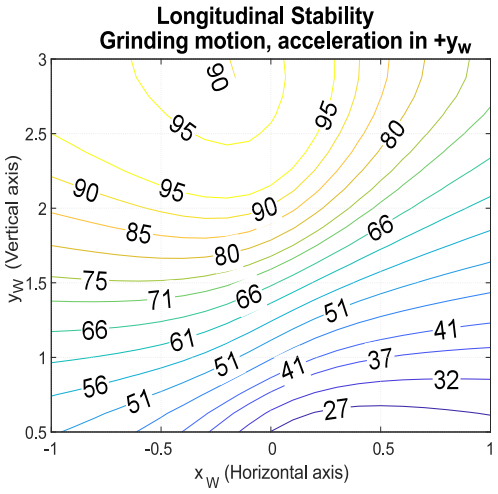

Figure 5.24: Dynamic longitudinal stability of prototype V2 when tool grinds towards $+y_w$

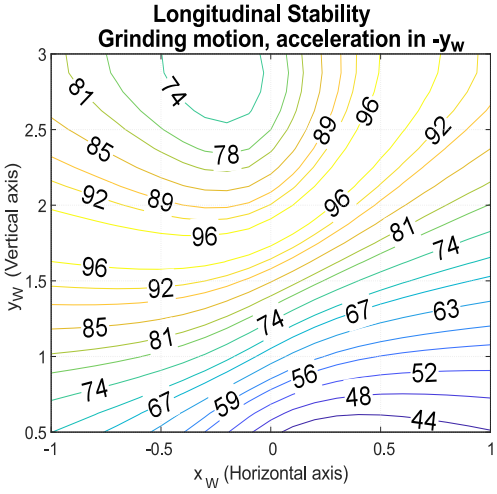

Figure 5.25: Dynamic longitudinal stability of prototype V2 when tool grinds towards $-y_w$

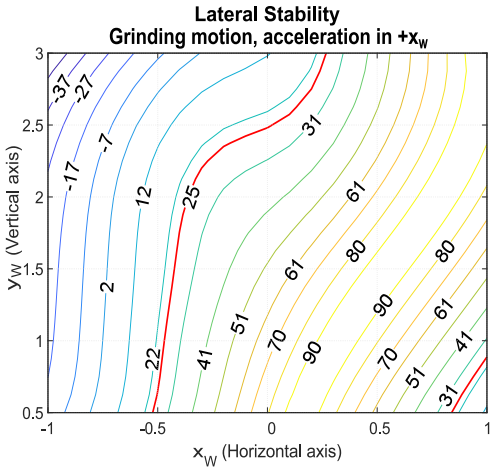

Figure 5.26: Dynamic lateral stability of prototype V2 when tool grinds towards $+x_w$

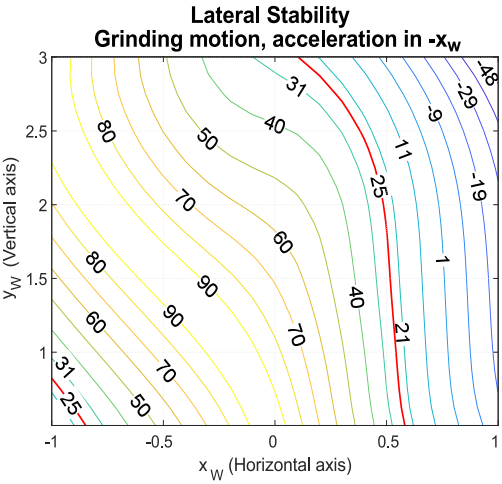

Figure 5.27: Dynamic lateral stability of prototype V2 when tool grinds towards $-x_w$

y_w axis. This hints towards difficulty in achieving coverage path planning.

– **Motion along** $-x_w$: For this motion, tangential forces are along $+x_w$. The two red lines of 25% stability are indicated in figure 5.23. Reduction in the area of laterally stable zone is visible similar to previous case.

5.6 Kinematic performance indices

Manipulability index (w) proposed by [Yoshikawa, 1985] provides a quantitative measure of closeness of the robotic manipulator to a state of singularity. Manipulability

is widely used for achieving optimal control performance of kinematically redundant manipulators.

Condition number of the kinematic jacobian matrix is used as an index to describe accuracy, dexterity as well as closeness to the singularity of the given pose. Ill conditioned jacobian has low maneuverability which implies need of high joint torques to obtain even a small velocity output of the end-effector [Tsai and Chiou, 1990]. Inverse of condition number (κ^{-1}) is bounded between $[0 \quad 1]$ where the value of 1 indicates condition of isotropy.

5.6.1 Wall scenario

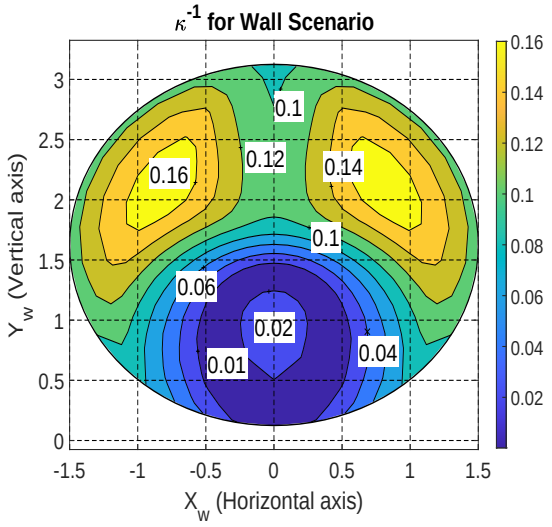

Figure 5.28: Inverse of condition number (κ^{-1}) for wall scenario

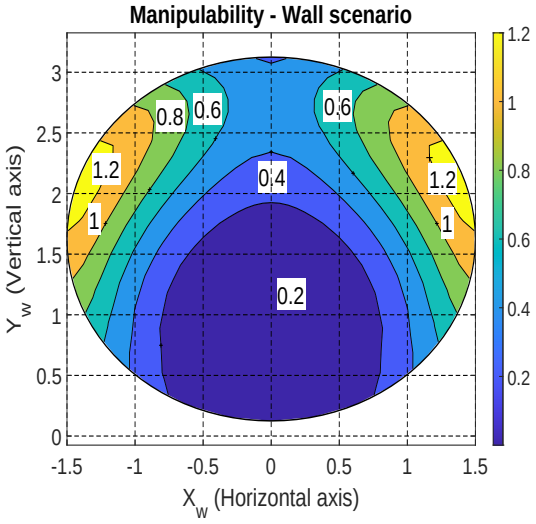

Figure 5.29: Manipulability (w) for wall scenario

Figure 5.28 presents a contour plot of distribution of (κ^{-1}) over wall accessible workspace. As can be seen from the figure, it is symmetric about $X_w = 0$. Value of κ^{-1} lies above 0.1 for $Y_w > 1.5\,\text{m}$ and goes below 0.1 for $Y_w < 1.5\,\text{m}$.

Manipulability index (w) shown in figure 5.29 implies a trend similar to that of the (κ^{-1}). A central region around $Y_w = 1.5m$ has the lowest value of w. It is noteworthy that, w shows a higher value near boundary of the stable accessible workspace (which is not a boundary of the total accessible workspace) on lateral sides.

5.6.2 Ceiling scenario

Figure 5.30 shows (κ^{-1}) contour for ceiling scenario that is symmetric about $Y_c = 0$. The index has the lowest value (0.02) in the center. This clearly indicates that the pose of the robotic arm is near singularity. For the area defined by $X_c = [-1 \quad 1]$ and $Y_c = [-0.375 \quad 0.375]$. Beyond this area value of (κ^{-1}) gradually increases on both sides indicating, arm is now moving away from singularity.

Manipulability index (w) for ceiling scenario is shown in figure 5.31. Similar to κ^{-1}, manipulability is symmetric about $Y_c = 0$ and has lowest value located near center and increases gradually on both sides of $X_w = 0$.

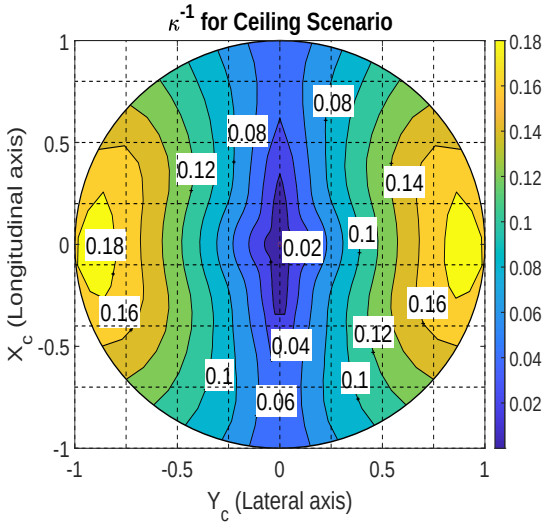

Figure 5.30: Inverse of condition number (κ^{-1}) for ceiling scenario

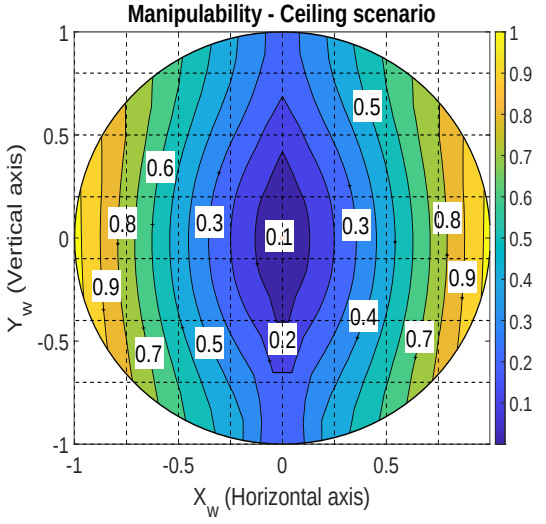

Figure 5.31: Manipulability (w) for ceiling scenario

5.6.3 Ground scenario

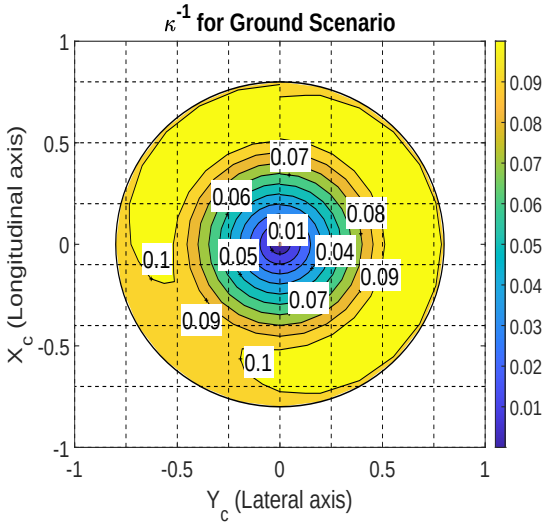

Figure 5.32: Inverse of condition number (κ^{-1}) for ground scenario

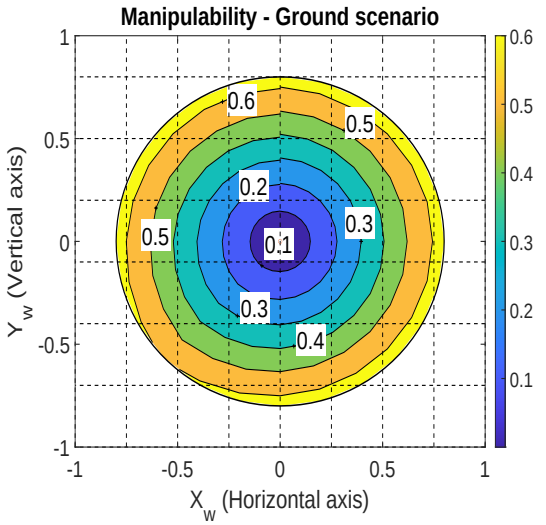

Figure 5.33: Manipulability (w) for ground scenario

For ground cleaning scenario, both inverse of condition number κ^{-1} (figure 5.32) and manipulability w (figure 5.31) have gradually increasing concentric circles. The central area is obviously occupied by mobile base. Beyond that, condition number doesn't increase significantly and the maximum value reached is 0.1. Manipulability however, shows a good rise in the value. Yet, cleaning ground is not a promising scenario due to low value of κ^{-1}.

5.7 Stability based trajectory using Version-1 prototype

This section demonstrates a grinding trajectory using Version-1 prototype [Maraje et al., 2019]. Since, most of the cleaning walls are rectangular in shape, we assume a rectangle of dimensions (1.38 m × 1.13 m) inside circle (C). Here, slider height is h = 1.675 m. Robotic unit is placed in at a distance of 0.75 m from the cleaning wall.

Dynamic stability conditions

Important conclusions of the dynamic analysis of Version-1 prototype are recalled below.

- Figure 5.16 shows that when the tool moves along x_w, a red line of critical lateral dynamic stability appears in the region $(x_w < 0)$ while the region $(x_w > 0)$ is dynamically stable.
- Similarly, figure 5.17 shows when the tool moves along $-x_w$ direction, the region $(x_w < 0)$ is dynamically stable while portion of the area from $(x_w > 0)$ develops instability.
- Figures 5.12 and 5.13 imply that at this slider height, dynamic longitudinal stability is above the critical limit of %25. Thus, motion of the tool in both $\pm y_w$ directions is permitted.

Conditions of motion

The conclusions derived above yield important conditions of motion.

- For motion along axis x_w in the region $(x_w < 0)$, the tool direction should be along $-x_w$.
- For motion along axis x_w in the region $(x_w > 0)$, the tool direction should be along $+x_w$.

Grinding trajectory

From these two conditions. The continuous path E_1-E_2 is divided into two sub-paths (see figure 5.35):

(i) **SE_1**: While tracing this path the tool moves in the region $(x_w < 0)$ and direction of the motion is along $-x_w$.

(ii) **SE_2**: While tracing this path the tool moves in the region $(x_w > 0)$ and direction of the motion is along $+x_w$.

Validation of stability

To perform the grinding trajectory, multibody dynamic model of the Version-1 prototype was made in ADAMS software (see figure 5.34). Figure 5.36 shows front half of the support polygon. Axis AB defines the front axle. The black dotted lines are 25% stability lines. The figure shows variation of ZMP obtained for the cleaning trajectory. The black line shows ZMP trace calculated using numerical approach while the pink line traces ZMP from cosimulation. The approximate overlapping of the two traces validates the numerical approach.

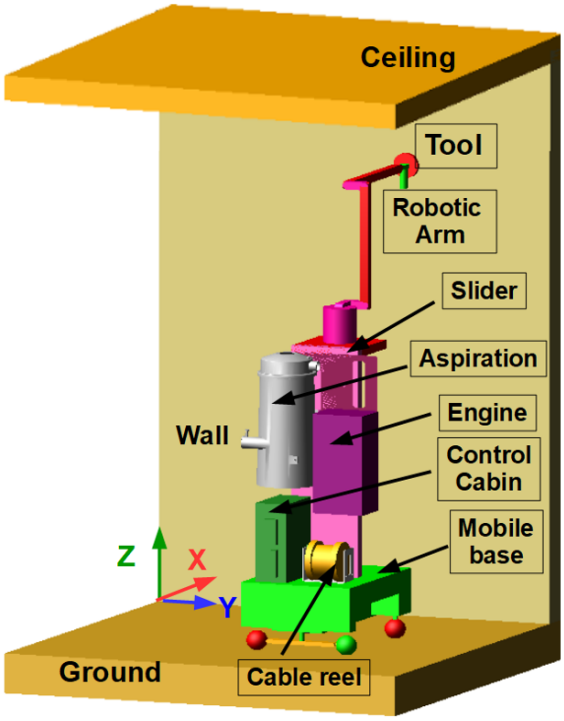

Figure 5.34: Multibody dynamic model of the Version-1 prototype

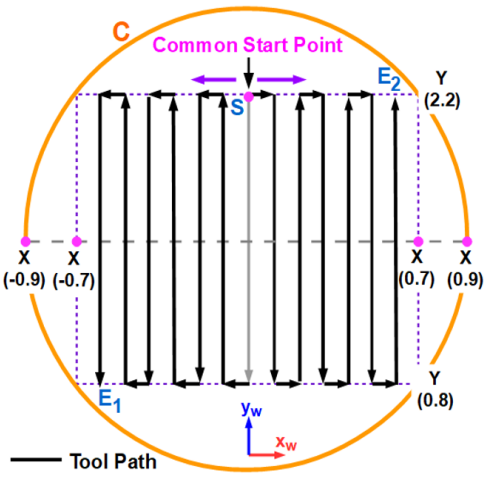

Figure 5.35: Path traced by tool on the wall

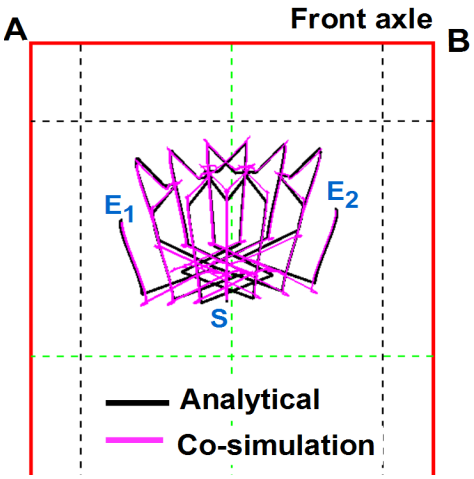

Figure 5.36: ZMP estimation through analytical and co-simulation

Conclusion

This chapter presented stability analyses of the two prototype versions. Firstly, static stability of Version-1 prototype having an arm of P6R kinematics (6R robotic arm mounted on the vertical slider) was evaluated. This version showed a stable static longitudinal and lateral behavior throughout the accessible surface. Dynamic analysis performed at two different slider heights revealed occurrence of lateral instabilities.

Version-2 prototype that has 7R redundant kinematic arm was statically analyzed for three cleaning scenarios (wall, ground and ceiling). This version was found to have limited static lateral stability for the wall case. For the ceiling case, static stability was

always maintained. However, the ground case turned out to be unsuitable for cleaning due to instabilities and reduction in the accessible area due to presence of the mobile base. Dynamic analysis of this version revealed reduction in the surface available for cleaning due to loss of dynamic lateral stability.

Finally, a stable grinding trajectory using Version-1 prototype was demonstrated. The traditional continuous zigzag path was split into two sub-paths based on the conditions of motion derived from dynamic analysis. Numerical evaluation of stability was validated through cosimulation.

Conclusions and future work

This chapter summarizes contributions and conclusions of the thesis and invokes perspectives.

Synopsis

The primary focus of this doctoral thesis was structural selection of the arm kinematics and stability management of the robotic unit while performing asbestos removal operation from real world rehabilitation sites.

Initially, the use-case of manual asbestos removal was reviewed to study the cleaning environment. The study led to formulate requirements and constraints imposed by the cleaning environment on the robotized asbestos removal. Design rules were inferred from requirements and a redundant P-6R kinematics (i.e. 6R anthropomorphic arm mounted on a vertical slider) was selected and integrated with the mobile base. Moreover, dimensional synthesis of the arm was performed to satisfy critical constraints such as tall ceiling height, narrow entry door and cleaning in narrow corridors. The prototype resulting from the integration of P-6R with the mobile compact base was called Version-1 prototype. It was shown that the arm had a sufficient workspace to access ground, wall and ceiling from the given pose of the mobile base. As Version-1 was not optimal in terms of compactness, a Version-2 was proposed with a 7R arm kinematics preserving the volume of the control box and more suitable for ground cleaning around the mobile base and wall cleaning in narrow corridors.

Further, the robot-environment dynamic interaction model was presented and the need to create dynamic simulation was emphasized. This was followed by geometric modeling of the cleaning environment consisting of wall, ceiling and ground. Thereafter, the effect of grinding reaction forces on the dynamic stability of the robotic unit for three cleaning scenarios was identified. Based on this a numerical methods for stability assessment was proposed to evaluate the dynamic stabilities of two versions of the robotic unit. Additionally, a co-simulation model (multibody dynamic simulation software + numerical solver) was developed to validate the numerical approach.

Stability analysis consisted of studying static and dynamic stabilities of the two versions for the three cleaning scenarios. Kinematic performance indices- (manipulability and inverse of condition number) were evaluated to assess suitability of the arm in different cleaning scenarios. This revealed difficulties in cleaning ground while both the prototypes showed acceptable performance for cleaning the wall and the ceiling. The analysis led to identify cleaning directions which comply with the longitudinal and lateral stability requirement. In the end, cleaning of the wall surface using stable cleaning trajectories was demonstrated.

Contributions

1 Structural selection and dimensional synthesis of the robotic arm

Structural selection and dimensional synthesis of P-6R (that is a 6R manipulator mounted on a vertical slider) was presented in Chapter 3.

1.1 Asbestos removal use case was geometrically modeled using an interactive geometric software (Geogebra). This allowed to formalize 11 requirements from which were derived 8 design rules.

1.2 The two long links (arm and fore-arm) were designed sufficiently short to avoid collision in the corridor scenario. As they are too short to reach the ceiling, the additional range was provided by the vertical slider.

2 Dynamic modeling of the robotic unit for stability evaluation

2.1 A dynamic interaction model of the robotized asbestos removal was proposed. A geometric model was developed to represent the robotic unit and cleaning environment. Reaction forces appearing during the grinding and their effect on the stability of the robotic unit were identified.

2.2 Using the above information, a numerical approach for stability evaluation was developed using ZMP based stability margin. The method of pseudo-inverse was used to solve the inverse kinematic problem of the redundant arm.

2.3 Multibody dynamic models of the two prototypes of the robotic unit were developed and were coupled with the control model for co-simulation.

3 Static and dynamic stability evaluation for trajectory planning

3.1 Static stability of the Version-1 prototype was first studied. It was found that the prototype has stable static behavior over the entire accessible surface of the wall at a given position of the mobile base. Dynamic stability behavior however showed occurrence of instabilities at specific slider heights.

3.2 Version-2 prototype was analyzed for three scenarios - ground, wall and ceiling of static stability. In cases of wall, static lateral stability was found to limit the accessible area. In case of ceiling, the robotic unit showed a stable behavior. However, for ground scenario, robotic arm was found to be close to singularity.

3.3 Based on the conclusions of stability analysis, safe grinding trajectory was demonstrated for cleaning wall scenario. Original design rules for path planning were extracted. For instance, it was shown that dynamic stability for wall cleaning is better when horizontal motions start from the center of the workspace and move away towards the sides.

Future work

1 Arm design based on dynamic stability criteria

It was found that the arm that has been designed based on the geometric modeling and the dimensional synthesis approach provided a good accessible workspace for cleaning walls. However, due to loss of static stability, a part of the accessible area was inappropriate for grinding. One future work could be to construct an optimization problem to maximize the dynamic stability on a standard trajectory and deduce optimal dimensions of the arm.

2 Stability optimization for a redundant mobile manipulator

As the arm has already a redundant kinematics for the task and is also supported by a mobile base that adds two or three other mobilities, the mobile manipulator can be optimally controlled online for maximizing its stability. Control can deal only with the arm for a given pose of the mobile base, or can simultaneously address the arm and mobile base motions. Our developments on stability evaluation will be directly usable in such control approaches.

3 Multi-robot collaboration

The conceptual framework of the Bots2ReC project imagined robot-robot collaboration for achieving the cleaning task. However, numerous challenges faced during the development and the limited time span, the idea of collaboration remained at conceptual level.

The application of asbestos removal can be performed with two or three specialized robots one for each scenario (wall-ceiling and ground). In such case productivity of the cleaning operation can be further optimized. Collaboration can also enhance stability of the robotic units if connected by mechanical links. This can significantly enhance the cleaning workspace for both of the robots working side-by-side.

Acknowledgment

The Bots2ReC (Robots to Re-Construction, [Bots2ReC, 2016]) project has received funding from the European Union's Horizon 2020 research and innovation program under - grant agreement No: **687593**.

Appendix A

Online tool path planning algorithm

Contents

This section elaborates theoretical framework for the a stability based trajectory planning algorithm.

A.1 Aspects of path planning

To study this dependency, a systematic approach is proposed to plan operational trajectories of the arm by assessing dynamic stability. Some of the issues to be addresses while planning the trajectory are presented below:

- *Identifying line of safety* :
- *Defining dynamic task workspace* : It is clear from previous discussion that, lateral stability plays an important role in deciding stable operational zone since postural longitudinal stability never reaches zero. Figure A.2 shows stability contours of (0, 5, 10, 15, 20, 25)%. These lines indicate potential threshold for deciding which line should be considered as a safety margin for the operation. Choice of the line affects how much area is selected as a safe zone. In figure A.3, two zones defined based on two stability contours are shown. Zone 1 is set of all points inside 20% static stability line while zone 2 is set of all points 10%. Two area's differ, such that (Zone 2)>(Zone 1) by $1.5m^2$.

  To identify which line to be taken as a safety limit, robotic arm is applied with acceleration in all directions from the point on each stability line.
- *Complete area coverage* :

  While performing the task that involves covering the entire wall, issue of determining optimal adjacent positions of the robotic unit arises. A challenge here is not to let any area uncovered. At the same time too much overlapping of areas can result

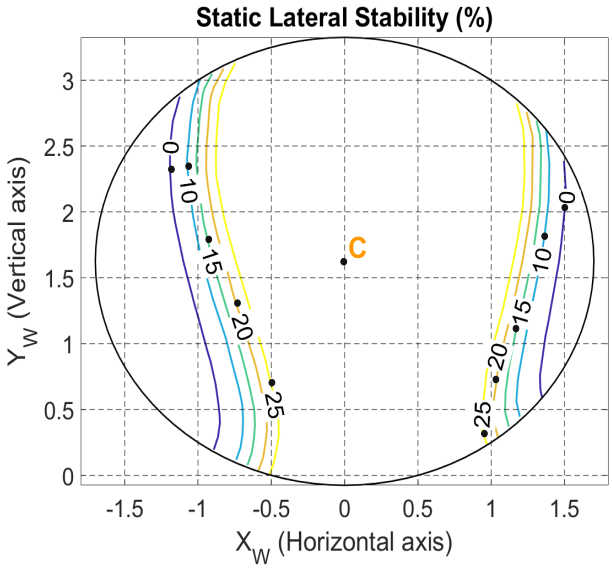

Figure A.1: Contour: Static lateral stability lines

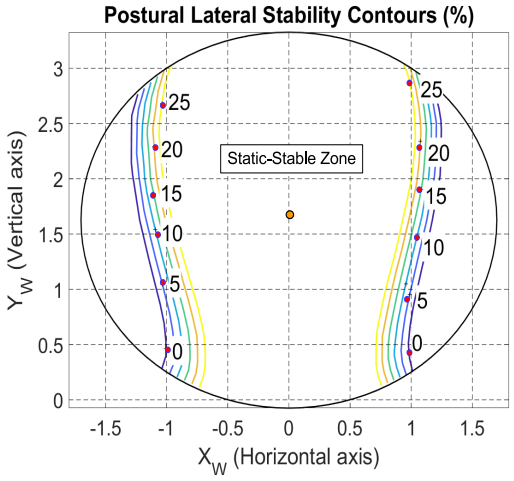

Figure A.2: Contour: Postural lateral stability

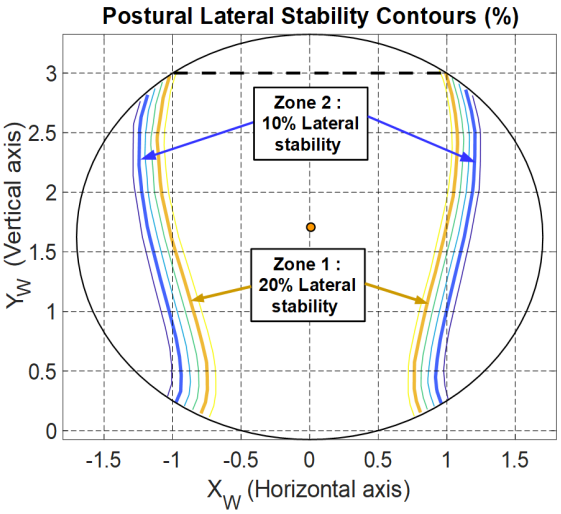

Figure A.3: Defining zones based on stability lines of 10% and 20%

in frequent repositioning of the robotic unit increasing task completion time. The region show in figure A.3 is an irregular concave shape. However, to cover entire wall during operation, this shape needs to be replicated several times. Figure A.4 shows two operational areas, A and B resulting from two adjacent positions of the robotic unit. Two regions namely, overlapped region (R_O) and uncovered region (R_U) are indicated. For time-efficient operation,

1. Area of uncovered region (R_U) must be zero
2. Area of overlapped region (R_O) must be minimized

– *Contact vs Non-contact*

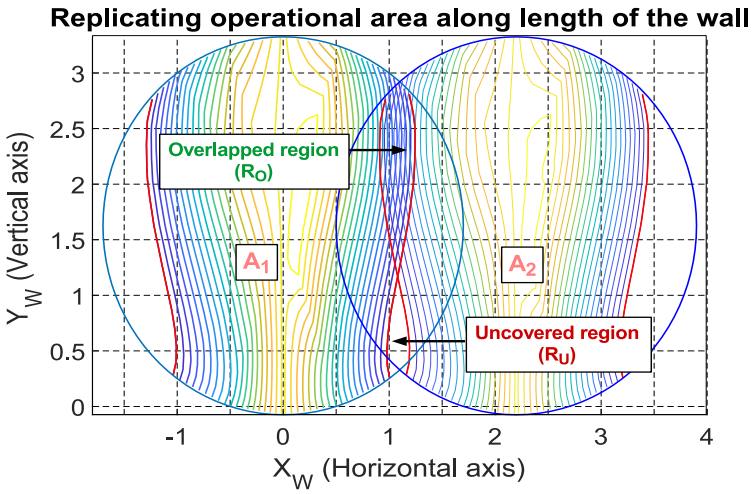

Figure A.4: Scenario of adjacent operational areas

Depending on the type of operation, i.e. whether end-effector makes any contact with the operating surface, dynamics of the system changes. Thus, two cases need to be studied separately.

A.2 Definition of path

Initial step in planning trajectory is to define a **path** inside the static stability zone such that, it covers all points within the zone at least once in a single trace. Let, such path be denoted by p and l_p be the total path length (figure A.5).

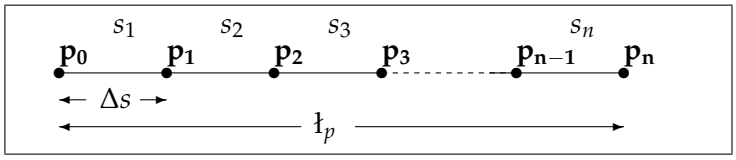

Figure A.5: Definition of the path followed during operation

Path p is divided into 'n' segments ($s_1, s_2 ... s_n$) using '$n+1$' points ($\mathbf{p_0}, \mathbf{p_1}, \mathbf{p_2}, ... \mathbf{p_{n-1}}, \mathbf{p_n}$). Thus, $\mathbf{p_0}$ and $\mathbf{p_n}$ are **start** and **end** points of the path respectively, whereas all the other in between points ($\mathbf{p_1}, \mathbf{p_2}, \mathbf{p_3}, ... \mathbf{p_{n-1}}$) are **intermediate** points. Each segment (s_i) has an equal length of Δs.

$$n \times \Delta s = l_s \tag{A.1}$$

(A.2)

A.3 Types of T_{CP} motions

Tool centre point (T_{CP}) undergoes accelerated and decelerated motions during the operation which can be classified into following types:

– Start motion :
At the beginning of path (i.e. point $\mathbf{p_0}$) involving acceleration of T_{CP}.

– Stop motion :
At the end of path (i.e. point $\mathbf{p_n}$) involving deceleration of T_{CP}.

– Intermediate motions :
While T_{CP} travels through intermediate points ($\mathbf{p_1}, \mathbf{p_2}, ..., \mathbf{p_{n-1}}$), it may pass from the point of higher stability zone to the lower one or vice a versa. This may generate accelerations and decelerations of T_{CP}.

– Emergency stop motion :
As soon as, operator hits the emergency stop switch, T_{CP} must come to rest within specified stopping distance. Intuitively, higher stopping distance would allow planning stop motion with lower deceleration. Even though this would generate lower dynamics, time taken to complete the stop motion will be higher compared to the motion planned over lower stopping distance. However, in case of motion over lower stopping distance, higher dynamics will be generated, making dynamic stability a critical issue.

From this classification, initial and final conditions of velocity and acceleration of the tool can be determined.

A.4 Boundary conditions for T_{CP} motion

Let, V_{t_i} and a_{t_i} be the velocity and acceleration of T_{CP} for the i^{th} point on path p. Here, $\mathbf{p_0}$ and $\mathbf{p_n}$ are the start and the end points, respectively. At these points, T_{CP} is assumed to have zero velocity and acceleration. Thus, we have

$$\begin{aligned} V_{t_0} = 0,\ V_{t_n} = 0 \\ a_{t_0} = 0,\ a_{t_n} = 0 \end{aligned} \tag{A.3}$$

Boundary conditions on velocity and acceleration expressed through equation A.3 will be useful while calculating start and stop motions of the trajectory.

A.5 Trajectory Planning Algorithm

Once the path to be followed by the tool during operation is defined, positions acquired by T_{CP} with respect to time need to be identified, which indeed defines **trajectory** of the entire motion. To achieve this, we need to determine minimum possible time interval Δt_i for the motion of the frame T_{CP} along Δs_i under constraints of static and dynamic stabilities.

– *Planning start motion* :
For starting motion, tool centre point T_{CP} is initially positioned at point p_0. Initial conditions of velocity and acceleration are expressed in equation A.3. To achieve time-efficient trajectory, an attempt should be to reach maximum transnational velocity '$V_{t_{max}}$' in shortest possible time while reaching the successive point p_1 on the path. Since, Δs is the length of the segment s_1 between points $\mathbf{p_0}$ and $\mathbf{p_1}$, the planning problem becomes: coverage of distance Δs in shortest time interval Δt_1 under the constraint of **dynamic stability**.

– *Computing* Δt_1 :
According to equations of motion,

$$v^2 = u^2 + 2.a.s$$
$${V_{t_1}}^2 = {V_{t_0}}^2 + 2.(a_{\Delta s_1}).\Delta s \tag{A.4}$$

Here,
$V_{t_0} = 0$
$a_{\Delta s_1}$ = uniform acceleration over segment Δs.

Rearranging, eqn.A.4 for acceleration we have,

$$(a_{\Delta s_1}) = \frac{{V_{t_1}}^2}{2.\Delta p} \tag{A.5}$$

Also,

$$v = u + a.t$$
$$t = \frac{v - u}{a} \tag{A.6}$$

Using, $u = 0$, and the value of acceleration (a) from equation A.5,

$$\Delta t_1 = \frac{2.\Delta s}{V_{t_1}} \tag{A.7}$$

Equation A.7 shows that, value of Δt_1 depends on the choice of velocity V_{t_i}. To achieve minimum possible Δt_1, intuitive choice of V_{t_i} is $V_{t_{max}}$. However, choice of V_{t_i} is responsible for generating uniform acceleration $a_{\Delta p_{s_1}}$ (equation A.5) and hence the magnitude of **dynamic** effects. The total dynamic effect in turn governs stability of the system. Therefore, choice of V_{t_1} is constrained by dynamic stability. If, for $V_{t_i} = V_{t_{max}}$, dynamic stability is within the limit of stability criterion, computed Δt_1 is valid. Else, another Δt_1 must be calculated that does not result into instability of the robotic unit.

– *Critical limit of stability* :

Figure A.6 shows support polygon $S_1S_2S_3S_4$. Axes x_s and y_s define frame of the support polygon. Segment S_1S_2 represents front side of the support polygon while segment S_3S_4 is the rear one. Based on the signs of x_s and y_s coordinates, we have $\pm$ *critical longitudinal stability line* $\pm$ *critical lateral stability line*. Every point on the critical stability line is a critical value of ZMP.

– *Computing optimal* Δt *based on critical stability :*
Reminding equation of zero-moment point we have,

$$x_{zmp} = \frac{\sum_{i=1}^{n} m_i(\ddot{z}_i + g)x_i - \sum_{i=1}^{n}(m_i\ddot{x}_i)z_i - \sum_{i=1}^{n}(\mathcal{L}_y)_i}{\sum_{i=1}^{n} m_i(\ddot{z}_i + g)} \tag{A.8a}$$

$$y_{zmp} = \frac{\sum_{i=1}^{n} m_i(\ddot{z}_i + g)y_i - \sum_{i=1}^{n}(m_i\ddot{y}_i)z_i - \sum_{i=1}^{n}(\mathcal{L}_x)_i}{\sum_{i=1}^{n} m_i(\ddot{z}_i + g)} \tag{A.8b}$$

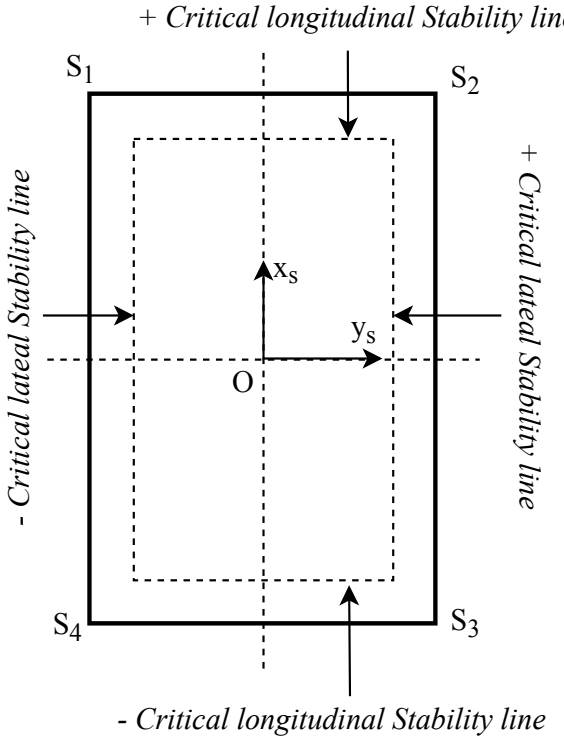

Figure A.6: Longitudinal and lateral critical stability lines

Last terms in both the equations are derivatives of angular moments. Since, angular velocities ω of all the links are low, value of the last terms is negligible compared to the first two. Thus, contribution of the last term in deciding ZMP is negligible.
Also, terms of accelerations can be represented in terms of time derivatives to separate time variable. Ignoring last terms in the numerator of equations A.8a can be expressed as,

$$x_{zmp} = \frac{\sum_{i=1}^{n} m_i(\frac{\Delta z_i}{\Delta t^2} + g)x_i - \sum_{i=1}^{n}(m_i\frac{\Delta x_i}{\Delta t^2})z_i}{\sum_{i=1}^{n} m_i(\frac{\Delta z_i}{\Delta t^2} + g)} \tag{A.9a}$$

Equation A.9a can be re-organised to express in terms of t as follows:

$$x_{zmp} = \frac{\sum_{i=1}^{n} m_i(\Delta z_i + g\Delta t^2)x_i - \sum_{i=1}^{n}(m_i\Delta x_i z_i)}{\sum_{i=1}^{n} m_i(\Delta z_i + g\Delta t^2)} \tag{A.10}$$

$$x_{zmp} = \frac{\sum_{i=1}^{n} m_i(\Delta z_i)x_i + \sum_{i=1}^{n} m_i g\Delta t^2 x_i - \sum_{i=1}^{n} m_i\Delta x_i z_i}{\sum_{i=1}^{n} m_i(\Delta z_i) + \sum_{i=1}^{n} m_i g\Delta t^2}$$

$$(x_{zmp} - \sum_{i=1}^{n} x_i)\sum_{i=1}^{n} m_i(\Delta z_i) + (x_{zmp} - \sum_{i=1}^{n} x_i)\sum_{i=1}^{n} m_i g\Delta t^2 = -\sum_{i=1}^{n}(m_i\Delta x_i z_i)$$

$$(x_{zmp} - \sum_{i=1}^{n} x_i)\sum_{i=1}^{n} m_i g\Delta t^2 = -(\sum_{i=1}^{n}(m_i\Delta x_i z_i) + (x_{zmp} - \sum_{i=1}^{n} x_i)\sum_{i=1}^{n} m_i(\Delta z_i))$$

$$\Delta t^2 = \frac{-[\sum_{i=1}^{n}(m_i \Delta x_i z_i) + (x_{zmp} - \sum_{i=1}^{n} x_i)\sum_{i=1}^{n} m_i(\Delta z_i)]}{(x_{zmp} - \sum_{i=1}^{n} x_i)\sum_{i=1}^{n} m_i g}$$

$$\Delta t = \pm\sqrt{\frac{-[\sum_{i=1}^{n}(m_i \Delta x_i z_i) + (x_{zmp} - \sum_{i=1}^{n} x_i)\sum_{i=1}^{n} m_i(\Delta z_i)]}{(x_{zmp} - \sum_{i=1}^{n} x_i)\sum_{i=1}^{n} m_i g}}$$

Negative value of Δt is infeasible and hence, the value of Δt to be taken is;

$$\Delta t_x = \sqrt{\frac{-[\sum_{i=1}^{n}(m_i \Delta x_i z_i) + (x_{zmp_C} - \sum_{i=1}^{n} x_i)\sum_{i=1}^{n} m_i(\Delta z_i)]}{(x_{zmp} - \sum_{i=1}^{n} x_i)\sum_{i=1}^{n} m_i g}} \tag{A.11}$$

Here, subscript x in Δt_x indicates time interval evaluated based on critical value of ZMP - x_{zmp_C}. This critical value can be the point on the *longitudinal dynamic safety margin* drawn inside the support polygon.
Similarly, based on critical value of the lateral stability y_{zmp_C}, another time interval namely, Δt_y can be calculated as,

$$\Delta t_y = \sqrt{\frac{-[\sum_{i=1}^{n}(m_i \Delta y_i z_i) + (y_{zmp_C} - \sum_{i=1}^{n} y_i)\sum_{i=1}^{n} m_i(\Delta z_i)]}{(y_{zmp} - \sum_{i=1}^{n} y_i)\sum_{i=1}^{n} m_i g}} \tag{A.12}$$

– *Planning stop motion* :
Stop motion occurs at the end of trajectory i.e. while going from point p_{n-1} to p_n. Time interval Δt_n for stop motion can be calculated using equations A.5, A.6 and A.7 as,

$$\Delta t_n = \frac{2.\Delta p}{V_{t_{n-1}}} \tag{A.13}$$

– *Planning intermediate motion* :
Since, stability of the robotic unit varies due to arm acquiring different positions during the operation, intermediate motions are associated with uniform acceleration, uniform deceleration or constant velocity motion.

- Accelerated motion : For any motion from p_{i-1} to p_i (i.e. along p_{s_i}), if tool translational velocity ($V_{t_{i-1}}$) is less than,

– *Planning emergency stop motion* :

At any time instance during the trajectory, arm must be able to stop within specified stopping distance in case of emergency. Thus, arm must be able to decelerate the tool and come to rest without being dynamically unstable.

To satisfy the criteria of stability during deceleration, from each point on the trajectory, arm is decelerated to come to rest within the stopping distance. To illustrate this, let's consider that while performing trajectory, tool center point T_{cp} is passing through an intermediate point p_{int} shown in fig.A.7.

Let, $V_{t_{int}}$ be the velocity and $a_{t_{int}}$ be the acceleration of T_{cp}. Let, p_{stop} be a point at stopping distance d_{stop} from the point p_{int}. At p_{stop}, both velocity and acceleration,i.e. $V_{t_{stop}}$ and $a_{t_{stop}}$ are zero. Stopping time Δt_{stop} can then be calculated as below.

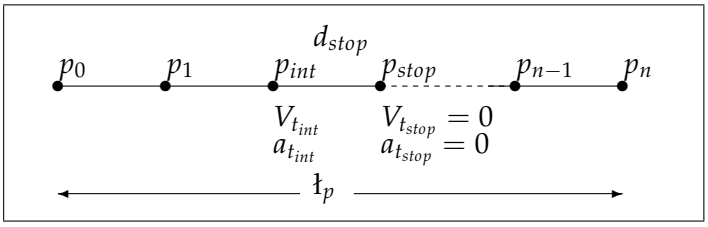

Figure A.7: Deceleration to achieve emergency stop

In equation, A.4 when, $v = 0$, it becomes

$$a = -\frac{u^2}{2.s} \tag{A.14}$$

Also,

$$\begin{aligned} v &= u + a.t \\ t &= \frac{v - u}{a} \end{aligned} \tag{A.15}$$

Using, $v = 0$, and the value of a from A.14,

$$\begin{aligned} t &= \frac{-u.(2.s)}{-u^2} \\ t &= \frac{2.s}{u} \end{aligned} \tag{A.16}$$

Here, $s = d_{stop}$, $u = V_{t_{int}}$ and $t = \Delta t_{stop}$. Thus,

$$\Delta t_{stop} = \frac{2.(d_{stop})}{V_{t_{int}}} \tag{A.17}$$

From eqn.A.17, it is clear that time required to stop the motion of tool in the stopping distance depends on the velocity of the tool at the time of pressing emergency stop.

– Value of Δt_{stop} can then be used to evaluate stability while executing stopping motion from p_{int} to p_{stop}.

– Value of Δt_{i+1} will decide velocity and acceleration of the motion.

– Finally, addition of all Δt_{i+1} will yield total time taken to complete the path. Since, we attempt to find out minimum possible time interval, the resulting time of path completion is the minimized one.

Input: $p = \sum_{i=0}^{i=n} p_i$
initialization: Start point $p_i = p_0$, $V_{t_i} = 0$, $t_p = 0$;
for $i = 0 : (n-1)$ **do**
  compute $\rightarrow \Delta t_{i+1} = \Delta p / V_{t_{max}}$;
  compute $\rightarrow (\lambda_{D_{Lo}}, \lambda_{D_{Lt}})_{acc}, (\lambda_{D_{Lo}}, \lambda_{D_{Lt}})_{dec}$;
  if $[(\lambda_{D_{Lo}}, \lambda_{D_{Lt}})_{acc}, (\lambda_{D_{Lo}}, \lambda_{D_{Lt}})_{dec}] > \lambda_{D_C}$ **then**
    execute motion from p_i to p_{i+1};
    store Δt_{i+1};
  else if $(\lambda_{D_{Lo}})_{acc} < \lambda_{D_C}, [(\lambda_{D_{Lt}})_{acc}, (\lambda_{D_{Lo}}, \lambda_{D_{Lt}})_{dec}] > \lambda_{D_C}$ **then**
    compute $\rightarrow \Delta t_{x_{i+1}}$;
    execute motion from p_i to p_{i+1} using $\Delta t_{x_{i+1}}$;
    store $\Delta t_{i+1} = \Delta t_{x_{i+1}}$
  else if $(\lambda_{D_{Lt}})_{acc} < \lambda_{D_C}, [(\lambda_{D_{Lo}})_{acc}, (\lambda_{D_{Lo}}, \lambda_{D_{Lt}})_{dec}] > \lambda_{D_C}$ **then**
    compute $\rightarrow \Delta t_{y_{i+1}}$;
    execute motion from p_i to p_{i+1};
    store $\Delta t_{i+1} = \Delta t_{y_{i+1}}$;
  else if $(\lambda_{D_{Lo}})_{dcc} < \lambda_{D_C}, [(\lambda_{D_{Lo}}, \lambda_{D_{Lt}})_{acc}, (\lambda_{D_{Lt}})_{dec}] > \lambda_{D_C}$ **then**
    compute $\rightarrow \Delta t_{x_{i+1}}$;
    execute motion from p_i to p_{i+1};
  else
    evaluate Δt_{i+1} using eqn(A.11);
    excute motion from p_i to p_{i+1};
    store Δt_{i+1};
  end
end
At End point: $i = n$, $p_i = p_n$, $V_{t_n} = 0$, $t_p = \sum_{i=0}^{n} \Delta t_{i+1}$;

Algorithm 2: Tool motion planning

Bibliography

Rotor Shaft Assembly using the KUKA LWR. 2012. URL https://www.youtube.com/watch?v=bR77UhcS0z4.

L'union sociale pour l'habitat. amiante., 2014. URL https://www.union-habitat.org/centre-de-ressources/patrimoine-maitrise-d-ouvrage/amianteficheS-de-communication-de-crise. Visited on 24/10/2017.

Bouygues construction and audencia junior conseil., 2015. Étude du marché du désamiantage en europe.

Home | Geogebra, 2016. URL https://www.geogebra.org. viewed on 2018/11/12.

Abo-Shanab, R. F. and Sepehri, N. On dynamic stability of manipulators mounted on mobile platforms. *Robotica*, 19(4):439–449, 2001.

Abo-Shanab, R. F. and Sepehri, N. Dynamic modeling of tip-over stability of mobile manipulators considering the friction effects. *Robotica*, 23(2):189–196, 2005.

Ackerman, E. Boston dynamics' spotmini is all electric, agile, and has a capable face-arm, June 2016. URL http://spectrum.ieee.org/automaton/robotics/home-robots/boston-dynamics-spotmini. Consulté le 24/10/2018.

Agah, A. and Tanie, K. Human interaction with a service robot: Mobile-manipulator handing over an object to a human. *Proceedings - IEEE International Conference on Robotics and Automation*, 1(April):575–580, 1997.

Alipour, K. and Moosavian, S. A. A. Dynamically stable motion planning of wheeled robots for heavy object manipulation. *Advanced Robotics*, 29(8):545–560, 2015.

Alipour, K., Hasanpour, A., and Daemy, P. Comparing two online tip-over avoidance algorithms for mobile manipulators. *2014 2nd RSI/ISM International Conference on Robotics and Mechatronics, ICRoM 2014*, pages 310–315, 2014.

Alipour, K., Daemi, P., Hassanpour, A., and Tarvirdizadeh, B. On the capability of wheeled mobile robots for heavy object manipulation considering dynamic stability constraints. *Multibody System Dynamics*, 41(2):101–123, 2017.

Angel, L., Pèrez, M. P., Diaz-Quintero, C., and Mendoza, C. ADAMS/MATLAB CO-SIMULATION: Dynamic Systems Analysis and Control Tool. *Applied Mechanisms and Materials*, 232:pp. 527–531, 2012.

Anses. French agency for food, environmental and occupational health and safety. asbestos:presentation, health effects, exposure and regulatory framework., 2017. URL https://www.anses.fr/en/content/asbestos. Visited on 24/10/2018.

Armada, E. G., Estremera, J., and Santos, P. G. D. A classification of stability margins for walking robots. *Proc. Int. Symp. ClimbingWalking Robots*, pages pp. 799–808, 2002. URL http://digital.csic.es/handle/10261/8031.

Bayle, B., Fourquet, J. Y., and Renaud, M. Manipulability of wheeled mobile manipulators: Application to motion generation. *The International Journal of Robotics Research*, 22(7–8):565–581, 2003.

Berenson, D., Kuffner, J., and Choset, H. An optimization approach to planning for mobile manipulation. *2008 IEEE International Conference on Robotics and Automation*, pages 1187–1192, 2008. URL http://ieeexplore.ieee.org/lpdocs/epic03/wrapper.htm?arnumber=4543365.

Bøgh, S., Hvilshøj, M., Kristiansen, M., and Madsen, O. Autonomous industrial mobile manipulation (aimm): From research to industry. 2011.

Bort, L. and del Pobil, A. P. Using speech to guide a mobile robot manipulator.

Bostelman, R., Hong, T., and Marvel, J. Survey of research for performance evaluation of mobile manipulators. *Journal of research of the national institute of standards and technology*, pages 342–366, 2017.

Bots2ReC. Home | Bots2ReC, 2016. URL https://www.bots2rec.eu. viewed on 2018/10/25.

Centre-Mosothelioma. A world of support for families affected by mesothelioma, 2006. URL https://www.asbestos.com/products/. Visited on 24/10/2018.

Chaventré, F. and Cochet, C. *Centre Scientifique et Technique du Bâtiment :*, 2005. URL L\T1\textquoterightamiantedansleparcdebâtimentsfrançais.http://docplayer.fr/1923126-L-amiante-dans-le-parc-de-batiments-francais.html.

Chen, M. and Zalzala, A. M. A genetic approach to motion planning of redundant mobile manipulator systems considering safety and configuration. *Journal of Robotic Systems*, 14(7):529–544, 1997.

Chen, X. and Li, Y. Cooperative transportation by multiple mobile manipulators using adaptive nn control. In *Neural Networks (IJCNN), International Joint Conference on*, pages 4193–4200. IEEE, 2006.

Chen, Z., Lii, N. Y., Wimböck, T., Fan, S., Liu, H., and Albu-Schäffer, A. Experimental analysis on spatial and cartesian impedance control for the dexterous DLR/HIT II hand. *International Journal of Robotics and Automation*, 29(1):1–13, 2014.

Chitta, S., Cohen, B., and Likhachev, M. Planning for autonomous door opening with a mobile manipulator. *Proceedings - IEEE International Conference on Robotics and Automation*, pages 1799–1806, 2010.

Clearpath Robotics. Husky UGV - Outdoor Field Research Robot by Clearpath, 2017. URL https://www.clearpathrobotics.com/husky-unmanned-ground-vehicle-robot/. Visited on 24/10/2018.

Davidson, J. K. and Schweitzer, G. A mechanics-based computer algorithm for displaying the margin of static stability in four-legged vehicles. *Journal of Mechanical Design, Transactions of the ASME*, 112(4):480–487, 1990.

de Défense des Victimes de l'Amiante, A. N.

Detert, T., Charaf Eddine, S., Fauroux, J.-C., Haschke, T., Becchi, F., Corves, B., Guzman, R., Herb, F., Linéatte, B., and Martin, D. Bots2rec: introducing mobile robotic units on construction sites for asbestos rehabilitation. *Construction Robotics*, pages 1–9, 2017.

Dharmawan, A. G., Foong, S., and Soh, G. S. Simultaneous optimal robot base placement and motion planning using expanded lagrangian homotopy. *ASME 2016 Dynamic Systems and Control Conference, DSCC 2016*, 2:1–10, 2016.

Diaz-Calderon, A. and Kelly, A. On-line stability margin and attitude estimation for dynamic articulating mobile robots. *International Journal of Robotics Research*, 24:1–41, 2005.

Ding, X., Liu, Y., Hou, J., and Ma, Q. Online dynamic tip-over avoidance for a wheeled mobile manipulator with an improved tip-over moment stability criterion. *IEEE Access*, 7:67632–67645, 2019.

DLR. Space Justin | National Auronaoutics and sapce administration, 2009. URL https://mars.nasa.gov/mer/. viewed on 25/03/2020.

Du, B., Zhao, J., and Song, C. Optimal base placement and motion planning for mobile manipulators. *Proceedings of the ASME Design Engineering Technical Conference*, 4 (PARTS A AND B):1227–1234, 2012.

Dubowsky, S. and Vance, E. Planning mobile manipulator motions considering vehicle dynamic stability constraints. *Proceedings, 1989 International Conference on Robotics and Automation*, pages 1271–1276, 1989.

Egerstedt, M. and Hu, X. Coordinated trajectory following for mobile manipulation. *Proceedings - IEEE International Conference on Robotics and Automation*, 4(April):3479–3484, 2000.

Fahimi, F. *Autonomous Robots: Modeling, Path Planning and Control*. Springer, 2009.

Fauroux, J.-C. "synthesis, design, modelling and experimentation of innovative machines - application to agile mobile robots", §4.5 synthesis methods for machine design,. *Habilitation à Diriger les Recherches*, pages 247–290, 2015.

Fetch. Assistive mobile manipulatror| Fetch Robotics, 2016. URL https://fetchrobotics.com/robotics-platforms. viewed on 25/03/2020.

Flannigan, C. Mobile Manipulation Robotics Automation Engineering, Southwest Research Institute. 2012.

FLIR Systems. iRobot 510 PackBot Multi-Mission Robot by FLIR, 1998. URL https://www.flir.com/products/packbot/. Visited on 01/04/2020.

FML. French ministry of labor. article r.4412-100 of the french labour code, as set out in ministerial order 2012-639., 2012. URL https://www.legifrance.gouv.fr/affichCodeArticle.do?cidTexte=LEGITEXT000006072050&idArticle=LEGIARTI000018490587&dateTexte=&categorieLien=cid. Online accessed 30-march-2019.

Foulon, G., Fourquet, J. Y., and Renaud, M. Coordinating mobility and manipulation using nonholonomic mobile manipulators. *Control Engineering Practice*, 7(3):391–399, 1999.

France-Goverment, 1996. URL https://www.legifrance.gouv.fr/affichTexte.do?cidTexte=JORFTEXT000000734637. Visited 24/14/2018.

Furuno, S., Yamamoto, M., and Mohri, A. Trajectory planning of mobile mainpulator with stability considerations. *International Conference on Robotics & Automation*, pages 3403–3408, 2003.

Garcia, E. and De Santos, P. G. *An improved energy stability margin for walking machines subject to dynamic effects*, volume 23. 2005.

Ghasempoor, A. and Sepehri, N. Measure of machine stability for moving base manipulators. *Proceedings - IEEE International Conference on Robotics and Automation*, 3: 2249–2254, 1995.

Guo, S., Song, T., (Jeff) Xi, F., and Mohamed, R. P. Tip-Over Stability Analysis for a Wheeled Mobile Manipulator. *Journal of Dynamic Systems, Measurement, and Control*, 139(5):054501–054501, 2017.

Guérin, J.-Y. and Joaun, A. Amiante et hlm : le plan a minima du gouvernement., 2014. URL http://www.lefigaro.fr/actualite-france/2014/09/23/01016-20140923ARTFIG00241-amiante-et-hlm-le-plan-a-minima-dugouvernement.php. Visited on 24/10/2017.

Hatano, M. and Obara, H. Stability evaluation for mobile manipulators using criteria based on reaction. volume 2, pages 2050 – 2055, 09 2003.

Hirose, S., Tsukagoshi, H., and Yoneda, K. Normalized energy stability margin and its contour of walking vehicles on rough terrain. *Proceedings 2001 ICRA. IEEE International Conference on Robotics and Automation (Cat. No.01CH37164)*, 1:181–186, 2001.

Holmberg, R. and Khatib, O. Development and control of a holonomic mobile robot for mobile manipulation tasks. *International Journal of Robotics Research*, 19(11):1066–1074, 2000.

Huang, Q., Sugano, S., and Kato, I. Stability control for a mobile manipulator using a potential method. *IEEE/RSJ/GI International Conference on Intelligent Robots and Systems*, 2:839–846, 1994.

Huang, Q., Kazuo, T., and Shigeki, S. Stability compensation of a mobile manipulator by manipulatorpaper motion: Feasibility and planning. *Advanced Robotics*, 13(1):25–40, 1998.

Huang, Q., Tanie, K., and Sugano, S. Planning for a mobile manipulator considering stability. pages 732–742, 2000.

Hvilshøj, M. and Bøgh, S. "Little helper" - An autonomous industrial mobile manipulator concept. *International Journal of Advanced Robotic Systems*, 8(2), 2011.

IFR. International federeation of robotics: Executive summary world robotics 2018 service robots, 2017. URL https://ifr.org/downloads/press2018/WR_Presentation_Industry_and_Service_Robots_rev_5_12_18.pdf. Visited on 24/10/2018.

Jain, A. and Kemp, C. C. EL-E: An assistive mobile manipulator that autonomously fetches objects from flat surfaces. *Autonomous Robots*, 28(1):45–64, 2010.

J.E., A. and Mossman, B. Experimental analysis on spatial and cartesian impedance control for the dexterous DLR/HIT II hand. *Asbestos revisited*, 277(1)(1):70–75, 1997.

Joanneum. CHIMERA | Joanneum Research Robotics, 2016. URL https://ottomotors.com/platform.

Khalil, W., D. E. *Modeling, Identification and Control of Robots*. CRC Press, 2002.

Khalil, W. and Creusot, D. Symoro+: a system for the symbolic modelling of robots. *Robotica*, 15:pp. 153–161, 1997.

Khatib, O., Yokoi, K., Chang, K., Ruspini, D., Holmberg, R., Casal, A., and Baader, A. Force Strategies for Cooperative Tasks in Multiple Mobile Manipulation Systems. *Robotics Research*, pages 333–342, 1996a.

Khatib, O., Yokoi, K., Chang, K., Ruspini, D., Holmberg, R., Casal, A., and Baader, A. Force Strategies for Cooperative Tasks in Multiple Mobile Manipulation Systems. *Robotics Research*, pages 333–342, 1996b.

Kim, J., Chung, W. K., Youm, Y., and Lee, B. H. Real-time ZMP compensation method using null motion for mobile manipulators. *Proceedings - IEEE International Conference on Robotics and Automation*, 2:1967–1972, 2002.

King, A. Asbestos explained, 2017. URL https://www.chemistryworld.com/news/whyasbestos-is-still-used-around-the-world/3007504.article. Visited on 24/10/2018.

KUKA. Mobile Robots from KUKA | KUKA, 2015. URL https://www.kuka.com/en-de/products/mobility/mobile-robots.

LBR-iiwa. Mobile Robots from KUKA | KUKA, 2013. URL https://www.kuka.com/en-de/products/robot-systems/industrial-robots/lbr-iiwa.

Lee, J. H., Park, J. B., and Lee, B. H. Turnover prevention of a mobile robot on uneven terrain using the concept of stability space. *Robotica*, 27(5):641–652, 2009.

Lenain, R., Bouton, N., Fauroux, J.-C., and Thuilot, B. Dynamic modeling of all terrain vehicles designed for dynamic stability analysis. *ECCOMAS Thematic Conference*, (June):25–28, 2007.

Lin, B.-S. and Song, S.-M. Dynamic modeling, stability and energy efficiency of a quadruped walking machine. *IEEE International Conference on Robotics and Automation*, 18(11):367–373, 1993.

Mahdi, A. and Nestinger, S. S. Foot force criterion for robot stability. (July):23–26, 2012.

Maraje, S., Fauroux, J.-C., Bouzgarrou, C.-B., and Adouane, L. Stability analysis of an asbestos removal mobile manipulator for safe grinding trajectories. In *Advances in Mechanism and Machine Science*, pages 2349–2358. Springer International Publishing, 2019.

McGhee, R. and Frank, A. On the stability properties of quadruped creeping gaits. *Mathematical Biosciences*, 3:331–351, 1968.

Mcghee, R. B. and Iswandhi, G. I. Adaptive locomotion of a multilegged robot over rough terrain. *IEEE Transactions on Systems, Man, and Cybernetics*, 9(4):176–182, 1979.

Medrobotics. Flex Robotic System | Medrobotics, 2016. URL https://fetchrobotics.com/robotics-platforms. viewed on 25/03/2020.

Meghdari, A., Naderi, D., and Eslami, S. Optimal stability of a redundant mobile manipulator via genetic algorithm. *Robotica*, 24(6):739–743, 2006.

Messuri, D. A. and Klein, C. A. Automatic Body Regulation for Maintaining Stability of a Legged Vehicle During Rough-Terrain Locomotion. *IEEE Journal on Robotics and Automation*, 1(3):132–141, 1985.

Moosavian, S. and Alipour, K. Moment-height tip-over measure for stability analysis of mobile robotic systems. *2006 IEEE/RSJ International Conference on Intelligent Robots and Systems*, pages 5546–5551, 2006.

Moosavian, S. A. A. and Alipour, K. On the dynamic tip - over stability of wheeled mobile manipulators. *International Journal of Robotics and Automation*, 22(4), 2007.

Moosavian, S. A. A., Alipour, K., and Bahramzadeh, Y. Dynamics modeling and tip-over stability of suspended wheeled mobile robots with multiple arms. *IEEE International Conference on Intelligent Robots and Systems*, pages 1210–1215, 2007.

MSH. Le repérage de l'amiante dans les bâtiments., 2019. URL https://solidarites-sante.gouv.fr/sante-et-environnement/batiments/article/le-reperage-de-l-amiante-dans-les-batiments. Online, accessed: 30th March, 2019.

Nagatani, K. and Yuta, S. Designing strategy and implementation of mobile manipulator control system for opening door. *Proceedings - IEEE International Conference on Robotics and Automation*, 3(April):2828–2834, 1996.

Nagatani, K., Hirayama, T., Gofuku, A., and Tanaka, Y. Motion planning for mobile manipulator with keeping manipulability. *IEEE International Conference on Intelligent Robots and Systems*, 2:1663–1668, 2002.

NASA. Opportunity Rover | MARS Exploration Rovers, 2003. URL https://mars.nasa.gov/mer/. viewed on 25/03/2020.

Norouzi, M., Miro, J. V., and Dissanayake, G. A statistical approach for uncertain stability analysis of mobile robots. *2013 IEEE International Conference on Robotics and Automation*, pages 191–196, 2013.

Osumi, H. and Terasawa, M. *Proceedings of the 1998 IEEE International Conference on Robotics Automation Leuven, Belgium*.

Pal-Robotics. TIAGo | Pal Robotics, 2016. URL https://tiago.pal-robotics.com. viewed on 25/03/2020.

Papadopoulos, E. and Poulakakis, J. Planning and model-based control for mobile manipulators. In *Intelligent Robots and Systems, 2000.(IROS 2000). Proceedings. 2000 IEEE/RSJ International Conference on*, volume 3, pages 1810–1815. IEEE, 2000.

Papadopoulos, E. and Rey, A. A new measure of tipover stability margin for mobile manipulators. In *Robotics and Automation, 1996. Proceedings., 1996 IEEE International Conference on*, volume 4, pages 3111–3116. IEEE, 1996.

Papadopoulus, E. and Rey, D. A new measure of tipover stability margin for mobile manipulators. *Proceedings of the IEEE Internatioanal Conference on Robotics and Automation, Minneapolis, MN*, 4(April):3111–3116, 1996.

Peters, S. C. and Iagnemma, K. An analysis of rollover stability measurement for high-speed mobile robots. *Proceedings - IEEE International Conference on Robotics and Automation*, 2006(May):3711–3716, 2006.

Petersson, L., Austin, D., and Kragic, D. High-level control of a mobile manipulator for door opening. *IEEE International Conference on Intelligent Robots and Systems*, 3: 2333–2338, 2000.

Pin, F. G. and Culioli, J. C. Optimal positioning of combined mobile platform-manipulator systems for material handling tasks. *Journal of Intelligent and Robotic Systems*, 6(2-3):165–182, 1992.

Rey, D. A. and Papadopoulos, E. G. On-line automatic tipover prevention for mobile manipulators. *IEEE International Conference on Intelligent Robots and Systems*, 3:1273–1278, 1997.

Roan, P. R., Burmeister, A., Rahimi, A., Holz, K., and Hooper, D. Real-world validation of three tipover algorithms for mobile robots. *Proceedings - IEEE International Conference on Robotics and Automation*, pages 4431–4436, 2010.

Seraji, H. Reachability Analysis. *Journal of Robotic Systems*, 12(1):29–43, 1994.

Seraji, H. Unified approach to motion control of mobile manipulators. *International Journal of Robotics Research*, 17(2):107–118, 1998.

Sreenivasan, S.V., W. B. H. Stability and TractSon control of an Actively Actuated Micro-Rover. *Journal of Robotic Systems*, 11(6):487–507, 1994.

Straif, K., Benbrahim-Tallaa, L., Baan, R., Grosse, Y., Secretan, B., Ghissassi, F. E., V. Bouvard, N. G., Freeman, C., and Galichet, L. A review of human carcinogens—part c: metals, arsenic, dusts, and fibres. *The lancet oncology*, 10((5)):453–454, 2009.

Sugano, S., Huang, Q., and Kato, I. Stability criteria in controlling mobile robotic systems. *Proceedings of 1993 IEEE/RSJ International Conference on Intelligent Robots and Systems (IROS '93)*, (C):832–838, 1993.

Sugar, T. and Kumar, V. Decentralized control of cooperating mobile manipulators. *Proceedings - IEEE International Conference on Robotics and Automation*, 4(May):2916–2921, 1998.

Tomizawa, T., Ohya, A., and Yuta, S. Remote book browsing system using a mobile manipulator. *Proceedings - IEEE International Conference on Robotics and Automation*, 1: 256–261, 2003.

Tsai, M. J. and Chiou, Y. H. Manipulability of manipulators. *Mechanism and Machine Theory*, 25(5):575 – 585, 1990.

UNRV.

Vukobratovic, M. and Juricic, D. Contribution to the synthesis of biped gait. In *Proceedings of IFAC Symposium on Technical and Biological Problems on Control, Erevan, USSR*, 1971.

Whitney, D. Resolved motion rate control of manipulators and human prostheses. *IEEE Transactions on man-machine systems*, 10(2):47–53, 1969.

Yamamoto, Y. and Yun, X. Coordinating locomotion and manipulation of a mobile manipulator. *IEEE Transactions on Automatic Control*, 39(6):1326–1332, 1994.

Yamamoto, Y. and Yun, X. Unified analysis on mobility and manipulability of mobile manipulators. *Proceedings - IEEE International Conference on Robotics and Automation*, 2: 1200–1206, 1999.

Yoneda, K. and Hirose, S. Stability Criterion of Integrated Locomotion an Manipulation. *Proc. IROS 96*, pages 870–876, 1996.

Yoshikawa, T. Manipulability of robotic mechanisms. *The International Journal of Robotics Research*, 4(2):3–9, 1985.

Yun, X. P. and Yamamoto, Y. Stability analysis of the internal dynamics of a wheeled mobile robot. *Journal of Robotic Systems*, 14(10):697–709, 1997.

Zhao, M., Ansari, N., and Hou, E. S. Mobile manipulator path planning by a genetic algorithm. *IEEE International Conference on Intelligent Robots and Systems*, 1(3):681–688, 1992.